UNIVERSITY OF CALIFORNIA
RIVERSIDE

Molecular Recognition by Synthetic Receptors in Biomimetic and Cellular Systems

A Dissertation submitted in partial satisfaction
of the requirements for the degree of

Doctor of Philosophy

in

Chemistry

by

Yoo-Jin Ghang

August 2015

Dissertation Committee:
Dr. Richard J. Hooley, Chairperson
Dr. Christopher Y. Switzer
Dr. Quan Cheng

The Dissertation of Yoo-Jin Ghang is approved:

_____

_____

_____

Committee Chairperson

University of California, Riverside

ABSTRACT OF THE DISSERTATION

Molecular Recognition by Synthetic Receptors in Biomimetic and Cellular Systems

by

Yoo-Jin Ghang

Doctor of Philosophy, Graduate Program in Chemistry
University of California, Riverside, August 2015
Dr. Richard J. Hooley, Chairperson

A deep water-soluble cavitand, a synthetic host molecule that can selectively recognize small molecules of the correct size, shape and charge, shows notable selectivity for trimethylammonium ($R\text{-}NMe_3^+$) salts through cation-π interactions in water. The cavitand possesses a negatively charged hydrophilic rim and a hydrophobic aromatic pocket, and can self-assemble into a vase-like conformation in aqueous solution via intramolecular hydrogen bonding. This host can be incorporated into supported lipid bilayers (SLBs) and retain its binding selectivity.

To study the scope of guests that can be recognized, several proteins were functionalized with $R\text{-}NMe_3^+$ binding handles and the recognition event between the functionalized proteins and cavitand:SLB system was monitored by Surface Plasmon Resonance (SPR) Spectroscopy. The binding was monovalent, and displayed a binding affinity of $>10^5\ M^{-1}$, showing that the cavitand is capable of recognizing suitably labeled large proteins via cavity-based recognition.

Underivatized proteins with high isoelectric points also showed strong binding to the cavitand:bilayer system under high salt conditions. This unique binding is due to charge-based interactions between the negatively charged rim of cavitand and the positively charged surfaces of proteins. Moreover, immobilized trypsin on the cavitand:SLB interface maintains its enzymatic function: the adhered trypsin is capable of digestion of insulin B. This indicates that the cavitand:SLB system is tolerant to enzymatic reactions.

From preliminary results on artificial SLBs, our interest has moved on to molecular recognition processes using cavitands in living cells. Shape-based molecular recognition with a synthetic receptor in living cells is far more challenging than in biomimetic membrane systems, simply due to the vast array of competitive species in a living cell. It was observed that the cavitand is capable of selective guest recognition and *transmembrane transport* in living cells despite the complexity of the environment. The host was combined with a R-NMe_3^+ labeled fluorescent guest in human cervical cancer cells (HeLa), and selective transport of the guest into the cells was observed. In the absence of cavitands minimal transport was observed, and no transport of fluorescein itself (without a R-NMe_3^+ binding handle) was observed. This was the first biological application of cavitands in cellular systems.

Table of Contents

Chapter Five: Cavitand-Mediated Endocytosis of Small Molecules into Live Cells

Chapter Six: Cavitands as New Transfection Agents for Living Cells

Chapter Seven: Experimental

List of Figures

List of Tables

Chapter One: Introduction to Molecular Recognition in Water

1.1 Molecular Recognition of Proteins and Enzymes within Biological Systems

Biological systems include many important recognition events, which occur between proteins or enzymes and other small molecules. These interactions include protein-ligand and protein-protein interactions. One of the most important factors of molecular recognition by proteins and enzymes is the unique physical and chemical properties exhibited by various binding pockets. When binding of proteins or enzymes to other molecules occur, various non-covalent interactions are involved, such as hydrogen bonding, electrostatic interactions, hydrophobic interactions, or cation-π interactions.

Acetylcholinesterase (AChE) is an enzyme involved in the termination of synaptic transmissions that acts by hydrolyzing the neurotransmitter acetylcholine.[1] AChE possesses a deep, narrow cavity called the "aromatic gorge"; this pocket is π-electron-rich and contains 14 aromatic amino acid residues.[2] X-ray crystallography and photoaffinity labeling experiments revealed that tryptophan (Trp) and phenylalanine (Phe) residues located within the aromatic gorge and the active site plays an important role in substrate binding.[3] When acetylcholine is bound inside of the gorge, it is drawn to the active site. The surface of the substrate has quaternary ammonium groups that possess a thin layer of positive charge and are responsible for interacting with the aromatic rings via cation-π interactions. The X-ray structure of the complex between AChE and *m*-(*N*,*N*,*N*-trimethylammonio)-2,2,2-trifluoroacetophenone (TMTFA, an inhibition analogue of AChE)[4] revealed that there are interactions between aromatic residues and the quaternary ammonium group of TMTFA.[5]

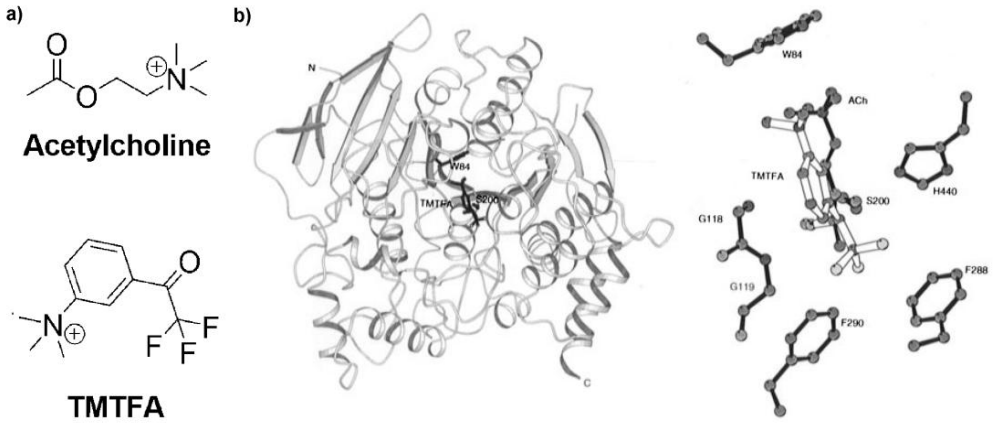

Figure 1.1: a) Structures of acetylcholine and *m*-(*N*,*N*,*N*-trimethylammonio)-2,2,2-trifluoroacetophenone (TMTFA); b) overall conformation (left) and close-up of the active site of the TMTFA-TcAChE (*Torpedo californica* acetylcholineasterase) complex.[5]

Membrane-bound proteins are also capable of recognizing small molecules while incorporating themselves within cellular membranes. P-glycoprotein is a large membrane-bound protein that recognizes and exports small molecules, such as positively charged cytotoxic molecules, across the cellular membranes. This protein is involved in the multidrug resistance of cancer cells to anticancer drugs,[6] and is thus a significant target for pharmaceutical therapeutics. In transmembrane domains, there are not many negatively charged residues, whereas a large portion of the internal channel is occupied by aromatic or polar amino acids like tyrosine (Tyr) or Phe.[7] Therefore, cationic compounds are able to bind to the transmembrane domain through cation-π interactions. When Tyr949 or Phe953 were mutated to alanine residues, the resistance to some drugs was reduced.[8] This supports that cation-π interactions are involved in the binding of positively charged compounds within the binding pocket of P-glycoprotein.

1.2 Molecular Recognition of Water-Soluble Synthetic Receptors

It is very difficult to mimic biological molecular recognition by synthetic receptors because there are not only host-guest interactions to be considered: interactions between the host, guest, solvent, and other components also contribute. When designing synthetic receptors, numerous factors must be considered: the host should have a hydrophobic pocket, good water-solubility, as well as being rigid in aqueous solution to facilitate guest binding. In addition, the hosts should bind substrates selectively with strong affinities while simultaneously overcoming many competing interactions. Several synthetic receptors capable of molecular recognition in aqueous solutions are introduced below.

One of the well-known synthetic receptors capable of host-guest interaction is cyclodextrin. It is composed of a number of α-D-glucopyranosides and these are linked by α-1,4-glycosidic bonds to form a ring structure. This is a truncated, cone-shaped macrocyclic molecule with good water solubility and has a hydrophobic interior cavity and a hydrophilic exterior surface. Based on the number of α-D-glucopyranoside units present - six, seven, or eight - it is named as α-cyclodextrin, β-cyclodextrin (**1.1**, Figure 1.2), and γ-cyclodextrin, respectively. Cyclodextrins are known to bind small hydrophobic substrates in aqueous solutions, but show poor selectivity as well as poor molecular recognition properties. However, they increase the water-solubility of lipophilic drugs drastically upon complexation with the drugs. For that reason, there have been numerous studies to apply cyclodextrins as agents for drug solubilization and delivery.[9,10] Huskens and co-workers employed β-cyclodextrin **1.1** as a host for the

immobilization of modified proteins.[11] Streptavidins labeled with adamantane-tagged biotin were immobilized by *β*-cyclodextrin (**1.1**) molecular printboards while nonspecific protein adsorption was inhibited.

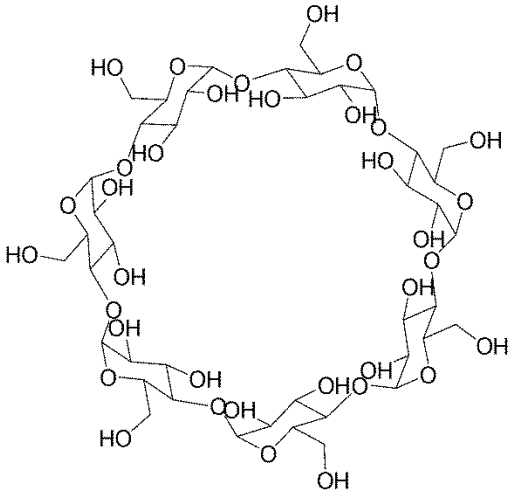

1.1

Figure 1.2: Structure of *β*-cyclodextrin **1.1**.

One group of artificial receptors that are capable of molecular recognition in aqueous solutions are the cyclophanes. Cyclophanes are molecules composed of bridged aromatic rings that form a hydrophobic cavity. Their water solubility can be increased by the employment of heterocyclic aromatic compounds or decoration of the linkers with water-solubilizing groups. Diederich synthesized cyclophane **1.2** (Figure 1.3a) that can extract extremely insoluble polycyclic aromatic hydrocarbons into aqueous solutions.[12] By the formation of 1:1 complexes with cyclophane **1.2** and the hydrocarbons via van der Waals and hydrophobic interactions, their water-solubility increased drastically. Later,

different types of cyclophanes, aromatic sulfur-linked macrocycles (**1.3a**, **1.3b**, Figure 1.3b), were synthesized to mimic protein or enzyme binding pockets.[13,14] These small molecule receptors demonstrate good binding affinities for ammonium ions via cation-π interactions, and the presence of carboxylate groups on the bridge increase their water solubility. Waters and co-workers reported that small molecule receptor **1.3a** mimics the HP1 chromodomain, which binds trimethyllysine residues on post-translationally modified histone 3. This receptor showed compatible affinities to native HP1 chromodomain. Impressively, its selectivity was better than native HP1 chromodomain: **1.3a** only binds to trimethyllysine groups while native HP1 chromodomain binds to other residues as well. Later, they increased the cavity size of the receptor by replacing phenyl derivative with naphthalene derivative, resulting in the receptor **1.3b**. This receptor still showed binding affinities for trimethyllysine groups, however, it showed stronger binding affinities for asymmetric dimethyl arginine($aRMe_2$) residues (Figure 1.3c).

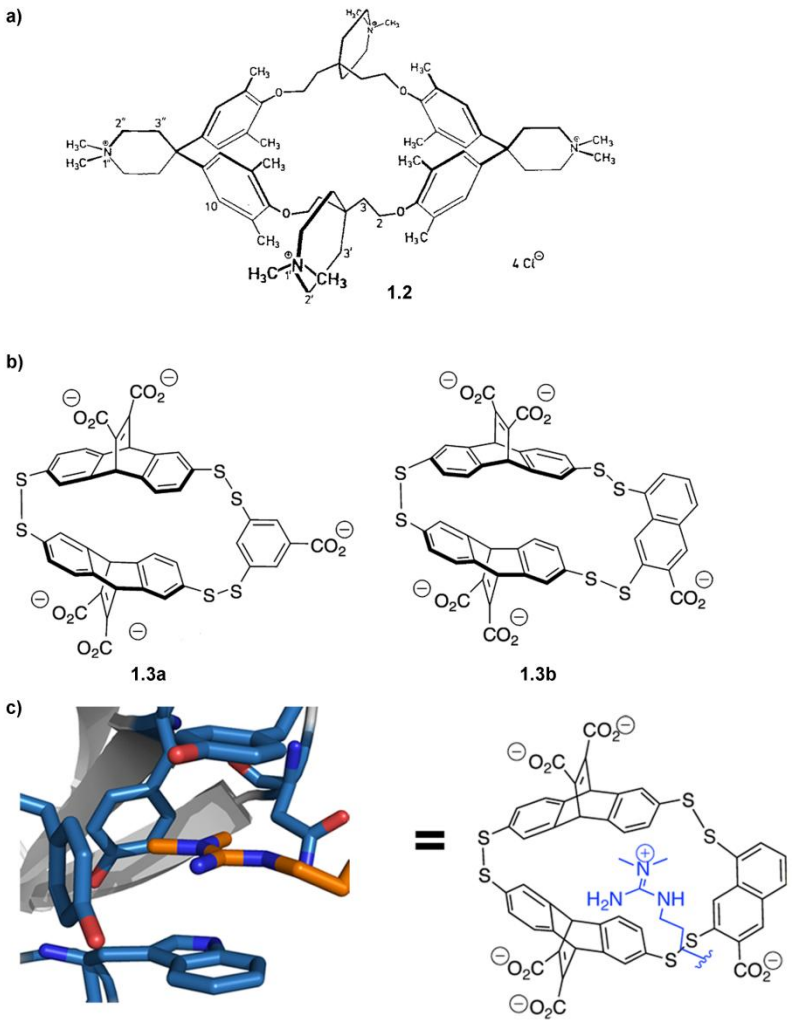

Figure 1.3: Structures of cyclophanes: a) **1.2**;[12] b) **1.3a** and **1.3b**;[14] c) molecular model of the SMN Tudor domain bound to $aRMe_2$ (left) and structure of **1.3b** bound to $aRMe_2$ (right).[14]

Raymond and co-workers reported that their self-assembled supramolecular host **1.4** can bind alkylammonium ions in water (Figure 1.4a).[15] This metal-ligand complex is a $[Ga_4L_6]^{12-}$ species with 1,5-bis(2',3'-dihydroxybenzamido)naphthalene functioning as the coordinating ligands. This host is water soluble and possesses a hydrophobic interior cavity whose size is approximately 250~430 Å based on the bound guests. Later, they

employed this cage as a supramolecular catalyst and were able to perform a unimolecular pericyclic rearrangement (Figure 1.4b).[16] Enammonium cations bind within the cavity of the cage in reactive conformations, and subsequently the cationic 3-aza Cope rearrangement occurs within the host. The product is then released from the cavity.

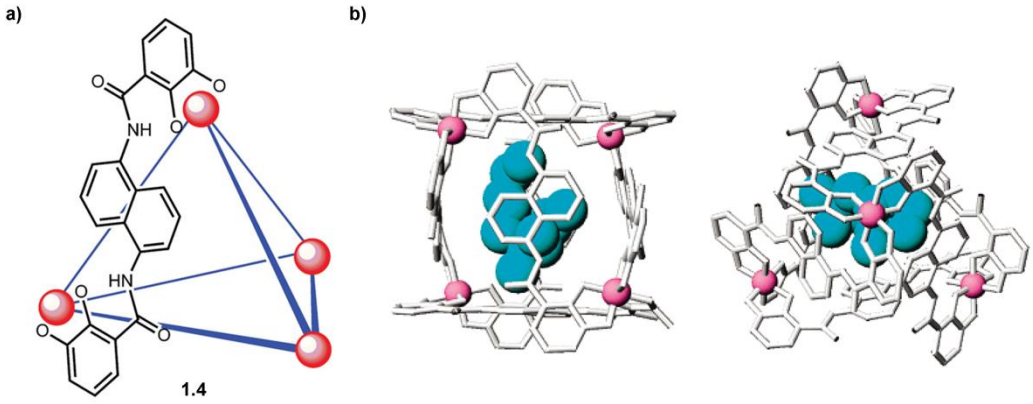

Figure 1.4: a) Structure of metal-ligand coordination complexes **1.4**;[15] b) molecular model of **1.4**, encapsulating an enammonium substrate.[16]

A calix[n]arene is an aromatic macrocyclic synthetic receptor composed of n number of phenolic units bridged by methylene groups which creates aromatic cavities for guest recognition. Calix[n]arenes have upper and lower rims that can be functionalized in order to control the binding properties and overall water solubility. Among many types of calixarenes, sulfonated calixarenes, containing sulfonate and carboxylate groups at the upper and lower rims respectively, are known to have good binding affinities for ammonium ions. Crowley and co-workers showed that *p*-sulfonatocalix[4]arene **1.5** (Figure 1.5a) is capable of recognizing lysine residues on cytochrome *c*.[17] The alkyl portion of the lysine group binds within the aromatic cavity

through Van der Waals interactions and the ammonium group of lysine has electrostatic interactions with the negatively-charged sulfonato groups. The binding of *p*-sulfonatocalix[4]arene **1.5** to lysine groups camouflaged cytochrome *c*, modifying the properties of its protein-protein interactions. In addition, Hof and co-workers reported that *p*-sulfonatocalix[4]arene **1.5** shows better binding affinity for trimethyllysine residues than unmethylated lysine groups.[18] These methylated lysine groups, resultants of post-translational modification of lysine residues, are mostly found in unstructured protein tails where reader protein binds. Thus, *p*-sulfonatocalix[4]arene **1.5** was applied as a histone-binding agent which disrupts protein-protein interactions (Figure 1.5b).[19]

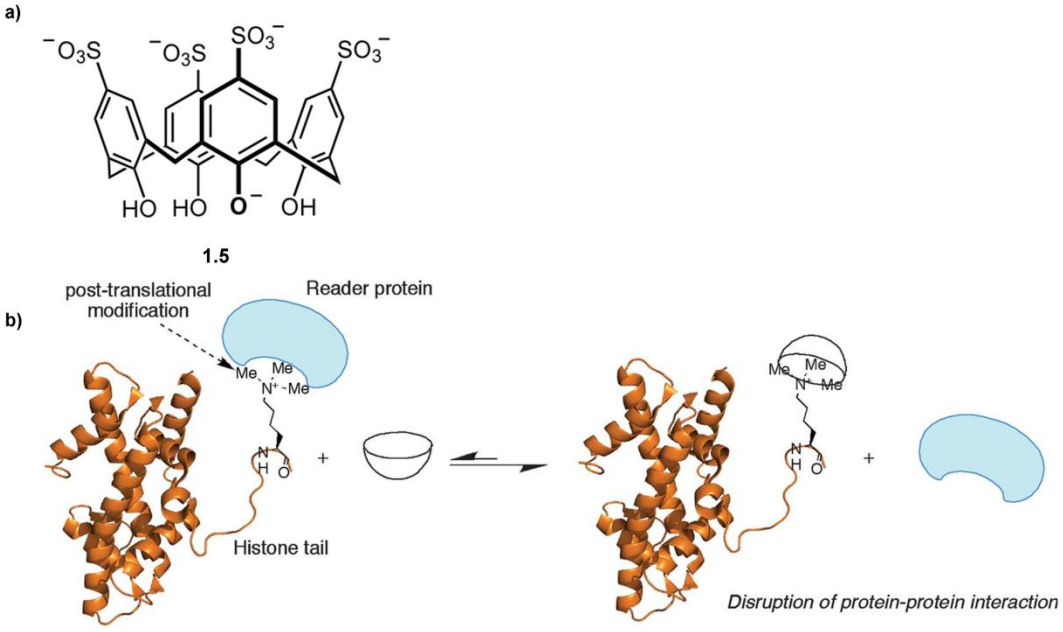

Figure 1.5: a) Structure of calix[4]arene **1.5**;[17] b) representation of a binding of reader protein to a trimethylated lysine residue on unstructured protein tail (left), and disruption of protein-protein interaction by **1.5**.[19]

Cucurbit[n]uril is another macrocyclic synthetic receptor that possesses a hydrophobic cavity and polar carbonyl groups surrounding each end of the cavity. They show good selectivity for binding organic cations in aqueous solutions. Inoue and co-workers reported that small peptides containing an N-terminal aromatic group are good guests for cucurbit[7]uril **1.6** (Figure 1.6a).[20] Later, Urbach and co-workers reported that cucurbit[7]uril **1.6** is capable of site-specific protein recognition (Figure 1.6b).[21] Cucurbit[7]uril **1.6** showed 1:1 binding for human insulin B-chain that possesses an N-terminal phenylalanine residue with a binding affinity of 10^6 M^{-1}. When the substrate is bound to cucurbit[7]uril **1.6**, the hydrophobic phenylalanine residue is placed within the cavity via hydrophobic interactions while the N-terminal ammonium group is stabilized by interactions with the carbonyl groups at the rim.

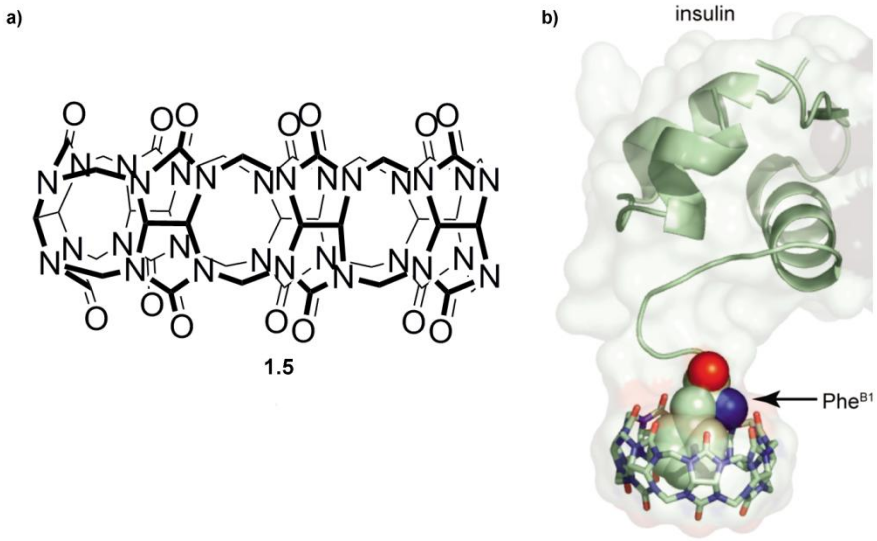

Figure 1.6: a) Structure of cucurbit[7]uril **1.6**; b) crystal structure of the human insulin B·**1.6** complex.[21]

Molecular tweezers functionalized with phosphate groups (**1.7**, Figure 1.7a) are another synthetic receptor that is capable of binding to lysine residues.[22] It has alternately connected norbornadiene and phenyl rings, and two phosphate groups are appended to the central hydroquinone ring. Lysine residues are effectively bound by **1.7**: the long side chain is capable of threading through the cavity, and the ammonium group has electrostatic attraction with one phosphate group. Sanchez-Garcia, Schrader, and Ottmann reported that **1.7** is capable of binding to a surface-exposed lysine group on 14-3-3 protein where partner proteins normally bind (Figure 1.7b).[23] This indicates that **1.7** can be applied to disrupt protein-protein interaction of 14-3-3 protein.

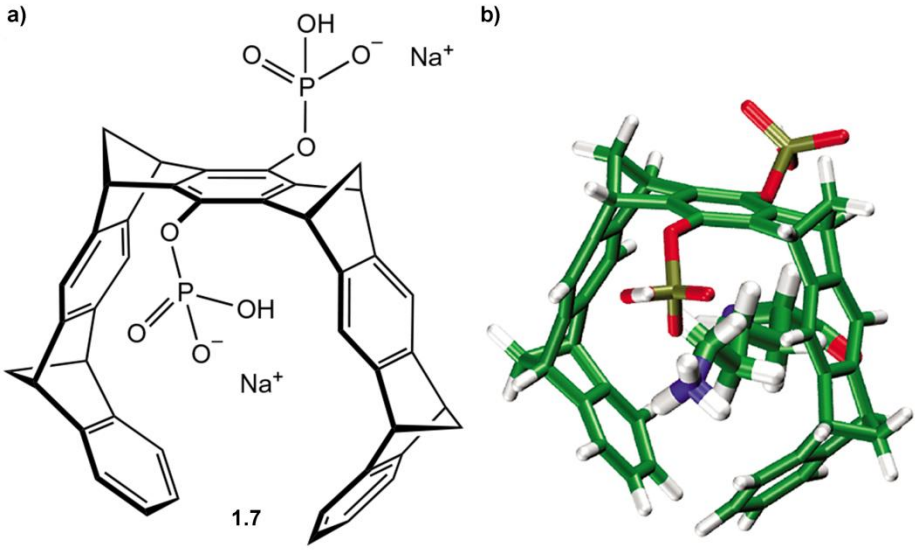

Figure 1.7: a) Structure of a molecular tweezer **1.7**;[23] b) molecular model of the lysine·**1.7** complex.[23]

These various kinds of water-soluble synthetic receptors show good molecular recognition properties in aqueous solution. However, these artificial receptors have

problems that need to be solved in order to further study the molecular recognition of membrane-bound proteins or enzymes. They are usually synthetically challenging to access, and often their scope of guest binding is poor. Moreover, most are not compatible with membrane environments. In order to apply synthetic receptors in complex membrane systems, these should be capable of functioning within the hydrophobic core of membranes while retaining their recognition properties in aqueous solution. The exterior portion of artificial receptors are usually decorated with polar or charged groups to increase their water solubility, but these groups make the hosts incapable of incorporating within lipid bilayers. Proteins or enzymes usually possess hydrophobic binding pockets for the recognition of the small organic substrates. However, this hydrophobic interaction is incompatible in membrane systems because any hydrophobic molecules can preferentially bind within the lipid bilayer.

1.3 Water-Soluble Deep Cavitands and their Binding Properties

Another synthetic receptor that mimics the binding pockets of proteins or enzymes is a cavitand. Resorcin[*n*]arene based cavitands possess concave aromatic cavities and are capable of binding guests in water. Resorcin[4]arene **1.8** is easily synthesized by the condensation of resorcinol with a variety of alkyl aldehydes (Figure 1.8).[24,25] Based on the aldehydes used, the "feet" of the resorcin[4]arene **1.8** can be varied. When excess NaOH is added to resorcin[4]arene **1.8**, only one hydroxyl group on each resorcinol unit is deprotonated.[26] This produces a tetraanionic resorcin[4]arene **1.9** that is capable of forming four strong intramolecular hydrogen bonds and delocalizing the

negative charges. Subsequently, a stable shallow bowl-like structure (C_{4v}) is formed. Since the host has a negatively charged rim, it can bind small tetraalkylammonium salts such as the tetramethylammonium ion or choline by electrostatic interactions with micromolar binding constants in water.

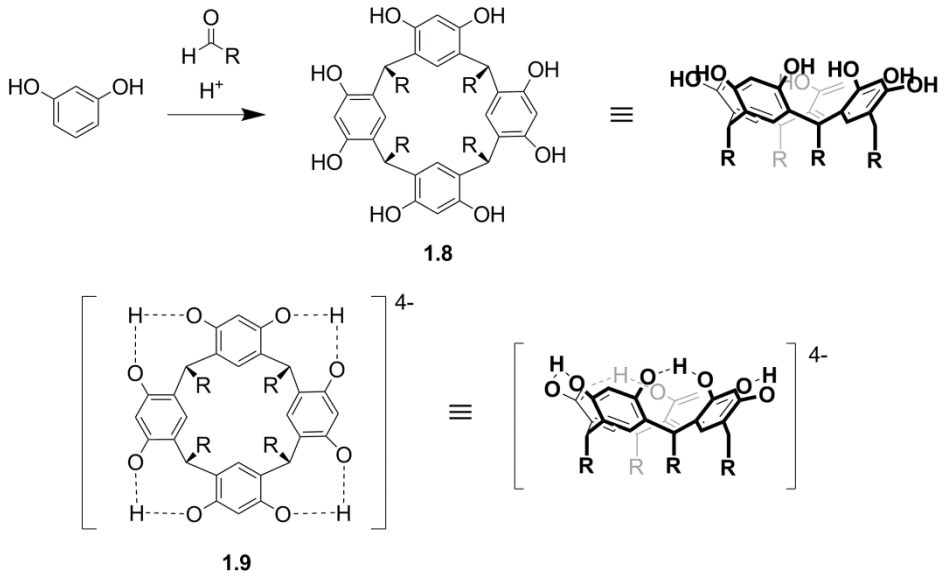

Figure 1.8: Synthesis of resorcin[4]arenes **1.8** and the formation of tetraanionic resorcin[4]arene **1.9**.

In order to build deeper and larger cavities, resorcin[4]arene **1.8** is treated with 4 equiv of 1,2-difluoro-4,5-dinitrobenzene in the presence of triethylamine to produce octanitro cavitand **1.10**.[27-29] Reduction of the octanitro cavitand **1.10** with tin chloride in the presence of hydrochloric acid leads to the formation of octaamine cavitand **1.11** (Figure 1.6), followed by the reaction with propionyl chloride produces octaamide cavitand **1.12** (Figure 1.9).[27,28] These cavitands possess four individual ammonium groups at the feet to increase water-solubility. When octaamide cavitand **1.12** is dissolved

in water in the absence of suitable guests, it does not form the vase-like formation, but instead exists in the C_{2v} kite-like conformation. Subsequently, it forms a D_{2d} dimer referred as a velcrand. This dimer is energetically preferred in order to minimize the exposure of the aromatic interior to water. Upon the addition of appropriate guests, however, it undergoes conformational changes from velcrand to the C_{4v} vase-like structure via intramolecular hydrogen bonding (C=O···H-N), and forms a 1:1 complex with the guests filling the hydrophobic cavity. The formation of the C_{4v} vase-like conformation can be easily confirmed by the ^{1}H NMR chemical shift of the methine CH proton, located at the bridging carbon of the aromatic groups at the resorcin[4]arene-based structure. When a cavitand is in a vase-like conformation, the methine CH proton resonates with the aromatic rings and its peak is observed around 5.5 ppm whereas the peak shows up below 5 ppm if a cavitand is in the kite-like conformation.

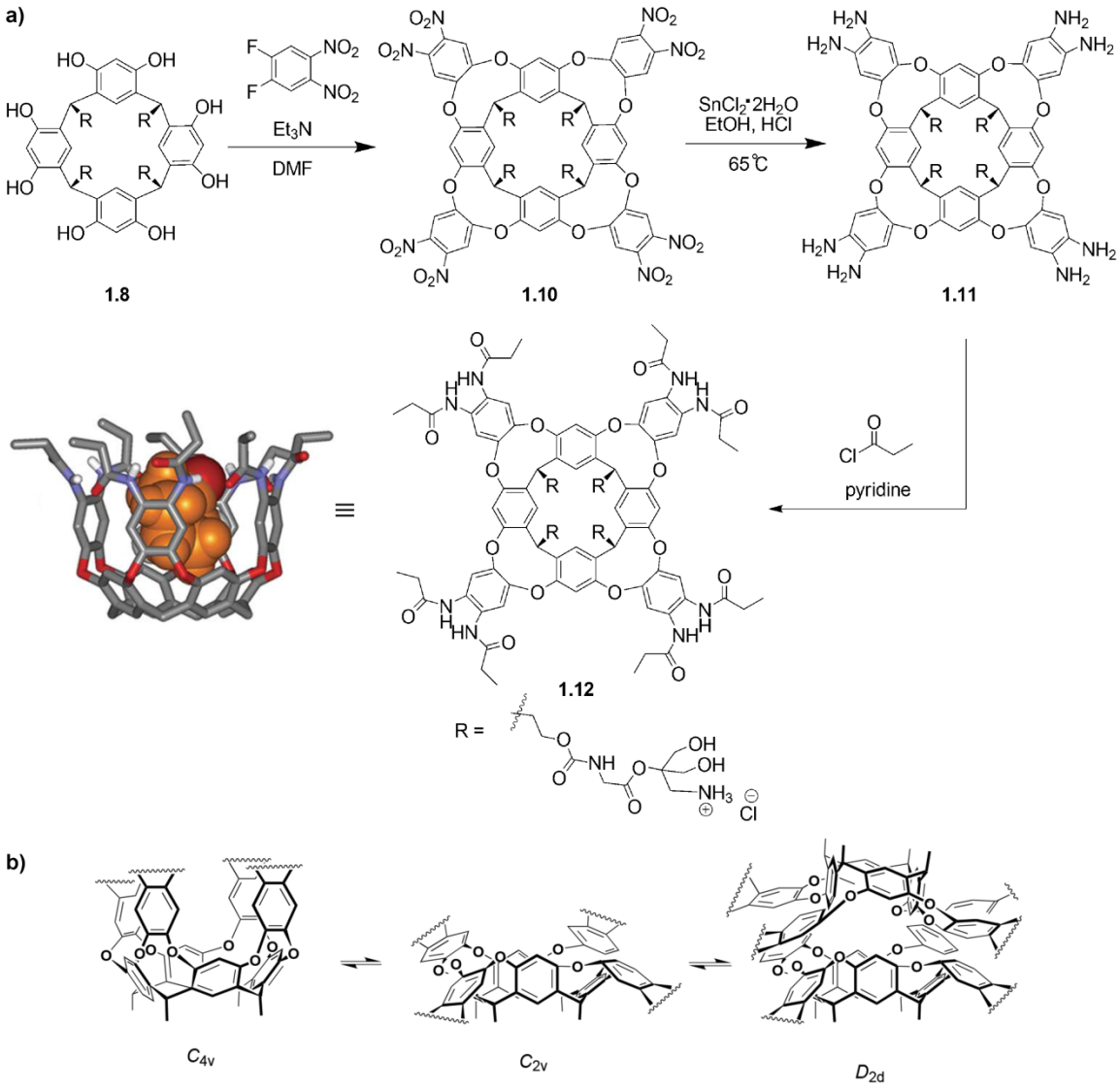

Figure 1.9: a) Synthesis of octaamide cavitand **1.12** and its molecular model;[30] b) proposed schematic representation of $C_{4v} \rightleftharpoons C_{2v} \rightleftharpoons D_{2d}$ conformation equilibrium for octaamide cavitand **1.12**.[28]

Another deep, water-soluble cavitand is synthesized by decorating the structure with water soluble units at the rim of cavitand. Condensation of the octaamine cavitand **1.11** with ethyl 3-ethoxy-3-iminopropionate produces the tetraester cavitand **1.13**, and subsequent saponification results in the tetracarboxylate cavitand **1.14** (Figure 1.10).[31,32] This cavitand **1.14** is in the C_{4v} vase-like formation in water even in the absence of proper

guests. Unlike the octaamide cavitand **1.12**, tetracarboxylate cavitand **1.14** forms intermolecular hydrogen bonding: the nitrogen atoms on the benzimidazole rings and four water molecules from the solvent have hydrogen bonds that hold the walls together. Interestingly, one tetrahydrofuran (THF) molecule from the saponification step remains bound within the cavity of the cavitand **1.14**, and this cannot be unencapsulated without the addition of guests of suitable size and shape.

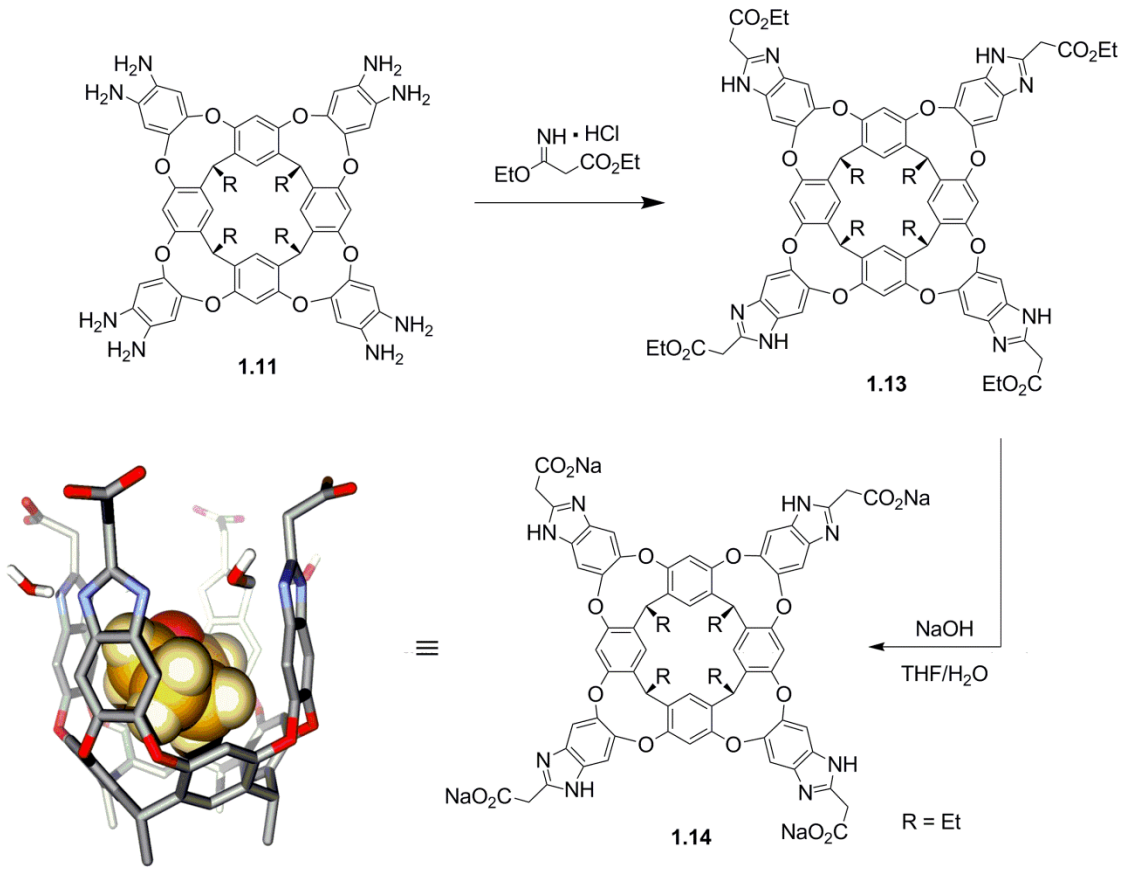

Figure 1.10: Synthesis of tetracarboxylate cavitand **1.14** and its molecular model cavitand **1.14** binding one THF molecule.

Tetracarboxylate cavitand **1.14** is capable of extracting water-insoluble molecules into water via hydrophobic stabilization. It was observed that *n*-alkanes are extracted into water and rapidly bind to the tetracarboxylate cavitand **1.14** via hydrophobic interactions.[33,34] These guests are coiled in a helical conformation and tumble rapidly within the cavity of the cavitand **1.14** on the NMR timescale. The selectivity of small guests, such as a cyclopentane, can be controlled by the attachment of rotating walls, such as a benzoate group, to the open end of the cavitand **1.14**.[35] The presence of the rotating "doors" at the cavity rim increases the selectivity for and reduces the exchange rate of small guests. However, haloalkanes and alkane thiols bind to cavitand **1.14** in a manner that is different from hydrocarbons.[36] Significant amounts of halides and thiols are present within the cavity due to the interaction between halide dipoles and the polarized aromatic surface of the cavity.

The cavitand **1.14** also shows good binding affinities for trimethylammonium salts ($R\text{-}NMe_3^+$), such as choline or acetylcholine, via cation-π interactions with binding constants $>10^4$ M^{-1}.[31-33] Interestingly, when both a long alkyl chain and a trimethylammonium group are present in one guest, the alkyl chain will preferentially bind inside the cavity over the trimethylammonium group.[32] This is due to the large hydrophobic driving force between hydrophobic chain and the aromatic interior of the cavity. The favorable electrostatic interactions between the positively charged trimethylammonium group of the guest and the negatively charged carboxylate groups at the rim of cavitand **1.14** are also involved with this process.

Interestingly, cavitand **1.14** is capable of promoting phase-transfer reactions.[37] A water-insoluble maleimide labeled with a hydrophobic binding handle is extracted into aqueous solution by the 1:1 complex formation with cavitand **1.14**, and it can react with thiols and sulfate groups. Once the bound-guest obtains water-soluble functionalities, the anionic product is released to the aqueous solution and another maleimide guest binds to cavitand **1.14**. This indicates that cavitand **1.14** catalyzes the phase-transfer process.

1.4 Molecular Recognition of Water-Soluble Deep Cavitands in Biomimetic Systems

As explained previously, deep water-soluble cavitand **1.14** possesses an aromatic body and negatively charged groups at the rim and selectively recognizes small molecules based on their size, shape, and charge.[32] It also recognizes surfactants containing long alkyl chains such as sodium dodecyl sulfate (SDS).[33,38] The alkyl chain of SDS coiled inside the hydrophobic cavity maximizes CH-π interactions with the aromatic surface of the interior, and the hydrophilic head group is positioned in the water layer. Interestingly, when the concentration of SDS is above the critical micelle concentration (cmc), the role of host and guest are reversed and cavitand **1.14** is incorporated within micelles of the surfactant: the hydrophobic body becomes buried in the core of a micelle layer and the hydrophilic rim is located on the surface with the cavity directed outwards towards the aqueous environment (Figure 1.11).[39] Cavitand **1.14** is also embedded into the dodecylphosphocholine (DPC) micelles when the concentration is above the cmc.[40] The micelle-bound cavitand **1.14** maintains its open cavity, allowing

for the recognition of guests with suitable size and shape such as cyclohexane and adamantane.

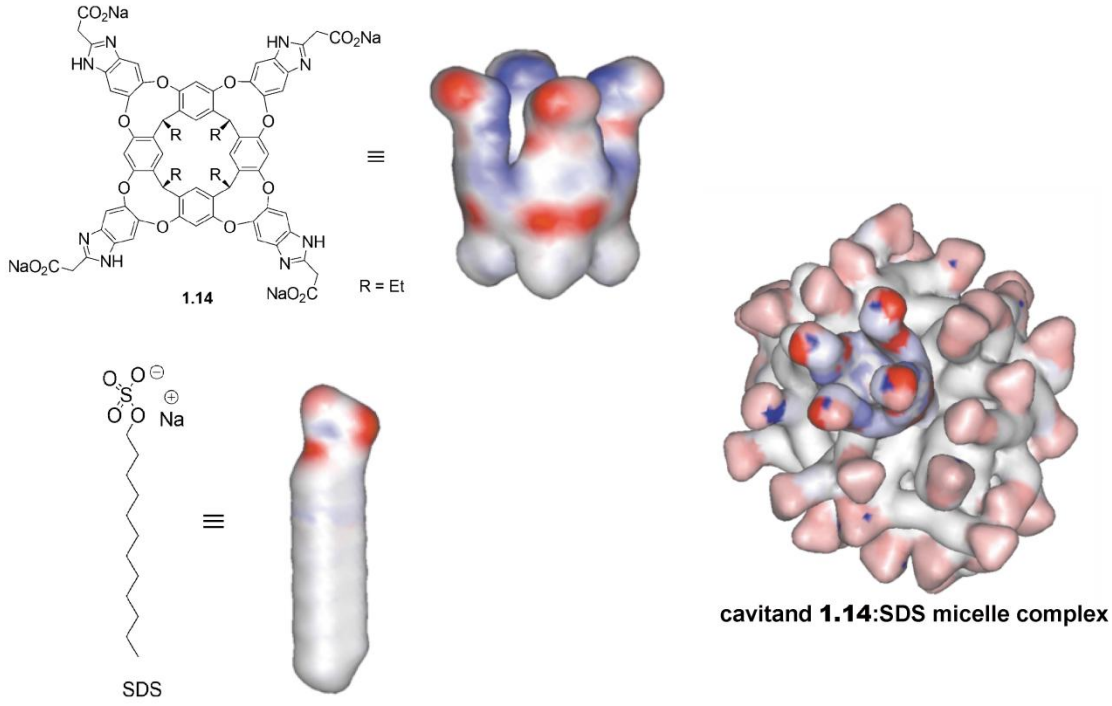

Figure 1.11: Structure and electrostatic surface representation of cavitand **1.14**, SDS, and a mixed micelle composed of SDS and cavitand **1.14**.[39]

Hooley and co-workers reported that the binding and immobilization of trimethylammonium-labeled guests to cavitand **1.14** attached to a clean gold surface was successfully monitored by surface Plasmon resonance (SPR) in real time.[41] Furthermore, by SPR method, they have shown that cavitand **1.14** can be self-incorporated into a supported lipid bilayer (SLB).[42] SPR is an optical, label-free technique that monitors chemical or biological non-covalent molecular interactions in real time (Figure 1.12).[43,44] The "Kretschmann" configuration is commonly employed for SPR instrument design as shown in Figure 1.9. When incident light strikes an electrically conducting gold layer that

is located at the interface of a glass substrate with a high refractive index and a liquid medium with low refractive index, the reflection of light occurs. When light is reflected, some electrical field intensity is leaked from the light beam into the liquid medium. This leaked electrical field is called the evanescent field. At a given angle, the electrons within the gold layer are excited by the evanescent wave and this subsequently produces surface plasmons. As a result, the intensity of the reflected light is reduced. The angle based on the intensity of reflected light is recorded as an SPR signal. A change in the refractive index of medium at the interface results in a change in SPR signal. This surface-sensitive technique is powerful for *in situ* investigation of molecular interactions.

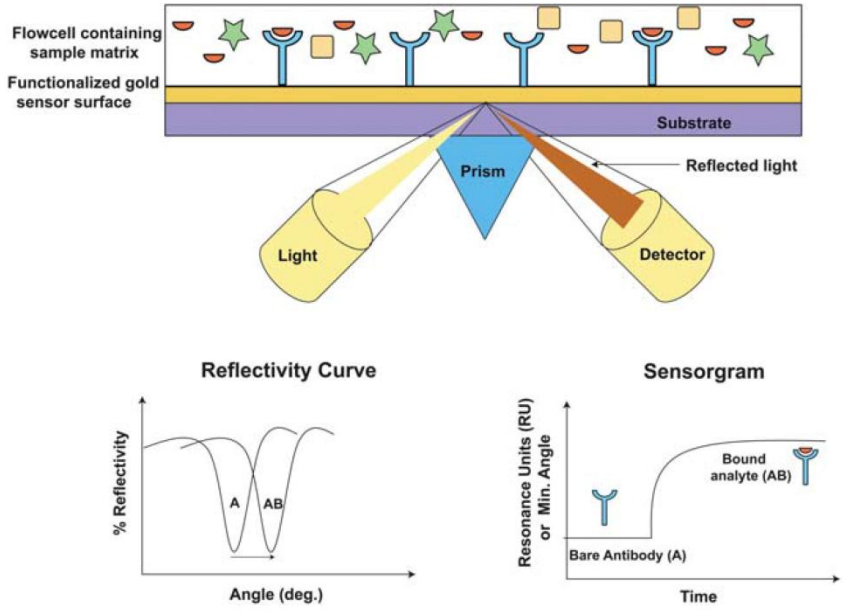

Figure 1.12: Sample biosensing interface for SPR with corresponding reflectivity curve and sensorgram.[44]

In order to investigate cavitand **1.14** incorporation into SLB and its binding properties, a calcinated nanoglassified gold substrate was installed in a SPR flowcell apparatus and the SLB was formed on the surface of the gold substrate by injecting 1-palmitoyl-2-oleoyl-*sn*-glycero-3-phosphocholine (POPC) vesicles in 20 mM PBS buffer.[42,45] When the POPC vesicles interact with a nanoglassified surface, the vesicles spontaneously adsorb onto the surface, rupture, and consequently form a SLB.[46] The cavitand **1.14** can then be embedded into the SLB by injection of a 10 % DMSO aqueous solution containing the cavitand.[42] When bound within the micelle, cavitand **1.14** is located in the upper leaflet of the SLB and the negatively charged rim is oriented toward the external surface, all the while retaining the open cavity (Figure 1.14). The disruption of the SLB is minimal during the cavitand **1.14** incorporation process, and no loss of viability is observed within the SLB. The membrane-bound cavitand **1.14** shows selectivity for a wide variety of small molecules containing a trimethylammonium group ($R\text{-}NMe_3^+$) with binding constants in the 10^2 M^{-1} range. When $R\text{-}NMe_3^+$ substituted species are bound within membrane-incorporated cavitand **1.14**, the $R\text{-}NMe_3^+$ group fills the cavity and the rest of the species is immobilized above the membrane, at the bilayer:water interface.

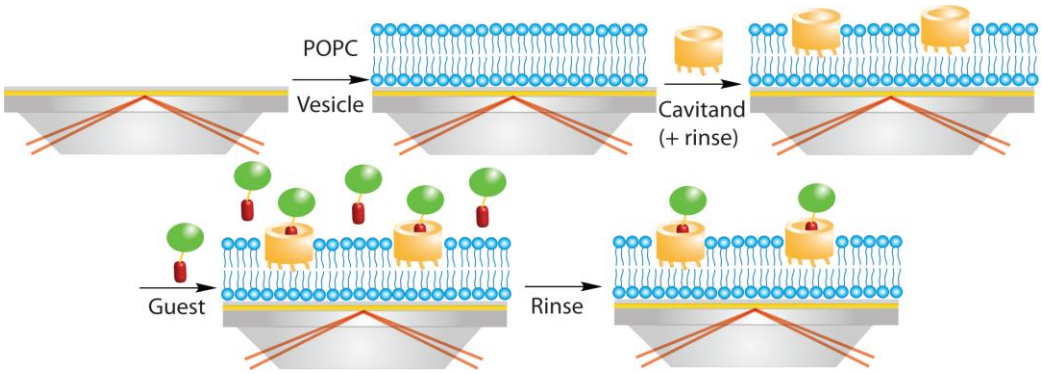

Figure 1.13: Representation of the formation of lipid bilayers on a glass substrate, the incorporation of cavitand# within the bilayers, and the guest binding to cavitand **1.14** embedded in a POPC bilayer membrane.

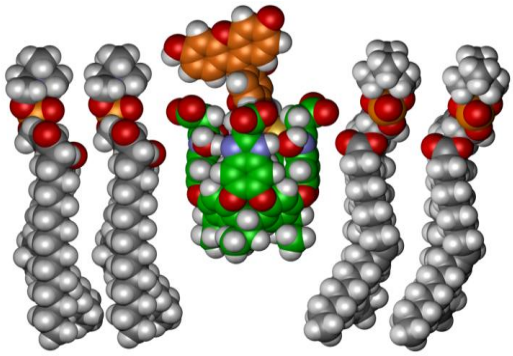

Figure 1.14: Representation of the cavitand **1.14**:guest complex in a POPC lipid membrane.

Interestingly, using the previous method, it was possible to perform chemical reactions at the SLB interface.[47] The reactive initiator for atom-transfer radical polymerization (ATRP) was derivatized to contain the R-NMe_3^+ binding handle (**1.15**) in one step. When it was bound to cavitand **1.14** that had been incorporated within the SLB, the active site of the derivatized initiator is displayed at the SLB interface. The exposure of methylmethacrylate (MMA) or 2-hydroxyethyl methacrylate (HEMA), caused hydrophobic or hydrophilic polymers to grow atop the SLB under mild conditions. The

hydrophilic poly(HEMA) was easily removed by washing with PBS buffer, while no loss of poly(MMA) was observed. Interestingly, not all of the cavitand bound initiator molecules were reacted with HEMA during the polymerization. As a result, the reacted initiators were removed along with poly(HEMA) from the membrane-bound cavitand **1.14** upon washing. However, the unreacted initiator molecules remained bound to the cavitand **1.14**:SLB system. When HEMA was injected a second time after washing, the growth of poly(HEMA) was observed again.

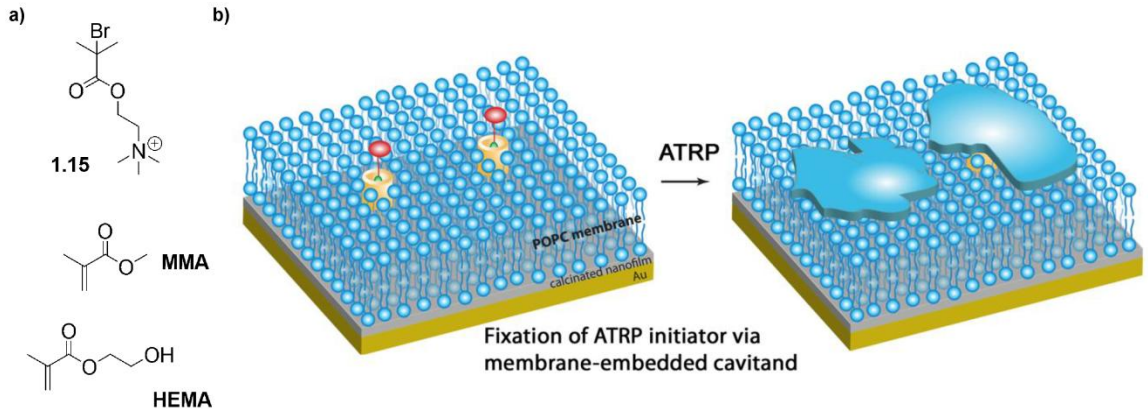

Figure 1.15: a) Structure of R-NMe_3^+ labeled initiator molecule **1.15**, MMA, and HEMA; b) representation of polymer growth atop a SLB.

Deep water-soluble cavitand **1.14** is a good synthetic receptor that mimics molecular recognition properties of membrane-bound proteins or enzymes. It is not synthetically challenging and it shows good selectivity with strong binding affinities to suitable guests. Furthermore, water-soluble cavitand **1.14** is capable of self-incorporating into SLB while maintaining its guest binding properties. The molecular recognition

properties of the cavitand **1.14** in biomimetic and cellular environments will be investigated in this dissertation.

1.5 References

1. Rosenberry, T. L. “Acetylcholinesterase.” *Adv. Enzymol. Relat. Areas Mol. Biol.*, **1975**, *43*, 103-218.

2. Sussman, J. L.; Harel, M.; Frolow, F.; Oefner, C.; Goldman, A.; Toker, L.; Silman, I. “Atomic Structure of Acetylcholinesterase from Torpedo California: a Prototypic Acetylcholine-Binding Protein.” *Science*, **1991**, *253*, 872-879.

3. Harel, M.; Schalk, I.; Ehret-Sabatier, L.; Bouet, F.; Goeldner, M.; Hirth, C.; Axelsen, P. H.; Silman, I.; Sussman, J. L. “Quaternary Ligand Binding to Aromatic Residues in the Active-Site Gorge of Acetylcholinesterase.” *Proc. Natl. Acad. Sci. U. S. A.*, **1993**, *90*, 9031-9035.

4. Brodback, U.; Schweikert, K.; Gentinetta, R.; Rottenberg, M.; “Fluorinated Aldehydes and Ketones Acting as Quasi-Substrate Inhibitors of Acetylcholinesterase.” *Biochim. Biophys. Acta – Enzymol.*, **1979**, *567*, 357-369.

5. Harel, M.; Quinn, D. M.; Nair, H. K.; Silman, I.; Sussman, J. L. “The X-Ray Structure of a Transition State Analog Complex Reveals the Molecular Origins of the Catalytic Power and Substrate Specificity of Acetylcholinesterase.” *J. Am. Chem. Soc.*, **1996**, *118*, 2340-2346.

6. Putman, M.; van Veen, H. W.; Konings, W. N. “Molecular Properties of Bacterial Multidrug Transporters.” *Microbiol. Mol. Biol. Rev.*, **2000**, *64*, 672-693.

7. van Veen, H. W.; Higgins, C. F.; Konings, W. N. “Molecular Basis of Multidrug Transport by ATP-Binding Cassette Transporters: A Proposed Two-Cylinder Engine Model.” *J. Mol. Microbiol. Biotechnol.*, **2001**, *3*, 185-192.

8. Hanna, M.; Brault, M.l Kwan, T.; Kast, C.; Gros, P. “Mutagenesis of Transmembrane Domain 11 of P-Glycoprotein by Alanine Scanning.” *Biochemistry*, **1996**, *35*, 3625-3635.

9. Szente, L.; Szejtli, J. “Highly Soluble Cyclodextrin Derivatives: Chemistry, Properties, and Trends in Development.” *Adv. Drug Deliv. Rev.*, **1999**, *36*, 17-28.

10. Rajewski, R. A.; Stella, V. J. "Pharmaceutical Applications of Cyclodextrins. 2. *In Vivo* Drug Delivery." *J. Pharm. Sci.*, **1996**, *85*, 1142-1169.

11. Ludden, M. W.; Mulder, A.; Tampé, R.; Reinhoudt, D. N.; Huskens, J. "Molecular Printboards as a General Platform for Protein Immobilization: A Supramolecular Solution to Nonspecific Adsorption." Angew. *Chem. Int. Ed.*, **2007**, *46*, 4104-4107.

12. Diederich, F. "Complexation of Neutral Molecules by Cyclophane Hosts." *Angew Chem. Int. Ed. Engl.*, **1988**, *27*, 362-386.

13. Ingerman, L. A.; Cuellar, M. E.; Waters, M. L. "A Small Molecule Receptor That Selectively Recognizes Trimethyl Lysine in a Histone Peptide with Native Protein-Like Affinity." *Chem. Comm.*, **2010**, *46*, 1839-1841.

14. James, L. I.; Beaver, J. E.; Rice, N. W.; Waters, M. L. "A Synthetic Receptor for Asymmetric Dimethyl Arginine." *J. Am. Chem. Soc.*. **2013**, *135*, 6450-6455.

15. Caulder, D. L.; Powers, R. E.; Parac, T. N.; Raymond, K. N. "The Self-Assembly of a Predesigned Tetrahedral M_4L_6 Supramolecular Cluster." *Angew. Chem. Int. Ed.*, **1998**, *37*, 1840-1843.

16. Fiedler, D.; van Halbeek, H.; Bergman, R. G.; Raymond, K. N. "Supramolecular Catalysis of Unimolecular Rearangements: Substrate Scope and Mechanistic Insignts." J. *Am. Chem. Soc.*, **2006**, *128*, 10240-10252.

17. McGovern, R. E.; Fernandes, H.; Khan, A. R.; Power, N. P.; Crowly, P. B. "Protein Camouflage in Cytochrome *c*-Calixarene Complexes." *Nature Chem.*, **2012**, *4*, 527-533.

18. Beshara, C. S.; Jones, C. E.; Daze, K. D.; Lilgert, B. J.; Hof, F. "A Aimple Calizarene Recognizes Post-Translationally Methylated Lysine." *Chem. Bio. Chem.*, **2010**, *11*, 63-66.

19. Daze, K. D.; Pinter, T.; Beshara, C. S.; Ibraheem, A.; Minaker, S. A.; Ma, M. C. F.; Courtemanche, R. J. M.; Campbell, R. E.; Hof, F. "Supramolecular Hosts That Recognize Methyllysines and Disrupt the Interaction Between a Modified Histone Tail and its Epigenetic Reader Protein." *Chem. Sci.*, **2012**, *3*, 2695-2699.

20. Rekharsky, M. V.; Yamamura, H.; Ko, Y. H.; Selvapalam, N.; Kim. K.; Inoue, Y. "Sequence Recognition and Self-Sorting of a Dipeptide by Cucurbil[6]uil and Cucurbit[7]uril." *Chem. Comm.,* **2008**, 2236-2238.

21. Chinai, J. M.; Taylor, A. B.; Ryno, L. M.; Hargreaves, N. D.; Morris, C. A.; Hart, P. J.; Urbach, A. R. "Molecular Recognition of Insulin by a Synthetic Receptor." *J. Am. Chem. Soc.*, **2011**, *113*, 8810-8813.

22. Talbiersky, P.; Bastkpwski, E.; Klärner, F. –G.; Schrader, T. "Molecular Clip and Tweezer Introduce New Mechanisms of Enzyme Inhibition." *J. Am. Chem. Soc.*, **2008**, *130*, 9824-9828.

23. Bier, D.; Rose, R.; Bravo-Rodriguez, K.; Bartel, M.; Ramirez-Anguita, J. M.; Dutt, S.; Wilch, C.; Klärner, F. –G.; Sanchez-Garcia, E.; Schrader, T.; Ottmann, C. "Molecular Tweezers Modulate 14-3-3 Protein-Protein Interactions." *Nature Chemistry*, **2013**, *5*, 234-239.

24. Niederl, J. B.; Vogel, H. J. "Aldehyde-Resorcinol Condensations." *J. Am. Chem. Soc.*, **1940**, *62*, 2512-2514.

25. Högberg, A G. S. "Two Stereoisomeric Macrocyclic Resorcinol-Acetaldehyde Condensation Products." *J. Org. Chem.* **1980**, *45*, 4498-4500.

26. Schneider, H. –J.; Güttes, D.; Schneider, U. "A Macrobicyclic Polyphenoxide as Receptor Analog for Choline and Related Ammonium Compounds." *Angew. Chem. In. Ed. Engl.*, **1986**, *25*, 647-649.

27. Haino, T.; Rudkevich, M.; Rebek, J., Jr. "Kinetically Stable Caviplexes in Water." *J. Am. Chem. Soc.*, **1999**, *121*, 11253-11254.

28. Haino, T.; Rudkevich, M.;Shivanyuk, A.; Rissanen, K. Rebek, J., Jr. "Induced-Fit Molecular Recognition with Water-Soluble Cavitands." *Chem. Eur. J.*, **2000**, *6*, 3797-3805.

29. Amrhein, P. Shivanyuk, A.; Johnson, D. W.; Rebek, J. Jr. "Metal-Switching and Self-Inclusion of Functional Cavitands." *J. Am. Chem. Soc.*, **2002**, *124*, 10349-10358.

30. Biros, S. M.; Rebek, J., Jr. “Structure and Binding Properties of Water-Soluble Cavitands and Capsules.” *Chem. Soc. Rev.*, **2007**, *36*, 93-104.

31. Hof, F.; Trembleau, L.; Ullrich, E. C.; Rebek, J., Jr. “Acetylcholine Recognition by a Deep, Biomimetic Pocket.” *Angew. Chem. In. Ed.*, **2003**, *42*, 3150-3153.

32. Biros, S. M.; Ullrich, E. C.; Hof, F.; Trembleau, L.; Rebek, J., Jr. “Kinetically Stable Complexes in Water: The Role of Hydration and Hydrophobicity.” *J. Am. Chem. Soc.*, **2004**, *126*, 2870-2876.

33. Hooley, R. J.; Van Anda, H. J.; Rebek, J., Jr. “Extraction of Hydrophobic Species into a Water-Soluble Synthetic Receptor.” *J. Am. Chem. Soc.*, **2007**, *129*, 13464-13473.

34. Hooley, R. J.; Biros, S. M.; Rebek, J., Jr. “Normal Hydrocarbons Tumble Repidly in a Deep, Water-Soluble Cavitand.” *Chem. Comm.*, **2006**, 509-510.

35. Hooley, R. J.; Van Anda, H. J.; Rebek, J., Jr. “Cavitands with Revolving Doors Regulate Binding Selectivities and Rates in Water.” *J. Am. Chem. Soc.*, **2006**, *128*, 3894-3895.

36. Hooley, R. J.; Gavette, J. V.; Mettry, M.; Ajami, D.; Rebek, J., Jr. “Unusual Orientation and Reactivity of Alkyl Halides in Water-Soluble Cavitands.” *Chem. Sci.*, **2014**, *5*, 4382-4387.

37. Hooley, R. J.; Biros, S. M.; Rebek, J., Jr. “A Deep, Water-Soluble Cavitand Acts as a Phase-Transfer Catalyst for Hydrophobic Species.” *Angew. Chem. Int. Ed.*, **2006**, *45*, 3517-3519.

38. Trembleau, L.; Rebek, J., Jr. “Helical Conformation of Alkanes in Hydrophobic Environments.” *Science*, **2003**, *301*, 1219-1220.

39. Trembleau, L.; Rebek, J., Jr. “Interactions between a Surfactant and Cavitand in Water Blur Distinctions between Host and Guest.” *Chem. Comm.*, **2004**, 58-59.

40. Schramm, M. P.; Hooley, R. J.; Rebek, J., Jr. “Guest Recognition with Micelle-Bound Cavitands.” *J. Am. Chem. Soc.*, **2007**, *129*, 9773-9779.

41. Liu, Y.; Taira, T.; Young, M. C.; Ajami, D.; Rebek, J., Jr.; Cheng, Q.; Hooley, R. J. "Protein Recognition by a Self-Assembled Deep Cavitand Monolayer on a Gold Substrate." *J. Am. Chem. Soc.*, **2012**, *28*, 1391-1398.

42. Liu, Y.; Liao, P.; Cheng, Q.; Hooley, R. J. "Protein and Small Molecule Recognition Properties of Deep Cavitands in a Supported Lipid Membrane Determined by Calcination-Enhanced SPR Spectroscopy." *J. Am. Chem. Soc.*, **2010**, *132*, 10383-10390.

43. Bakhtiar, R. "Surface Plasmon Resonance Spectroscopy: A Versatile Technique in a Biochemist's Toolbox." *J. Chem. Educ.*, **2013**, *90*, 203-209.

44. Linman, M. J.; Abbas, A.; Cheng, Q. "Interface Design and Multiplexed Analysis with Surface Plasmon Resonance (SPR) Spectroscopy and SPR Imaging." *Analyst*, **2010**, *135*, 2759-2767.

45. Phillips, K. S.; Han, J. –H.; Martinez, M.; Wang, Z.; Carter, D., Cheng, Q. "Nanoscale Glassification of Gold Substrates for Surface Plasmon Resonance Analysis of Protein Toxins with Supported Lipid Membranes." *Anal. Chem.*, **2006**, *78*, 596-603.

46. Keller, C. A.; Glasmästar, K.; Zhdanov, V. P.; Kasemo, B. "Formation of Supported Membranes from Vesicles." *Phys. Rev. Lett.*, **2000**, *84*, 5443-5446.

47. Liu, Y.; Young, M. C.; Moshe, O.; Cheng, Q.; Hooley, R. J. "A Membrane-Bound Synthetic Receptor that Promotes Growth of a Polymeric Coating at the Bilayer-Water Interface." *Angew. Chem. In. Ed.*, **2012**, *51*, 7748-7751.

Chapter Two: Labeled Protein Recognition by Synthetic Receptors at a Membrane Bilayer Interface

2.1 Introduction

The surface of cellular membrane is decorated with a variety of membrane bound receptors[1] that are capable of non-covalent and selective molecular recognition. These recognition processes are involved in controlling the transport of small and large molecules, metabolic regulation, and cell-cell communication, and are crucial for cellular responses to the external environment.[2] Most attempts to mimic extracellular recognition using synthetic receptor molecules have been made using covalent attachment of the receptor to lipids or steroids within biomimetic membranes.[3] Derivatization of receptors on membrane constructs, however, has limitations in the range of attachments and is synthetically challenging.

Previous work has shown that cavitand **1.14** can be self-incorporated into a supported lipid bilayer (SLB).[4] The membrane-bound cavitand **1.14** showed selectivity for a wide variety of small molecules containing a trimethylammonium (R-NMe_3^+) group such as choline and this binding event was monitored by surface plasmon resonance (SPR) in real-time. Furthermore, biomacromolecule recognition by cavitand **1.14** was possible using an alternative method. NeutrAvidin, a large protein with strong binding affinity to biotin (K_a = ~10^{15} M^{-1}), was immobilized by biotin guest **1.14** that was bound to cavitand **1.14** in a biomimetic environment.[4] This protein recognition method is, however, limited to only few proteins that show binding affinities to certain guest molecules and these molecules have to be synthesized with R-NMe_3^+ groups independently. To solve these limitations, proteins were directly labeled with a suitable

binding handle and the recognition of the labeled proteins by membrane-bound cavitands was demonstrated.[5]

2.2 Labeling Proteins with the R-NMe_3^+ Binding Handle

Recognition of large proteins is challenging for cavitand **1.14** because the size of proteins is considerably larger than the host itself. Moreover, the surface of proteins is hydrophilic: the binding affinity of guests for cavitand **1.14** decreases as hydrophilicity of guest molecules increases.[6] Since most proteins have R-NH_3^+ lysine groups but not the R-NMe_3^+ group naturally, a new protein labeling agent containing the R-NMe_3^+ binding handle is needed. To introduce the binding handle to proteins, a reactive functional group on the agent must react with proper residues found on proteins and not undergo hydrolysis. Most common labeling agents for proteins or live cells possess electrophilic functionality and react with nucleophilic lysine residues.[7,8] Among many electrophilic functional groups, isothiocyanate was chosen due to its selective reactivity with lysine residues and limited hydrolysis at pH 8. Thus, labeling agents containing both isothiocyanate and the R-NMe_3^+ binding handle were designed. Two labeling agents with different spacer lengths were synthesized since the binding affinity of modified large proteins may be affected by steric hindrance (Figure 2.1). The conversion of *N*,*N*-dimethylethylenediamine to isothiocyanate **2.1**[9] followed by quaternization with iodomethane gave a short trimethylammonium tag **2.2**. The reaction of isothiocyanate **2.1** with 4,7,10-trioxa-1,13-tridecanediamine extended the length of spacer (**2.3**), and following quaternization provided a long trimethylammonium tag **2.4**.

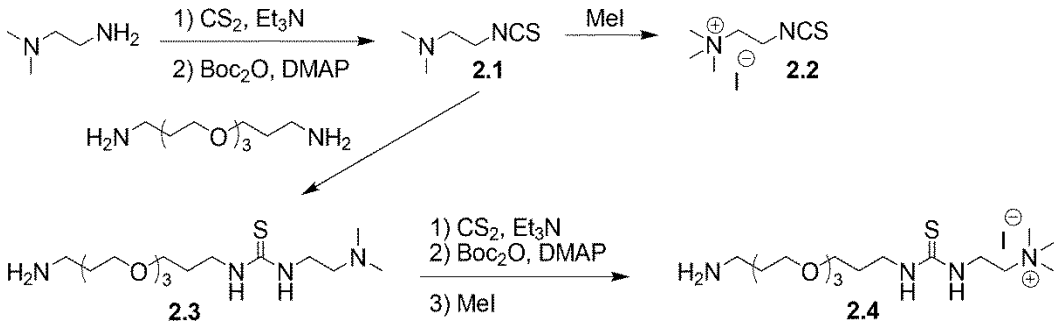

Figure 2.1: Synthesis of trimethylammonium tag molecules **2.2** and **2.4**.

In order to test the binding capabilities of labeling reagents with cavitand **1.14** when incorporated into SLB, the trimethylammonium tag **2.2** was added to the cavitand **1.14**:SLB system (Figure 2.2). Upon introducing labeling agent **2.2**, the resonance angle change in SPR was monitored. This implies that the trimethylammonium tag **2.2** was successfully recognized and bound by cavitand **1.14**. The purpose of the isothiocyanate group present on tag **2.2** is to react the tag **2.2** with lysine residues on proteins. Thus, bovine serum albumin (BSA, MW = 66.4 kDa) was injected after trimethylammonium tag **2.2** was bound to the cavitand **1.14**:SLB system (Figure 2.2). Labeling of native proteins with tag **2.2** was, however, not observed. There was no resonance angle change upon injection. This may be due to hydrolysis of the isothiocyanate group while incubating and washing. Another possibility is that trimethylammonium tag **2.2** was too short to expose isothiocyanate group above the SLB interface, thus the lysine groups on BSA were not able to reach and react with the isothiocyanate group.

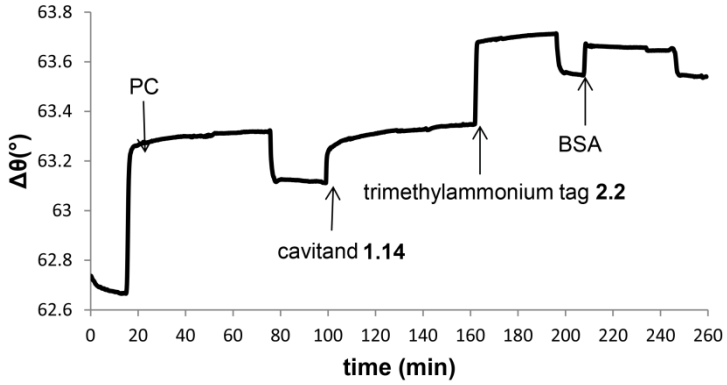

Figure 2.2: A SPR sensorgram of a binding event of trimethylammonium tag **2.2** to cavitand **1.14** incorporated within SLB and an introduction of BSA to tag **2.2**:cavitand **1.14**:SLB system.

The cavitand **1.14** incorporated within SLB was capable of recognizing the trimethylammonium tag **2.2**, but labeling proteins with the bound tag **2.2** in cavitand **1.14**:SLB system was not successful. Therefore, direct labeling of proteins with tags **2.2** and **2.4** was performed. Small and weakly hydrophilic proteins were considered since cavitand **1.14** shows reduced binding affinity for hydrophilic guests.[6] Thus, bovine heart cytochrome *c* (cyt *c*, MW = 12.4 kDa) was chosen as an initial test protein for tagging with the R-NMe_3^+ binding handle. Trimethylammonium tags, **2.2** and **2.4**, were labeled to cyt *c* via literature procedure,[10] and short and long tag-labeled cyt *c* derivatives were obtained (**R_1/R_2-cyt *c***, respectively) as shown in Figure 2.3. 1 mg/mL cyt *c* and either 10 mM **2.2** or **2.4** were incubated in 100 mM Phosphate Buffered Saline (PBS, pH 7.4) at 37 °C overnight. The labeled **R_1/R_2-cyt *c*** was purified from unreacted and hydrolyzed tags using centrifugal filters. Bradford Assay[11] was performed to determine the concentration of purified **R_1/R_2-cyt *c***. The Bradford Assay is a spectroscopic analytical technique that accurately measures the concentration of protein in solution. Various

concentrations of BSA (0.125 – 2 mg/mL) were prepared in PBS buffer, and Coomassie Brilliant Blue Dye was added into the samples. The absorbance at 595 nm was measured for all samples and the absorbance against BSA concentrations was plotted. The slope equation of the plotted graph was obtained, and the concentration of **R_1/R_2**-proteins was determined by the absorbance obtained from purified labeled proteins. Finally, each sample was adjusted to 15 µM by adding 100 mM PBS.

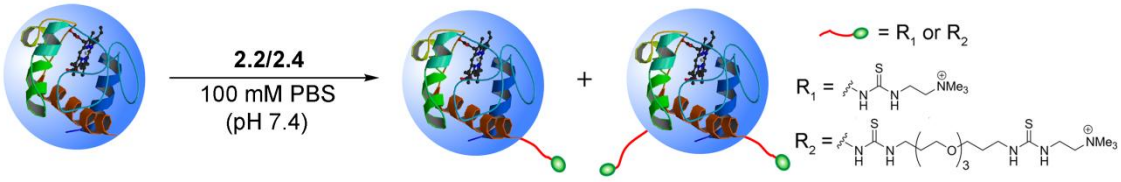

Figure 2.3: A representation of protein labeling procedure.

2.3 Labeled Protein Recognition by Membrane-Embedded Cavitand

The recognition of labeled proteins by membrane-bound cavitand **1.14** was monitored by SPR (Figure 2.4). The solution of **R_1/R_2-cyt *c*** was injected and the binding event was investigated.

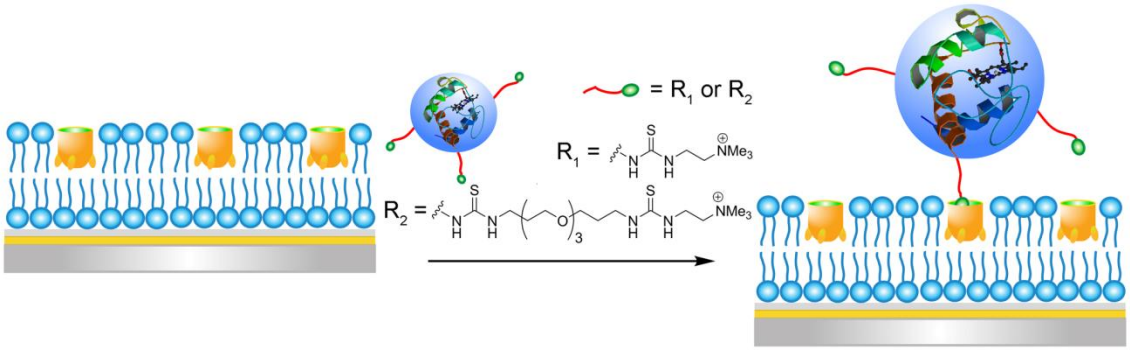

Figure 2.4: A representation of the recognition process with labeled cyt *c*.

As shown in Figure 2.5, the recognition of derivatized cyt *c* by the membrane-bound cavitand **1.14** was observed. The injection of **R_1-cyt *c*** into the cavitand **1.14**:SLB system showed a change in resonance angle ($\Delta\theta_{\text{cav }\mathbf{1.14}}$) of 0.22°, which was maintained even after washing for 30 min. A larger SPR response was observed with the longer chain labeled cyt *c*. The injection of **R_2-cyt *c*** to the system gave a change in resonance angle of 0.40°. When native cyt *c* or **R_2-cyt *c*** was exposed to a SLB in the absence of cavitand **1.14**, there was no change in resonance angle observed after washing. This indicates that there are no nonspecific interactions between native or derivatized cyt *c* and the SLB. The isoelectric point (pI) of cyt *c* is 10.5, so it is positively charged under the pH 7.4 conditions. In addition, the overall charge of cyt *c* is not changing by labeling with the trimethylammonium tags, **2.2** and **2.4**, since the lysine residues ($-NH_3^+$) are converted to R-NMe_3^+ groups. Therefore, the native and derivatized cyt *c*, a small positively charged hydrophilic protein, does not have any affinity for the zwitterionic surface of SLB.

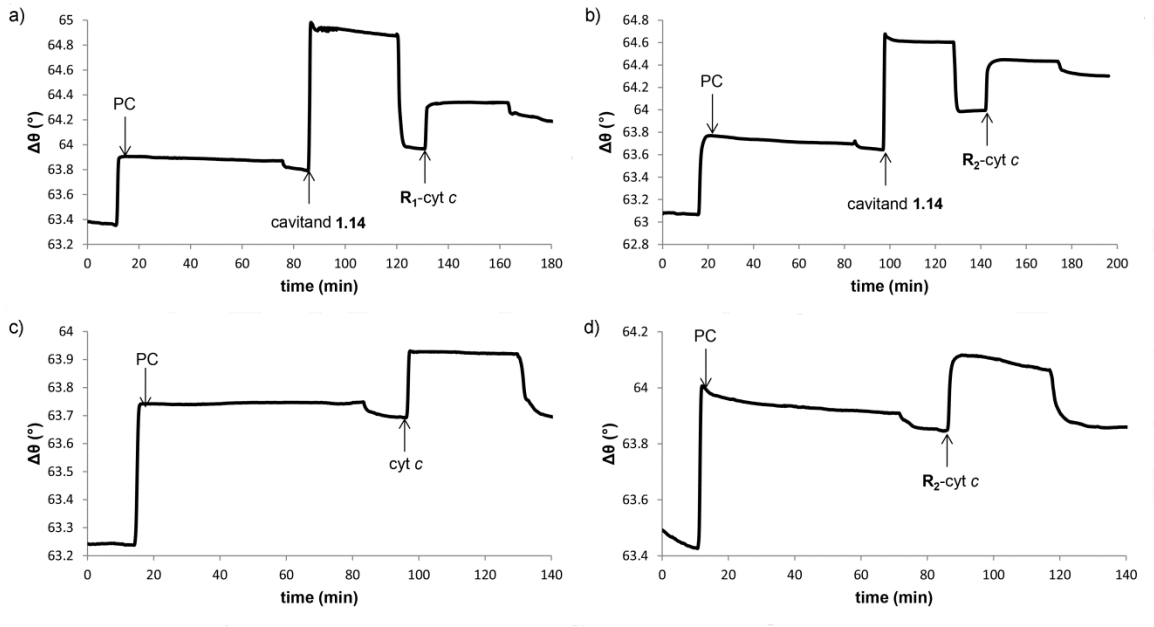

Figure 2.5: SPR sensorgrams of tagged cyt *c* immobilization by membrane-bound cavitand **1.14**: (a) **R_1-cyt *c***; (b) **R_2-cyt *c***; (c) native cyt *c* on a clean SLB; (d) **R_2-cyt *c*** on a clean SLB.

Since the labeling of BSA with trimethylammonium tag **2.2** bound to the cavitand **1.14**:SLB system was not successful, BSA was labeled with tag **2.2** and **2.4** directly, and subsequently exposed to the cavitand **1.14**:SLB system. As shown in Figure 2.6, the membrane-bound cavitand **1.14** was capable of recognizing **R_2-BSA** with a resonance angle change of 0.21°. No binding event was observed between **R_1-BSA** and the cavitand **1.14**:SLB system, however. It is possible that BSA is too large, so a short tag **2.2** labeled on a bulky BSA is not long enough to reach the cavity of the cavitand **1.14** embedded in a SLB. As a result, it cannot be recognized by the cavitand **1.14**:SLB system. When native BSA was injected into a clean SLB environment without cavitand **1.14**, native BSA did not show any binding affinity for the SLB after washing. In addition, no binding event was observed when **R_2-BSA** was exposed to a SLB in the absence of cavitand **1.14**.

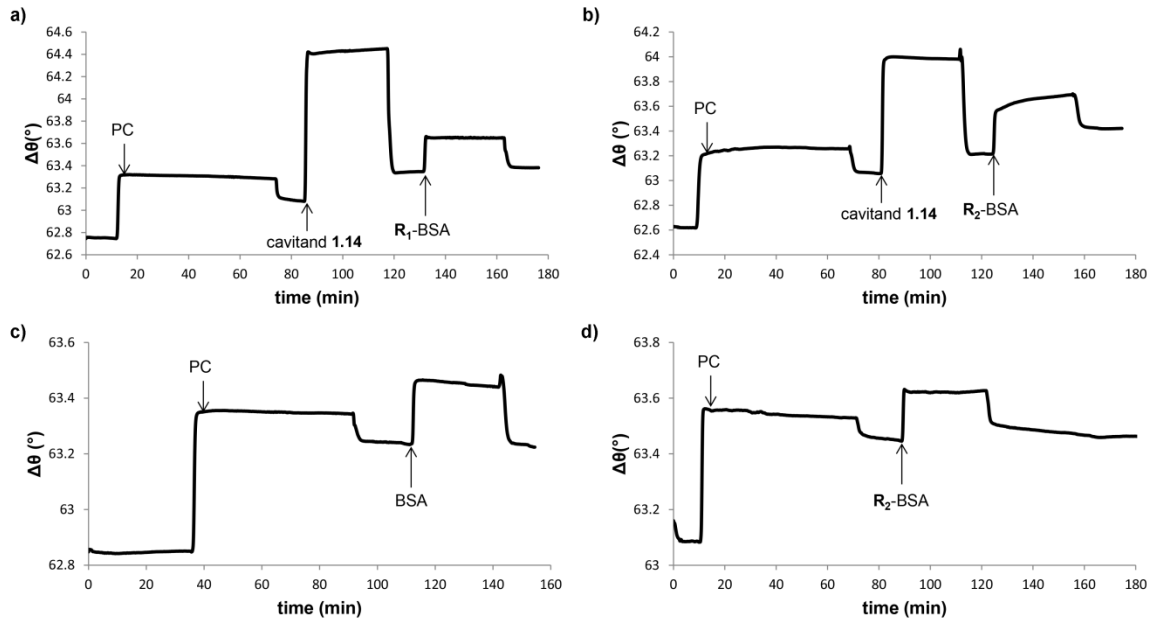

Figure 2.6: SPR sensorgrams of tagged BSA immobilization by membrane-bound cavitand **1.14**: (a) **R_1-BSA**; (b) **R_2-BSA**; (c) native BSA on a clean SLB; (d) **R_2-BSA** on a clean SLB.

Other proteins, equine myoglobin, bovine hemoglobin, and *β*-lactoglobulin from bovine milk, were labeled with the long trimethylammonium tag **2.4** and exposed to the cavitand **1.14**:SLB system. As shown in Figure 2.7, labeled proteins were successfully immobilized by membrane-bound cavitand **1.14**. The immobilization of **R_2-myoglobin**, **R_2-hemoglobin**, and **R_2-*β*-lactoglobulin** by embedded cavitand **1.14** showed $\Delta\theta_{\text{cav }\mathbf{1.14}}$ = 0.33°, 0.43°, and 0.15°, respectively. On the other hand, labeled myoglobin, hemoglobin, and *β*-lactoglobulin did not demonstrate any notable binding affinity for a SLB in the absence of cavitand **1.14** (Figure 2.7, Table 2.1). A small change in resonance angle was observed with **R_2-hemoglobin** on a SLB in the absence of cavitand **1.14** ($\Delta\theta_{\text{ctrl}}$ = 0.03°), however. This change is negligible as the binding affinity of the labeled protein for cavitand **1.14**:SLB system is much more stronger.

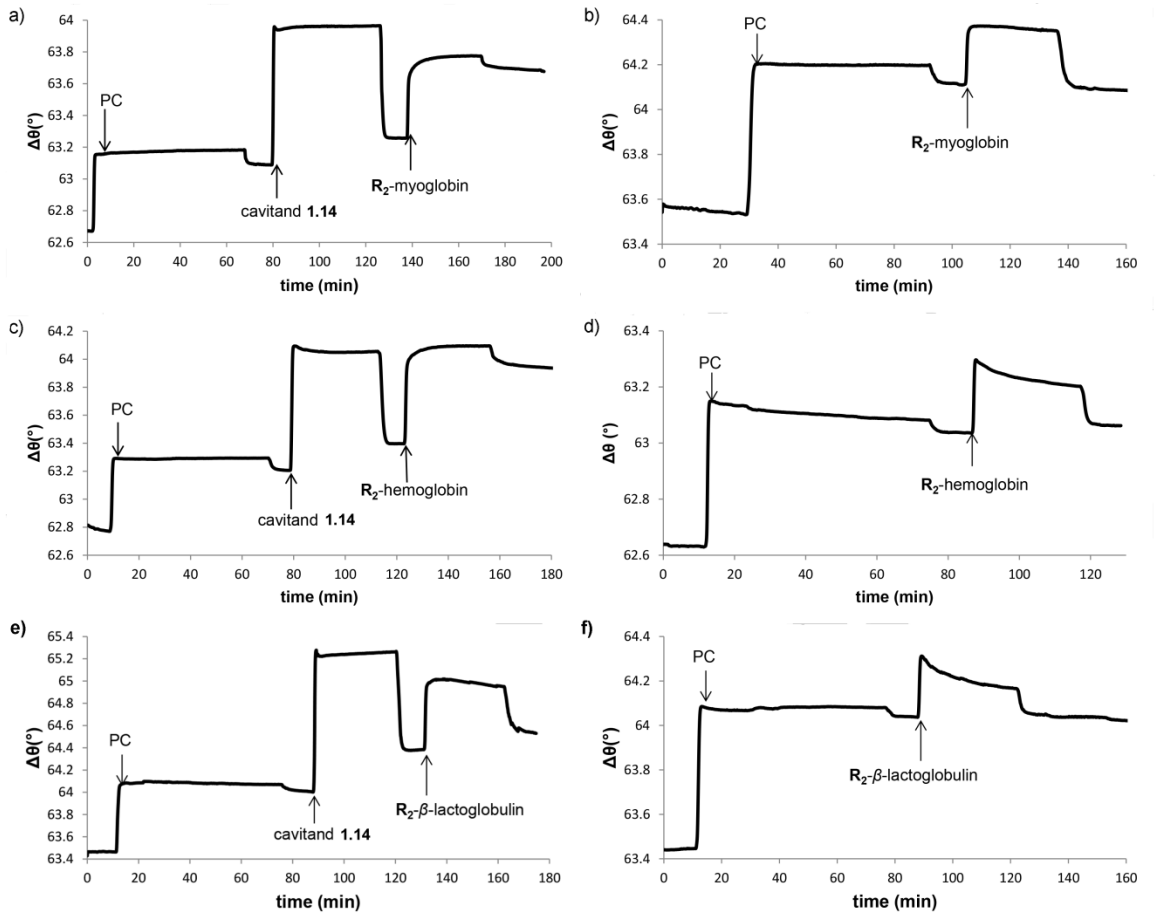

Figure 2.7: SPR sensorgrams for: (a) **R_2-myoglobin** on cavitand **1.14**:SLB system; (b) **R_2-myoglobin** on a clean SLB; (c) **R_2-hemoglobin** on cavitand **1.14**:SLB system; (d) **R_2-hemoglobin** on a clean SLB; (e) **R_2-*β*-lactoglobulin** on cavitand **1.14**:SLB system; (f) **R_2-*β*-lactoglobulin** on a clean SLB.

Table 2.1: Resonance angle change upon binding of labeled proteins to membrane-bound cavitand **1.14**.

R_2-protein	MW (kDa)	$\Delta\theta_{cav\ \mathbf{1.14}}$ (°)[a]	$\Delta\theta_{cntl}$ (°)[b]
cyt c	12.4	0.40	<0.01
BSA	66.4	0.21	<0.01
myoglobin	18	0.33	<0.01
hemoglobin	15.2 (α) / 16 (β)	0.43	0.03
β-lactoglobulin	18.4	0.15	<0.01

[a] $\Delta\theta_{cav\ \mathbf{1.14}}$ (°) = resonance angle change upon target binding in the presence of cavitand **1**. [b] $\Delta\theta_{cntl}$ (°) = resonance angle change upon target addition to clean SLB; injected [**1**] = 1.6 mM, [R_2-protein] = 15 μM, 100 mM PBS buffer.

2.4 Analysis of Labeled Proteins

When labeling proteins with the R-NMe_3^+ groups, excess trimethylammonium tags **2.2** or **2.4** were used in the reaction solution. Since proteins have several lysine groups that can be labeled with the tags, the number of labels attached to each protein was investigated. This is challenging because the labels do not have any chromophores or electroactive functional groups[12] that can be used for simple quantitation. Instead, mass spectrometry was used for tentative analysis. Unmodified cyt *c* and **R_2-cyt *c*** were analyzed by electrospray ionization mass spectrometry (ESI-MS) (Figure 2.8). The most abundant species were singly and doubly labeled proteins along with some other adducts, such as higher order labeled and methylated proteins. Although excess trimethylammonium tag **2.4** was used to label proteins, ESI-MS data showed the abundance of only one or two tag labeled proteins. This means that the efficiency of the labeling process is not high. The ESI spectrum of **R_2-cyt *c*** is complicated (Figure 2.8b)

because the archetypal ESI charge state distribution patterns for not only one and two R_2 tag labeled proteins but all other species were overlapped. Even though small amounts of several other species were present in the injected protein solution, only properly labeled proteins with R-NMe_3^+ groups were recognized by cavitand **1.14**. Other adducts that do not have R-NMe_3^+ groups were not capable of binding to the cavity, and consequently were SPR silent.

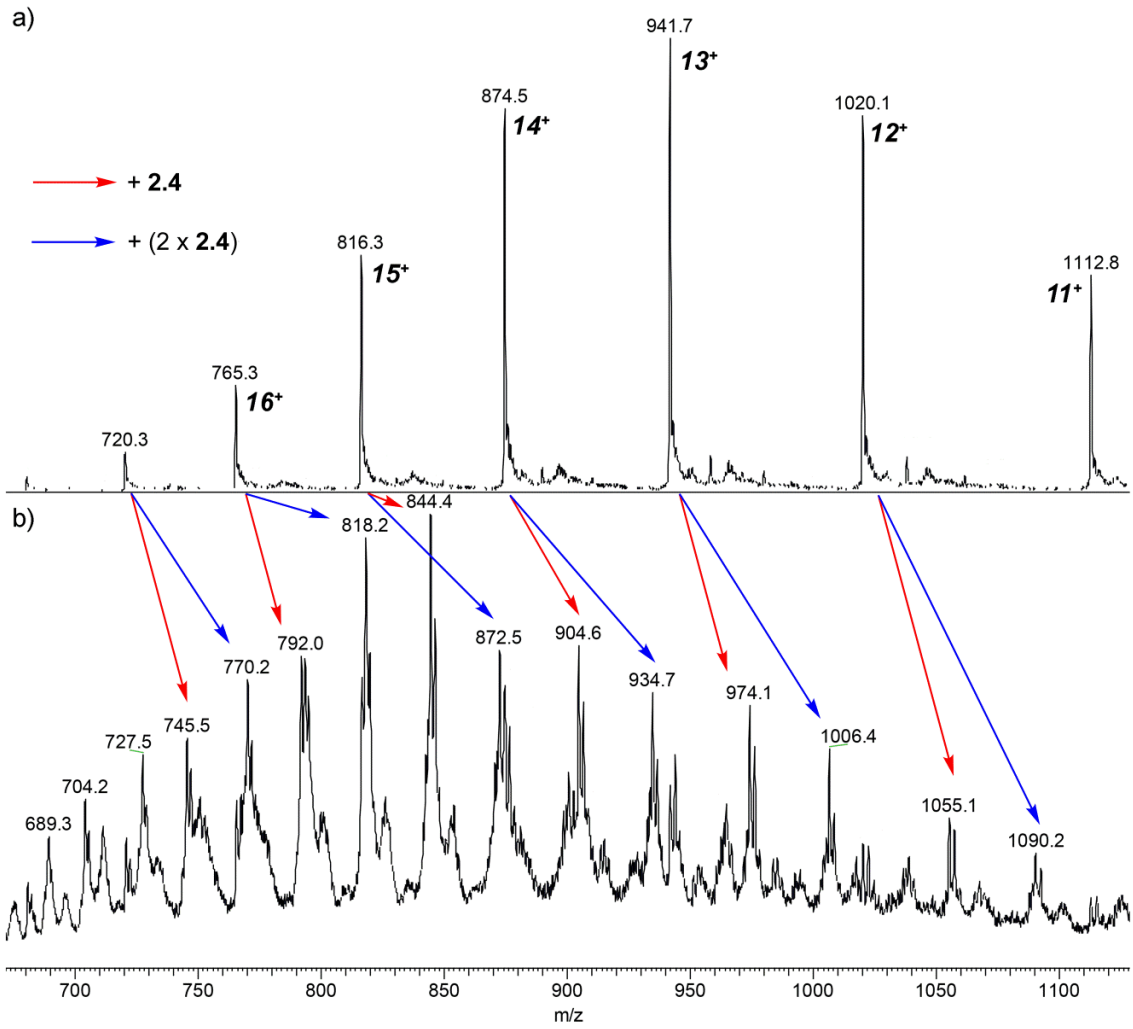

Figure 2.8: ESI-MS analysis of labeled **R_2-cyt *c***: (a) native cyt *c*; (b) **R_2-cyt *c***.

In addition, native myoglobin and **R_2-myoglobin** were analyzed by ESI-MS (Figure 2.9). Unlike **R_2-cyt *c***, a complicated collection of peaks was observed from **R_2-myoglobin**. This may be due to the presence of a mixture of myoglobins labeled with various numbers of tags. This result was different for the case of cyt *c*. Even though excess tag **2.4** was added when labeling proteins, the abundance of only one or two tag labeled cyt *c* was observed. Interestingly, unlike **R_2-cyt *c***, a peak at 616.25 Da, representing a heme group on myoglobin, was observed from both native myoglobin and **R_2-myoglobin**. This indicates that a heme group was detached from native and modified myoglobins while obtaining the ESI-MS data. Notably, the peak representing a heme group was more intense from modified myoglobin than that from native myoglobin. It is possible that the folding of myoglobin was weakened upon labeling with the trimethylammonium tag **2.4**, and the binding affinity of the heme group for myoglobin became weaker. As a result, the heme group was easily detached from the modified myoglobin while obtaining ESI-MS data. The weakening of protein folding can cause denaturing of proteins, this results in an exposure of buried lysine groups. As a result, more lysine groups were available for tagging and myoglobin was labeled with more than one or two tags. Since typical ESI charge state distribution patterns for a mixture of myoglobins labeled with varying numbers of tags were overlapped, the ESI-MS data of **R_2-myoglobin** is very complicated.

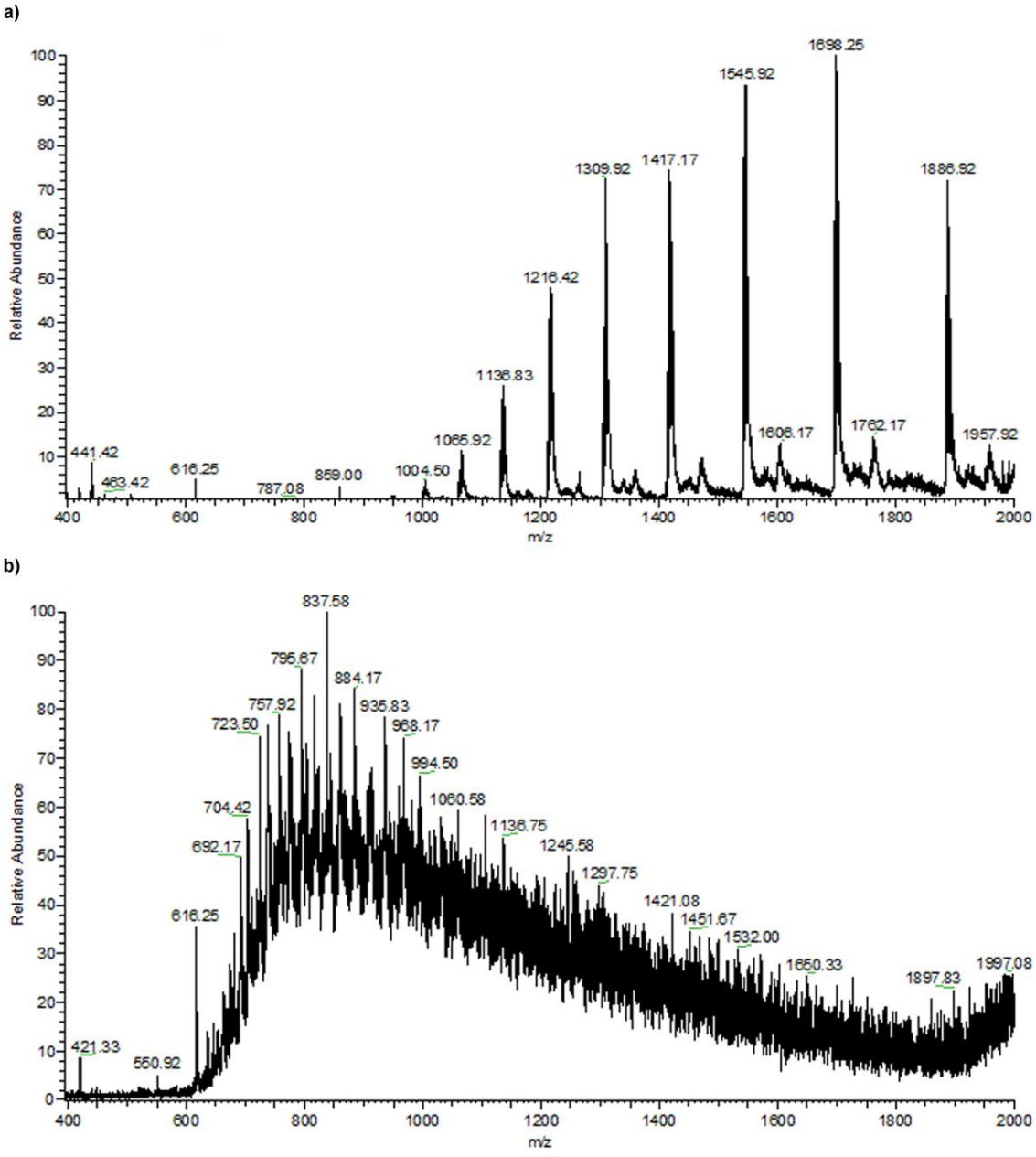

Figure 2.9: ESI-MS analysis of labeled **R_2-myoglobin**: (a) native myoglobin; (b) **R_2-myoglobin**.

2.5 Binding Affinities of Labeled Proteins for Membrane-Bound Cavitand

To investigate the strength of binding affinity of **R_2-cyt *c*** for membrane-bound cavitand **1.14**, excess choline chloride (a binding constant of $>10^4$ M^{-1} for cavitand **1.14** in D_2O[13]) was injected to prefill the host prior to the injection of **R_2-cyt *c***. Interestingly, **R_2-cyt *c*** was able to displace the bound choline and was immobilized by cavitand **1.14** (Figure 2.10). This indicates that the binding affinity of **R_2-cyt *c*** for the cavitand**1.14** embedded in a SLB is stronger than that of choline.

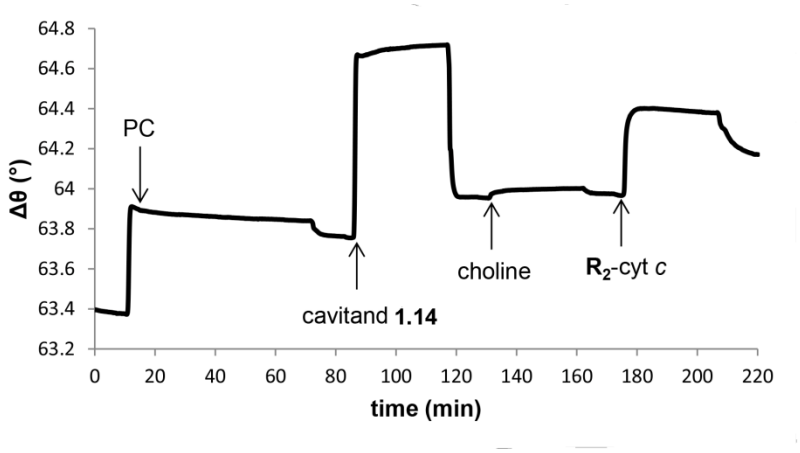

Figure 2.10: A SPR sensorgram of **R_2-cyt *c*** on a prefilled cavitand **1.14**:SLB system.

To determine the quantitative binding affinity of the long trimethylammonium tag **2.4**, labeled to proteins for cavitand **1.14** incorporated in a SLB, equilibrium dissociation constant (K_d) and equilibrium association constant (K_a) were calculated by SPR analysis in saturation binding mode.[4] The minimum change in resonance angle was obtained upon the injection of varying concentrations of R_2-labeled proteins to the cavitand **1.14**:SLB system, and saturation binding mode (eq 1)[14] was calculated.

$$AB_{eq} = AB_{max}(1/(1+K_d/[A])) \quad \text{(eq 1)}$$

Here, AB_{eq} is the average SPR response signal at equilibrium, AB_{max} is the maximum response obtained for R_2-labeled protein binding, and [A] is the concentration of injected R_2-labeled protein. In this case, the assumption that there was monovalent binding (1:1 complex) between cavitand **1.14** and R_2-labeled protein was made. AB_{max}/AB_{eq} against 1/[A] was plotted, and the slope was calculated. K_d is equal to the slop of the graph, and K_a is the reciprocal value of K_d. The data fit well with the 1:1 binding fit curve (Figure 2.11), and three R_2-labeled proteins - **R_2-cyt *c***, **R_2-myoglobin**, and **R_2-hemoglobin** - showed strong binding affinities for membrane-embedded cavitand **1.14** (Table 2.2). Even though the sizes of the R_2-labeled proteins are different, all three proteins (**R_2-cyt *c***, **R_2-myoglobin**, and **R_2-hemoglobin**) showed similar association constants with cavitand **1.14** incorporated into the SLB on the order of 10^5 M^{-1}. The binding affinities of R_2-labeled proteins for cavitand **1.14** under the analysis condition are an order of magnitude stronger than binding constants of choline chloride and acetylcholine chloride that are greater than 10^4 M^{-1} in D_2O.[13,15] This explains the result that **R_2-cyt *c*** was capable of displacing a bound choline molecule out of the cavity of the cavitand **1.14**:SLB system (Figure 2.10).

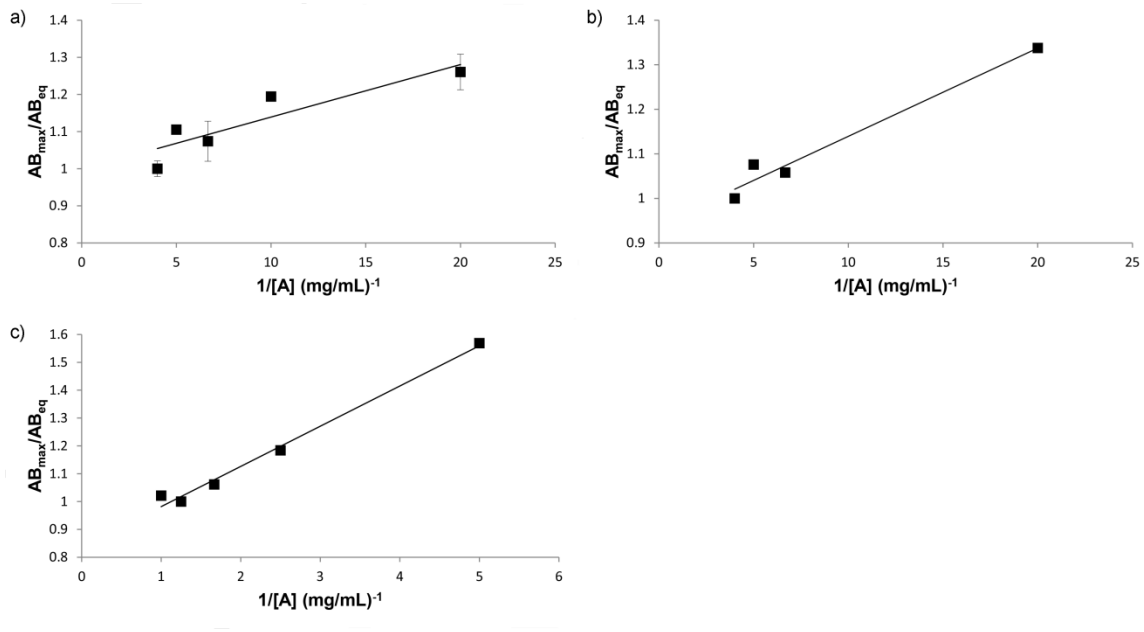

Figure 2.11: Equilibrium dissociation constant (K_d) determination for cavitand **1.14** binding with: (a) **R_2-cyt *c***; (b) **R_2-myoglobin**; (c) **R_2-hemoglobin**.

Table 2.2: Binding affinities of R_2-labeled proteins for membrane-embedded cavitand **1.14**.

R_2-protein	cyt *c*	myoglobin	hemoglobin
MW (kDa)	12.4	18	15.2 (α) / 16 (β)
K_a (1), M^{-1}	$(9.01 \pm 2.55) \times 10^5$	$(9.09 \pm 1.07) \times 10^5$	$(1.11 \pm 0.07) \times 10^5$
K_d (1), μM	1.11 ± 0.31	1.10 ± 0.13	9.03 ± 0.55

Injected [**1**] = 1.6 mM; [R_2-protein] = 15 μM, 100 mM PBS buffer.

Unfortunately, quantitative binding affinities of **R_2-BSA** for membrane-bound cavitand **1.14** could not be determined by SPR analysis in saturation binding mode.[4] This is due to the fact that the resonance angle changes upon injection of various concentrations of **R_2-BSA** did not correlate with the concentrations of the labeled protein.

It is possible that BSA aggregates as the concentration increases, thus accurate measurements of resonance angle change are not feasible.

2.6 Analysis of Binding Interactions

Cavitand **1.14** possesses negatively charged carboxylate groups at the rim and the surface of **R_2-cyt *c*** is positively charged under analysis conditions (pH 7.4). It is possible that the observed recognition is due to nonspecific charge-based interactions between R-NMe_3^+ groups on **R_2-cyt *c*** and cavitand **1.14** rather than cavity-based molecular recognition. To verify that the binding affinity of R_2-labeled proteins for cavitand **1.14** embedded in the SLB is a cavity-based interaction, neutral cavitand **2.5**[16] was employed. This cavitand does not have charged groups at the rim, but still possesses the same sized cavity as cavitand **1.14**. Its water solubility is not as good as cavitand **1.14**, thus another method was employed to incorporate the cavitand **2.5** into the SLB. Cavitand **2.5** was preincorporated into POPC vesicles during preparation. In the first step of making POPC vesicles, varied concentrations of cavitand **2.5** (0.5-5 mol%) in POPC lipids were prepared in chloroform, and the remaining steps were identical. As shown in Figure 2.12b, the cavitand **2.5** containing POPC vesicles were exposed to a calcinated nanoglassified gold substrate, and the formation of lipid bilayer was monitored by SPR. The formation of a robust SLB was observed if the concentrations of cavitand **2.5** was 2 mol% or lower. When POPC vesicles were contained >2 mol% of cavitand **2.5**, successful bilayer formation was not obtained. Therefore, POPC vesicles containing 2 mol% cavitand **2.5** were used for the bilayer formation to maximize binding of R_2-labeled proteins. In this

case, the upper POPC leaflet exposed to a bilayer:water interface consists of 1 mol% cavitand **2.5** if the cavitand was distributed evenly into the inner and outer leaflets of the vesicles.

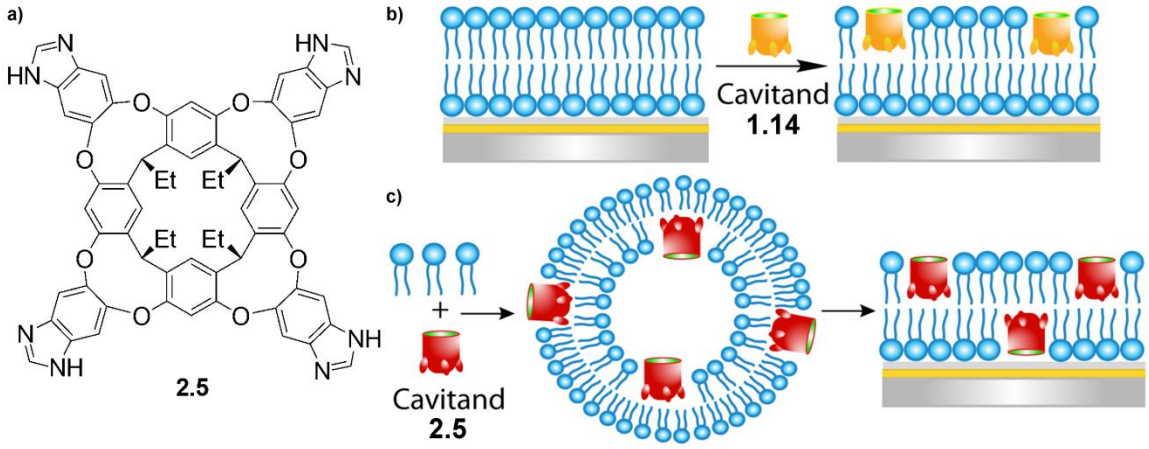

Figure 2.12: a) Structure of neutral cavitand **2.5**; representations of: b) the incorporation of cavitand **1.14** into a preformed SLB; c) 2 mol% cavitand **2.5**:POPC bilayer formation.

When **R_2-cyt *c*** was introduced to a preformed cavitand **2.5**:POPC bilayer, the recognition of the labeled protein was observed and showed a change in resonance angle ($\Delta\theta_{\text{cav 2.5}}$) of 0.29° (Figure 2.13). Other labeled proteins - **R_2-BSA**, **R_2-myoglobin**, and **R_2-hemoglobin** - also showed binding to the preformed SLB containing cavitand **2.5** (Table 2.1). This indicates that the recognition properties of the cavitand **2.5**:SLB system were functional. The SPR responses observed, however, were slightly lower when compared to those for cavitand **1.14**. This implies that a slight charge-based interaction between the surface of labeled proteins and cavitand **1.14** incorporated within a SLB exists but its proportion in the recognition is not large. In the case of cavitand **1.14**, hydrophilic carboxylate groups at the rim have an effect on the orientation of cavitand

1.14 when incorporating into the SLB. Neutral cavitand **1.14**, on the other hand, has no charged groups at the rim. The benzimidazole groups at the rim, however, are slightly more polar than the hydrophobic aromatic body of cavitand **2.5**. This makes the open cavity of cavitand **2.5** orient towards the exterior solvent in a significant proportion and the cavitand **2.5** can immobilize R_2-labeled proteins. Since cavitand **2.5** is still capable of recognizing R_2-labeled proteins, the binding of R-NMe_3^+ labeled proteins is cavity-based molecular recognition.

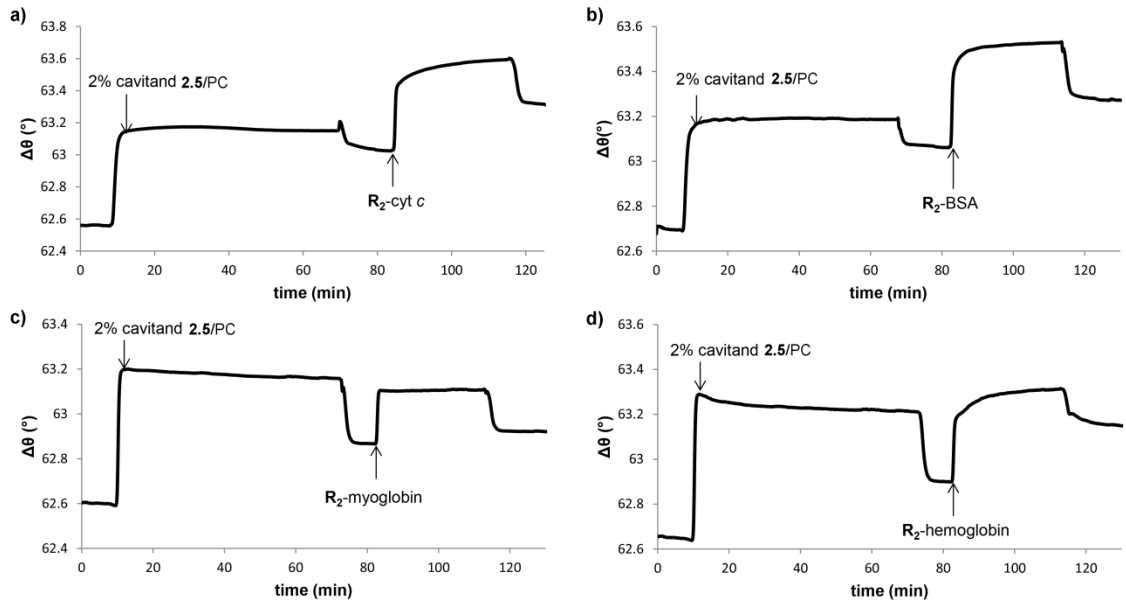

Figure 2.13: SPR sensorgrams of R_2-labeled protein immobilization by the cavitand **2.5**:SLB system: (a) **R_2-cyt *c***; (b) **R_2-BSA**; (c) **R_2-myoglobin**; (d) **R_2-hemoglobin**.

Table 2.3: Resonance angle change upon binding of labeled proteins to membrane-bound cavitand **2.5**.

R_2-protein	cyt *c*	BSA	myoglobin	hemoglobin
MW (kDa)	12.4	66.4	18	15.2 (α) / 16 (β)
$\Delta\theta_{cav\ \mathbf{2.5}}$ (°)[a]	0.29	0.21	0.05	0.25

[a] $\Delta\theta_{cav\ \mathbf{2.5}}$ (°) = resonance angle change upon target binding in the presence of cavitand **2.5**; injected [**1**] = 1.6 mM, [R_2-protein] = 15 μM, 100 mM PBS buffer.

2.7 Conclusion

New protein labeling agents containing both isothiocyanate and R-NMe_3^+ groups were synthesized and several proteins were labeled with these *in situ*. The labeled proteins showed strong binding affinities to cavitands incorporated into a SLB, with association constants of ~10^5 M^{-1}. ESI-MS data revealed that only one and two tags were labeled on proteins, and SPR analysis suggested that the recognition between membrane-bound cavitands and the labeled proteins is monovalent binding. In addition, immobilization of R-NMe_3^+ group labeled proteins by neutral cavitand **2.5** embedded into a SLB implied that the recognition event was cavity-based interactions.

2.8 References

1. Hymel, D.; Peterson, B. R.; "Synthetic Cell Surface Receptors for Delivery of Therapeutics and Probes." *Adv. Drug Deliv. Rev.*, **2012**, *64*, 797-810.

2. Conner, S. D.; Schmid, S. L. "Regulated Portals of Entry into the Cell." *Nature*, **2003**, *422*, 37-44.

3. Bertozzi, C. R.; Kiessling, L. L. "Chemical Glycobiology." *Science*, **2001**, *291*, 2357-2364.

4. Liu, Y.; Liao, P.; Cheng, Q.; Hooley, R. J. "Protein and Small Molecule Recognition Properties of Deep Cavitands in a Supported Lipid Membrane Determined by Calcination-Enhanced SPR Spectroscopy." *J. Am. Chem. Soc.*, **2010**, *132*, 10383-10390.

5. Ghang, Y. –J.; Lloyd, J. J.; Moehlig, M. P.; Arguelles, J. K.; Mettry, M.; Zhang, X.; Julian, R. R.; Cheng, Q.; Hooley, R. J. "Labeled Protein Recognition at a Membrane Bilayer Interface by Embedded Synthetic Receptors." *Langmuir*, **2014**, *30*, 10161-10166.

6. Hooley, R. J.; Biros, S. M.; Rebek, J. Jr. "A Deep, Water-Soluble Cavitand Acts as a Phase-Transfer Catalyst for Hydrophobic Species." *Angew. Chem. Int. Ed.*, **2006**, *45*, 3517-3519.

7. Chen, X.; Muthoosamy, K.; Pfisterer, A.; Neumann, B.; Weil, T. "Site-Selective Lysine Modification of Native Proteins and Peptides via Kinetically Controlled Labeling." *Bioconjugate Chem.*, **2012**, *23*, 500-508.

8. Takaoka, Y.; Ojida, A.; Hamachi, I. "Protein Organic Chemistry and Applications for Labeling and Engineering in Live-Cell Systems." *Angew. Chem. In. Ed.*, **2013**, *52*, 4088-4016.

9. Munch, H.; Hansen, J. S.; Pittelkow, M.; Christensen, J. B.; Boas, U. A. "New Efficient Synthesis of Isothiocyanates from Amines Using Di-*tert*-butyl Dicarbonate." *Tetrahedron Lett.*, **2008**, *49*, 3117-3119.

10. Nakamura, T.; Kawai, Y.; Kitamoto, N.; Osawa, T.; Kato, Y. "Covalent Modification of Lysine Residues by Allyl Isothiocyanate in Physiological Conditions: Plausible Transformation of Isothiocyanate from Thiol to Amine." *Chem. Res. Toxicol.*, **2009**, *22*, 536-542.

11. Bradford, M. M. “A Rapid and Sensitive Method for the Quantitation of Microgram Quantities of Protein Utilizing the Principle of Protein-Dye Binding.” *Anal. Biochem.*, **1976**, *72*, 248-254.

12. Badia, A.; Carlini, R.; Fernandea, A.; Battaglini, F.; Mikkelsen, S. R.; English, A. M. “Intramolecular Electron-Transfer Rates in Ferrocene-Derivatized Glucose Oxidase.” *J. Am. Chem. Soc.*, **1993**, *115*, 7053-7060.

13. Biros, S. M.; Ullrich, E. C.; Hof, F.; Trembleau, L.; Rebek, J., Jr. “Kinetically Stable Complexes in Water: The Role of Hydration and Hydrophobicity.” *J. Am. Chem. Soc.*, **2004**, *126*, 2870-2876.

14. Bieri, C.; Ernst, O. P.; Heyse, S.; Hofmann, K. P.; Vogel, H. “Micropatterned Immobilization of a G Protein-Coupled Receptor and Direct Detection of G Protein Activation.” *Nat. Biotechnol.*, **1999**, *11*, 1105-1108.

15. Hof, F.; Trembleau, L.; Ullrich, E. C.; Rebek, J., Jr. “Acetylcholine Recognition by a Deep, Biomimetic Pocket.” *Angew. Chem. Int. Ed.*, **2003**, *42*, 3150-3153.

16. Rafai Far, A.; Shivanyuk, A.; Rebek, J., Jr. “Water-Stabilized Cavitands.” *J. Am. Chem. Soc.*, **2002**, *124*, 2854-2855.

Chapter Three: Native Protein Adhesion by Synthetic Receptors at a Membrane Bilayer Interface

3.1 Introduction

Many attempts have been made to mimic molecular recognition at the extracellular membranes of natural systems. One common method is to exhibit a natural antibody or epitope at the membrane interface.[1-3] This technique, however, is usually met with a lot of synthetic challenges when it comes to displaying complex epitopes like mucins or their mimics.[4,5] Another technique for protein recognition is the attachment of a synthetic receptor at the membrane surface that can recognize biomolecules. Cyclodextrins can be attached on gold surface and mediate protein assembly,[6,7] but target molecules have to be modified in order to be recognized by the hosts. A synthetic receptor that can recognize native, unmodified proteins and enzymes is rare due to the fact that these structures do not possess suitable recognition motifs for a receptor. Some synthetic hosts, like sulfonatocalixarenes and cyclophanes, are known to recognize proteins in solution.[8-14] These hosts are not compatible with membrane-based recognition due to a lack of external lipophilicity that is required for incorporation into membranes.

As discussed in Chapter 2, cavitand **1.14** can self-incorporate into an SLB and recognize small molecules or biomacromolecules derivatized with a suitable binding handle.[15,16] Cavitand **1.14** displays carboxylate groups at the rim at SLB interface when it is bound within the SLB. This negatively charged rim makes cavitand **1.14** capable of ionically driven binding of proteins and enzymes at biomimetic membrane interface, and creates a bioreactive surface (Figure 3.1).[17]

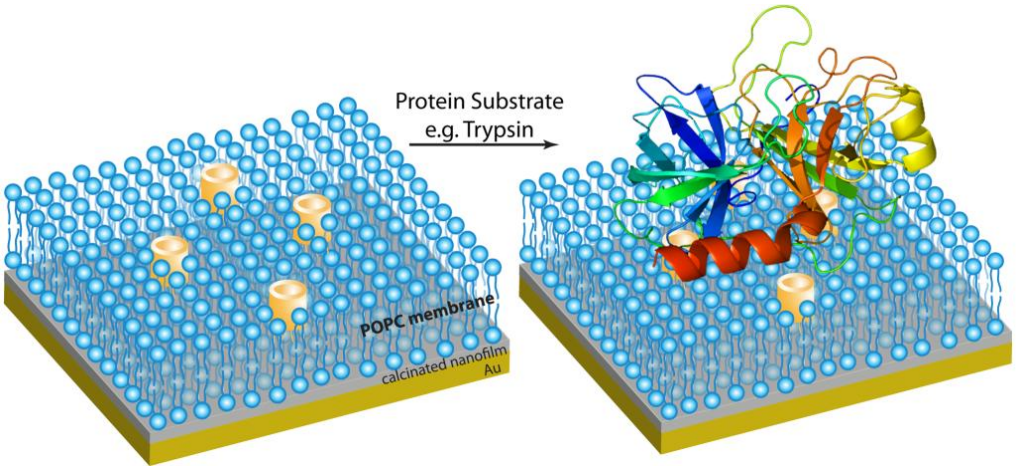

Figure 3.1: A representative of protein binding at the cavitand **1.14**:SLB surface.

3.2 Native Protein Adhesion by Embedded Synthetic Receptors

Our previous work revealed that R-NMe_3^+ labeled proteins showed stronger binding affinity to cavitand **1.14** than cavitand **2.5**.[16] From this observation, the assumption was made that not only cavity-based interaction but charge-based interaction between proteins and negatively charged carboxylate groups at the rim of cavitand **1.14** is also involved in the recognition event. As a preliminary experiment, native BSA, which does not have any binding handles for cavitand **1.14**, such as the R-NMe_3^+ group, was injected into cavitand **1.14**:SLB system and resonance angle change was monitored by SPR. Indeed, a large change in resonance angle was observed when BSA was injected into cavitand **1.14**:SLB system under low salt aqueous conditions ($\Delta_{\theta cav\ \mathbf{1.14}}$ = 0.40°) (Table 3.1, Figure 3.2). Even after 30 mins of extensive washing, the protein was immobilized at the surface. This indicates that BSA adhesion at the cavitand **1.14**:SLB surface was relatively strong. On the other hand, BSA did not show binding affinity to a clean SLB itself.

Table 3.1: Resonance angle change upon binding of proteins at cavitand **1.14**:SLB interface.

Protein	MW (kDa)	pI	$\Delta\theta_{\text{cav 1.14}}{}^{b}$ (°)	$\Delta\theta_{\text{cav 1.14}}{}^{c}$ (°)	$\Delta\theta_{\text{cntl}}{}^{d}$ (°)
BSA	66.4	4.8	0.40	<0.01	<0.01
cyt *c*	12.4	10.5	0.27	0.25	<0.01
myoglobin	18	7.3	0.19	<0.01	<0.01
trypsin	23.3	10.5	0.23	0.17	<0.01
TPCK trypsin	23.8	10.5	0.23	0.17	<0.01

[a]$\Delta\theta_{\text{cav 1.14}}$ (°) = resonance angle change upon target binding in the presence of cavitand **1.14**. [b]DI water as bulk medium. [c]100 mM PBS buffer as bulk medium. [d]$\Delta\theta_{\text{cntl}}$ (°) = resonance angle change upon target addition to POPC bilayer. [e]TPCK-trypsin = tosyl phenylalanyl chloromethyl ketone derivatized trypsin; injected [cavitand **1.14**] = 1.6 mM; [protein] = 15 μM.

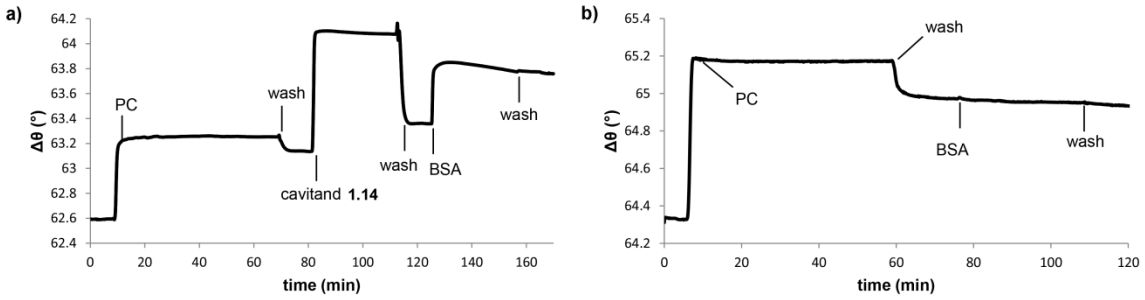

Figure 3.2: SPR sensorgrams of BSA binding in low salt concentrations at the surface of: (a) SLB containing cavitand **1.14**; (b) SLB itself.

Interestingly, a change in binding affinity of BSA to the cavitand **1.14**:SLB system was obtained under different salt concentrations (Figure 3.3). When BSA was injected to the system in 20 mM PBS buffer (pH 7.4), only a small change in resonance angle was detected ($\Delta\theta_{\text{cav 1.14}}$ = 0.04°). If 100 mM PBS buffer (pH 7.4) was used as the flow medium, BSA immobilization is not even detected. These observations imply that the ionic strength of the flow medium is involved in the interactions.

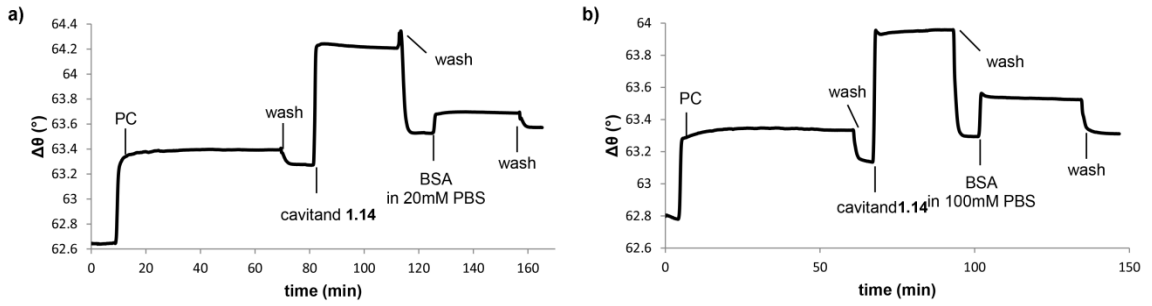

Figure 3.3: SPR sensorgrams of BSA binding at the surface of cavitand **1.14**:SLB system in PBS buffer concentrations of ; (a) 20mM; (b) 100mM.

To further examine the potential of the cavitand **1.14**:SLB surface for immobilization of biomacromolecules, other proteins possessing different sizes and charges from BSA were tested. BSA is a large protein with a molecular weight of 66.4 kDa and an isoelectrical point (pI) of 4.8, thus it is negatively charged overall in PBS buffer with pH 7.4. Cytochrome *c* (cyt *c*) is a small, well-characterized protein with a molecular weight of 12.4 kDa and a pI of 10.5. Unlike BSA that was only capable of adhesion with the system under low salt concentration, the immobilization of cyt *c* was more effective under various salt concentrations. The stronger affinity was shown in low salt concentration ($\Delta\theta_{\text{cav }\mathbf{1.14}}$ = 0.27°), but the immobilization was also observed in 100 mM PBS buffer ($\Delta\theta_{\text{cav }\mathbf{1.14}}$ = 0.25°) (Figure 3.4). In PBS buffer at pH 7.4, cyt *c* is positively charged while the carboxylate groups at the rim of cavitand **1.14** retain their negative charges.[18] As a result, the binding of cyt *c* at the cavitand **1.14**:SLB surface was observed under various salt concentrations. As a control experiment, cyt *c* was injected into a clean SLB and no binding was observed.

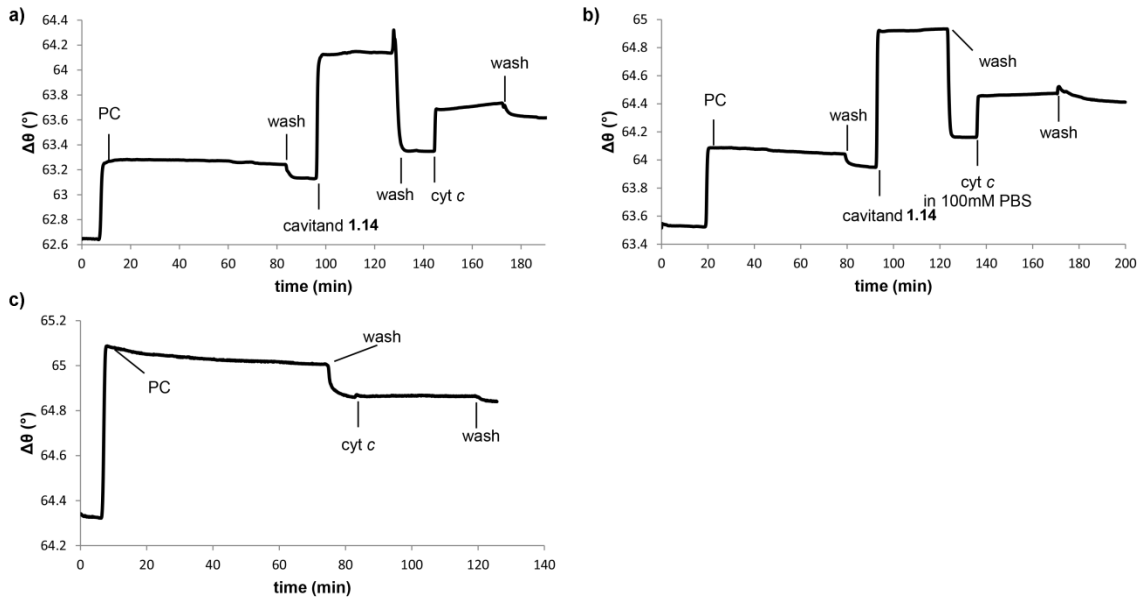

Figure 3.4: SPR sensorgrams of cyt *c* binding at the surface of: (a) SLB containing cavitand **1.14** in low salt concentrations; (b) SLB containing cavitand **1.14** in PBS buffer concentration of 100 mM; (c) SLB itself in low salt concentrations.

Myoglobin was also tested with this system. Myoglobin, with a molecular weight of 18 kDa and a pI of 7.3, was injected into the cavitand **1.14**:SLB system, and it showed binding affinity to the surface only under low salt concentration ($\Delta\theta_{\text{cav }\mathbf{1.14}}$ = 0.19°) as predicted (Figure 3.5). When the pH was adjusted to 7.4 with 100 mM PBS buffer, myoglobin exists in neutral state: therefore, there was no affinity between myoglobin and the negatively charged rim of cavitand **1.14**. Like other proteins, no binding was observed on SLB in the absence of cavitand **1.14**.

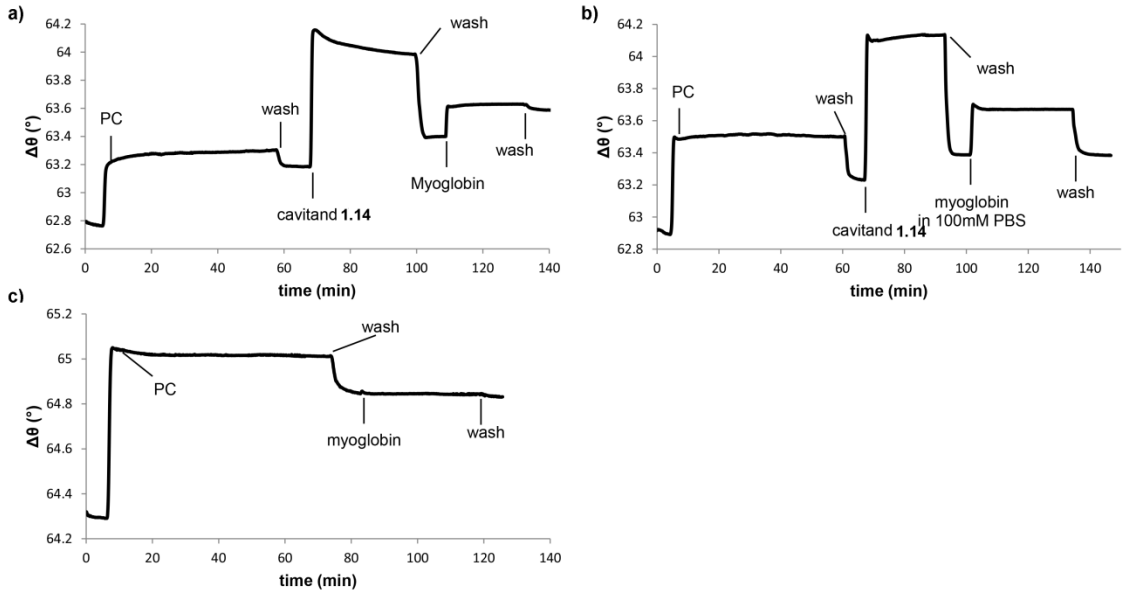

Figure 3.5: SPR sensorgrams of myogobin binding at the surface of: (a) SLB containing cavitand **1.14** in low salt concentrations; (b) SLB containing cavitand **1.14** in PBS buffer concentration of 100 mM; (c) SLB itself in low salt concentrations.

3.3 Analysis of Interactions between Native Proteins and Synthetic Receptors

To verify that the binding event between cyt *c* and cavitand **1.14** was a charge-based interaction, the interior of the cavity on cavitand **1.14** was blocked by choline (an association constant of $K_a > 10^4$ M^{-1} for cavitand **1.14** in D_2O[18]) by the addition of excess choline chloride to the cavitand **1.14**:SLB system prior to BSA injection. Once choline is bound within the cavitand, it blocks other properly sized binding molecules from entering the cavity. However, bound choline does not prevent interactions with the carboxylate groups at the rim because it does not protrude above the rim. When BSA was exposed to the choline-bound cavitand **1.14**:SLB surface, the attachment of BSA at the surface was not affected (Figure 3.6). This result supports that BSA adhesion at the cavitand **1.14**:SLB surface was a charge-based interaction.

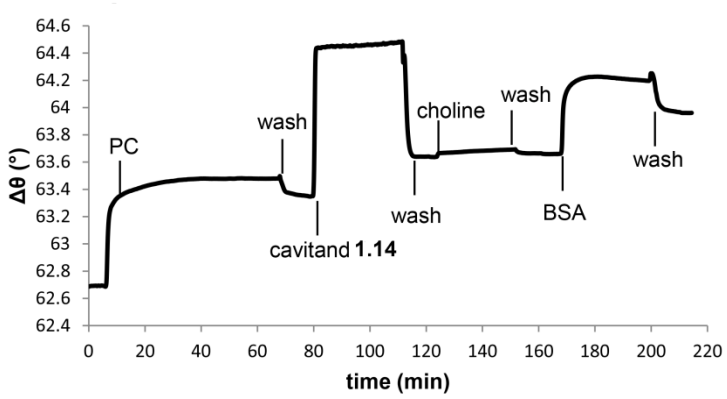

Figure 3.6: SPR sensorgram of BSA binding in low salt concentrations at choline-bound cavitand **1.14**:SLB surface.

In addition, cavitand **2.5**,[19] still possessing a cavity of identical size and similar guest binding properties to cavitand **1.14**, was employed to remove any effect of interactions with negatively charged groups at the rim. A SLB containing cavitand **2.5** was prepared via literature methods.[16] When BSA was injected into the cavitand **2.5**:SLB system, no binding was observed at both low and high salt concentrations (Figure 3.7). Other proteins such as cyt *c* and myoglobin also showed no adhesion at the cavitand **1.14**:SLB surface under both low and high salt concentrations. These results further suggest that the binding between BSA and the cavitand **1.14**:SLB surface was not a cavity-based but charge-based interaction. This host-guest charge interaction for deep cavitand is not common. Even though the functional groups at the upper rim have been used for biomimetic chemical reactions,[20] the molecular recognition process was always via complementary size and shape interactions between the guest and the cavity of the cavitand.

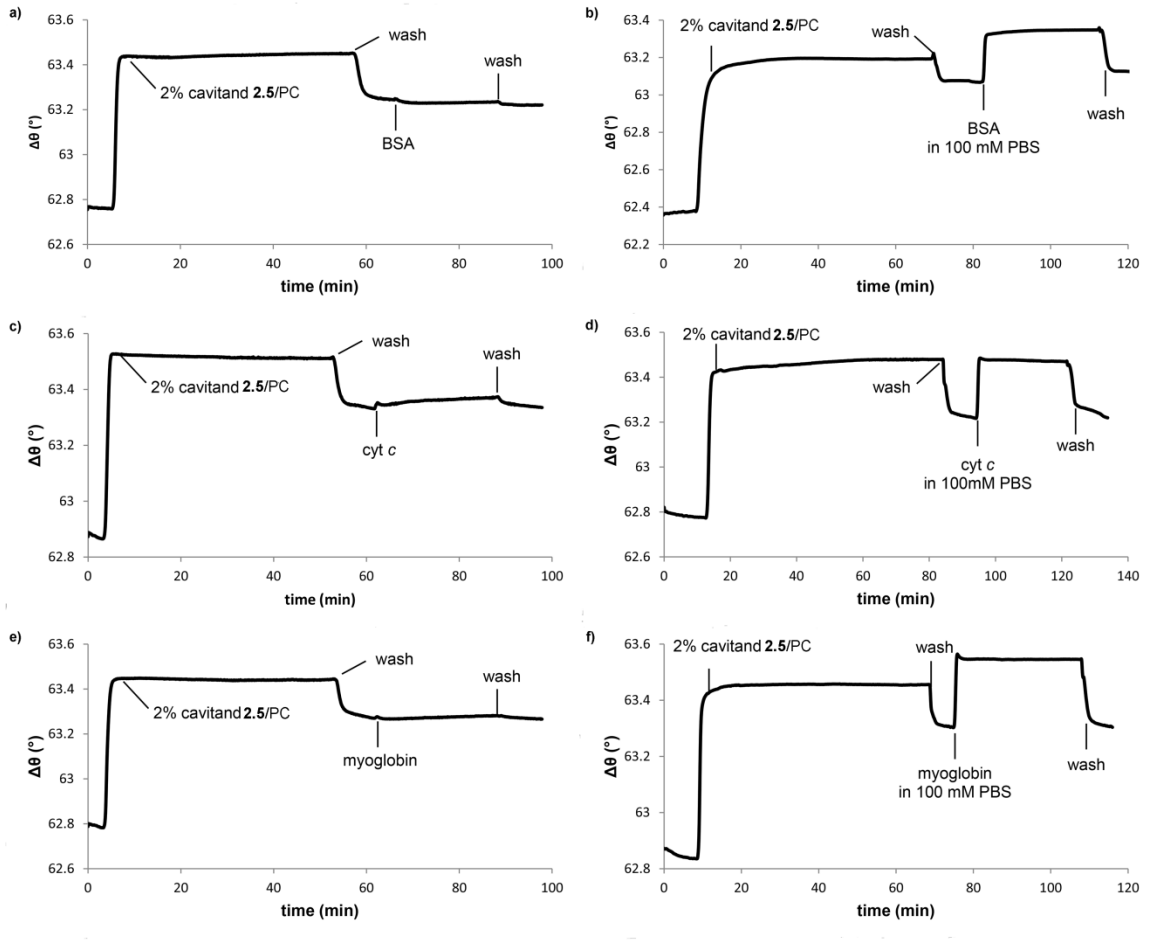

Figure 3.7: SPR sensorgrams of exposure of proteins at the cavitand **2.5**:SLB surface: (a) BSA in low salt concentration; (b) BSA in high salt concentration; (c) cyt *c* in low salt concentration; (d) cyt *c* in high salt concentration; (e) myoglobin in low salt concentration; (f) myoglobin in high salt concentration.

For quantitative analysis of the recognition event, the binding affinity of cyt *c* for cavitand **1.14**:SLB interface was determined. Preliminary attempts to calculate the equilibrium dissociation constant (K_d) were performed using SPR analysis in saturation binding mode.[15] However, this method was not suitable because cyt *c* tended to aggregate as the concentration increases. Thus, capillary electrophoresis (CE) experiments were employed in order to calculate K_d.[21] These were performed by a visiting student, Fang Si,

in Dr. Wenwan Zhong's lab. Even though it is not a perfect mimic for the cavitand **1.14**:SLB surface, the binding between cyt *c* and cavitand **1.14** incorporated into POPC vesicles can be measured by CE. First, the binding affinity between cyt *c* and cavitand **1.14** were measured. Cavitand **1.14** dissolved in the running buffer (17.5 mM phosphate buffer) was injected into the capillary and cyt *c* (3 μM) was subsequently injected. The mobility shift of cyt *c* was monitored at increasing concentrations of cavitand **1.14**, and the K_d was calculated as being 2.5 X 10^{-6} M (Figure 3.8). To measure the binding affinity of cyt *c* for the cavitand **1.14**:SLB surface, cavitand **1.14** was added at the first step of POPC vesicle formation and the mixture of cavitand **1.14** and POPC vesicle were prepared in the running buffer. The final POPC concentration was 15.8 μM, which is greater than 0.46 nM, the critical micelle concentration (cmc), but far lower than typical concentrations for coating capillary walls.[22] Not only was the separation baseline stable but the electroosmotic flow (EOF) did not change upon the injection of POPC vesicles containing cavitand **1.14** at this low POPC concentration. The cyt *c* was added after the injection of vesicles with cavitand **1.14**, and the mobility shift of cyt *c* was monitored. Similar to the result obtained from K_d measurements of cyt *c* for cavitand **1.14** itself, a K_d of 7.6 X 10^{-6} M was calculated (Figure 3.9). No binding event was observed between cyt *c* and POPC vesicle itself in the absence of cavitand **1.14**, and this observation corresponds with SPR results. This micromolar dissociation constant indicates that the binding is quite strong and this explains the observation that proteins stayed bound to the cavitand **1.14**:SLB surface even after 30 min of washing in SPR experiments. This persistence is likely due to the presence of multiple cavitands present in the SLB.

Although the on/off rate is rapid, the bound proteins do not dissociate completely and get washed away, but rather move from one position to another position on the cavitand **1.14**:SLB surface.

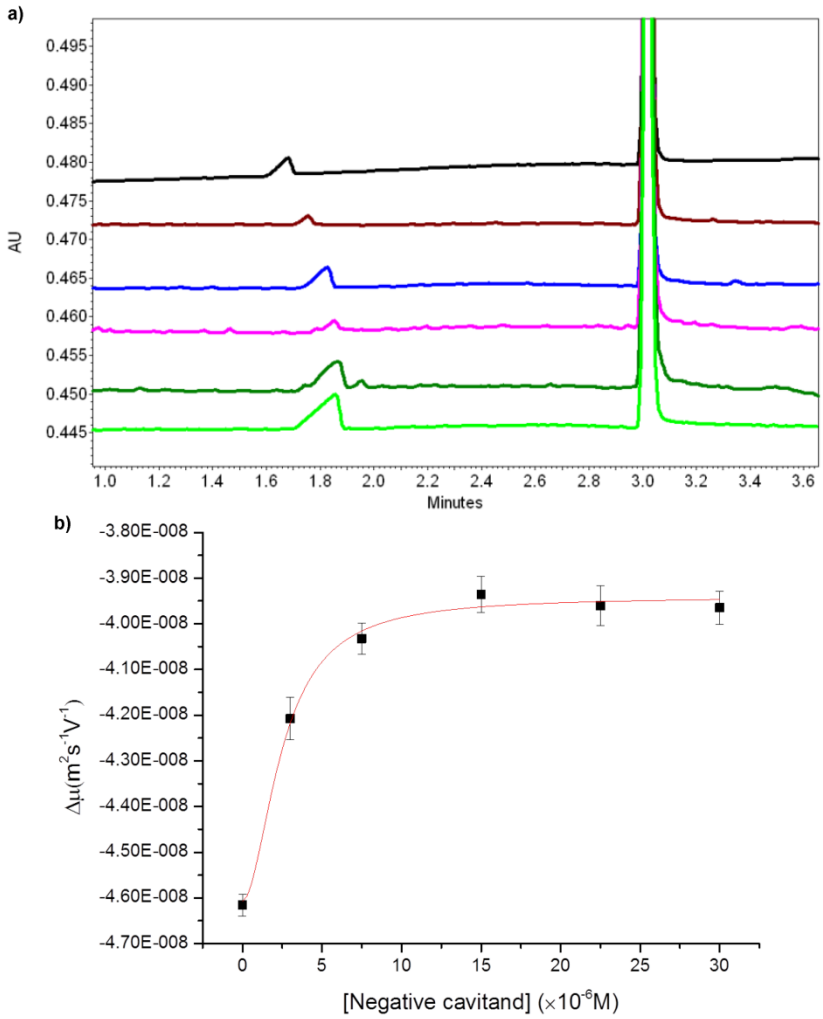

Figure 3.8: a) Electropherograms for cyt *c* incubated with cavitand **1.14** as running buffer at 191 nm, [cavitand **1.14**] = 3-30 µM, [cyt *c*] = 3 µM; b) Mobility shift of cyt *c* vs. [cavitand **1.14**].

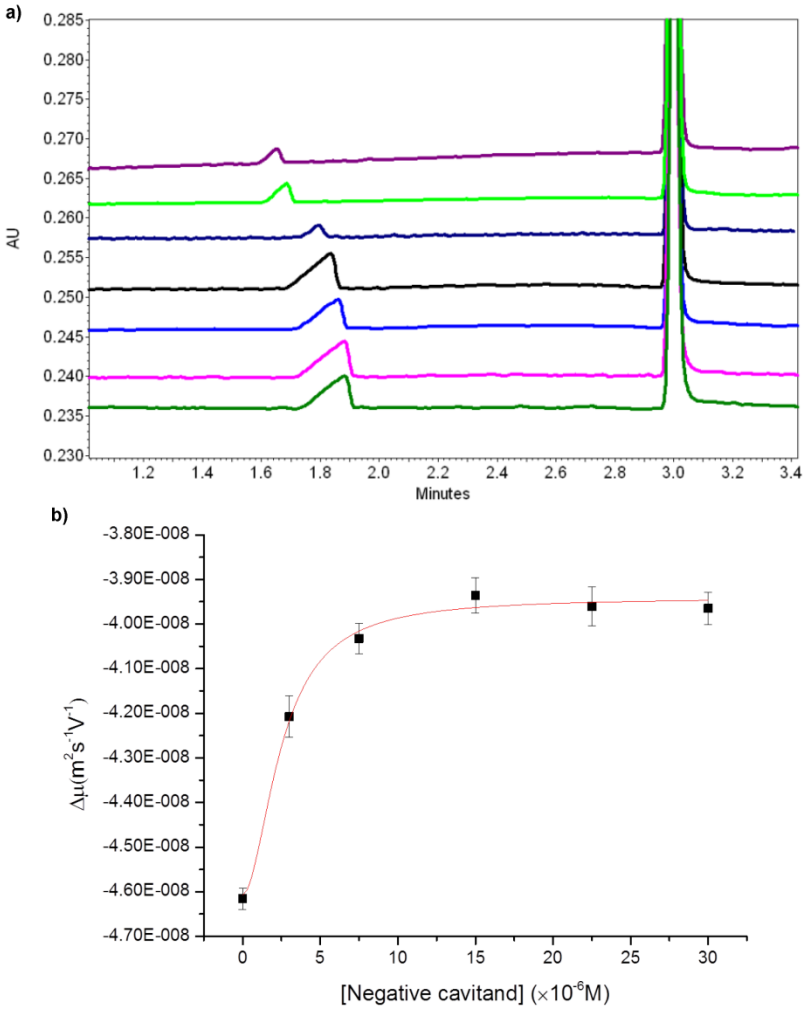

Figure 3.9: a) Electropherograms for cyt *c* incubated with cavitand **1.14** and POPC vesicles as running buffer at 191 nm, [cavitand **1.14**] = 3-30 μM, [cyt *c*] = 3 μM, [POPC] = 15.8 μM; b) Mobility shift of cyt *c* vs. [cavitand **1.14**] in the presence of POPC vesicles.

The recognition process occurs at the cavitand **1.14** containing SLB:water interface, and proteins do not have binding affinities for cavitand **1.14** in aqueous solution. In order to mimic the recognition event between proteins and cavitand **1.14** incorporated within the SLB, anionic lipids were employed. Anionic lipids are capable of incorporation into a SLB displaying carboxylate groups at the SLB:water interface and do not have binding affinity for proteins in aqueous solution.. When sodium palmitate

solution was injected into a SLB followed by the addition of BSA, an increase in resonance angle ($\Delta\theta$ = 0.16°) was observed (Figure 3.10). Moreover, the injection of sodium dodecyl sulfate into a SLB before the addition of BSA changed in resonance angle of 0.08°. Although the injection of sodium palmitate or sodium dodecyl sulfate into SLB did result in some loss of membrane due to their surfactant properties, BSA immobilization was still possible. The negatively charged lipids incorporated into the SLB acted in a manner similar to that of cavitand **1.14**; exposing carboxylate groups at the SLB:water interface. The binding affinity was, however, far less than cavitand **1.14** due to disruption of the membrane. Furthermore, like cavitand **1.14** embedded in the SLB, sodium dodecyl sulfate incorporated into the SLB was not capable of immobilization of BSA under high salt concentration. A possible assumption for the recognition event between cavitand **1.14** and proteins is that cavitand **1.14** is poorly solvated by water molecules at the SLB:water interface due to its hydrophobic surroundings. In other words, cavitand **1.14** is embedded in the hydrophobic lipid portion of the SLB, so conformational freedom of nearby water molecules is controlled. As a result, positively charged side chains on the proteins have a stronger interaction with cavitand **1.14** incorporated into the SLB, not only by hydrogen bonding but Coulombic attraction to the hydrophobic aromatic pocket of cavitand **1.14**.

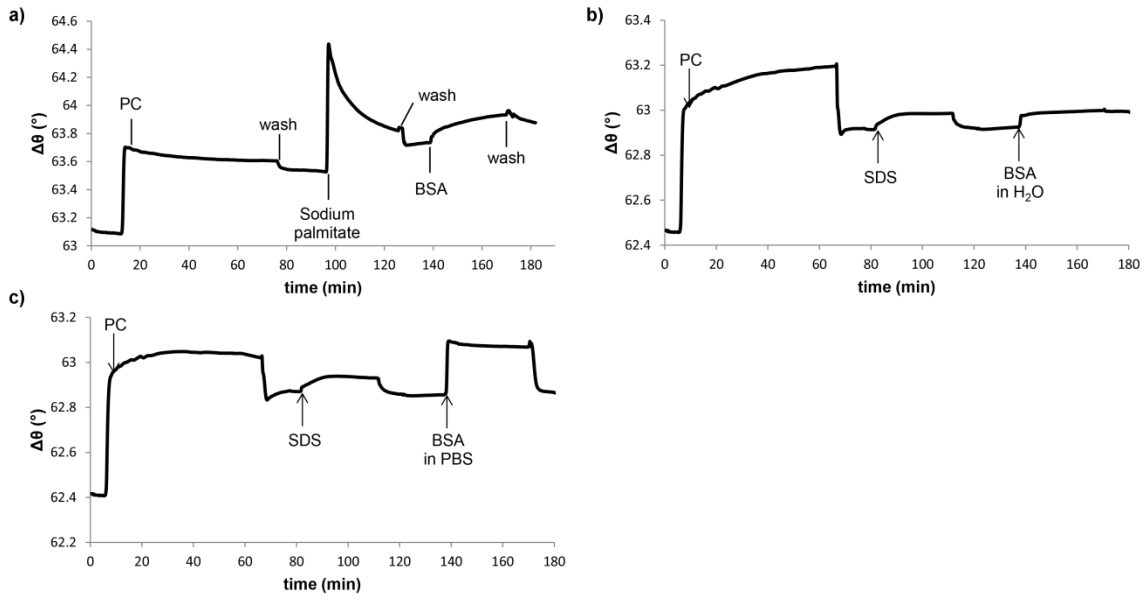

Figure 3.10: SPR sensorgrams of BSA binding event in low salt concentrations at: a) sodium palmitate:SLB surface; b) sodium dodecyl sulfate:SLB surface; c) SPR sensorgram of BSA binding event in high salt concentration at sodium dodecyl sulfate:SLB surface.

3.4 Cleavage of Insulin B by Immobilized Trypsin at a Membrane Bilayer Interface

The binding event between SLB embedded cavitand **1.14** and proteins occurs under mild conditions. It is non-covalent, and does not require protein labeling. In addition, the binding interaction occurs at ambient temperature and the binding process is rapid. Moreover, circular dichroism (CD) analysis of proteins in low or high salt concentrations revealed that there was no protein denaturing under either condition (Figure 3.11). Therefore, this cavitand **1.14**:SLB system is attractive due to its potential as a bioreactive surface.

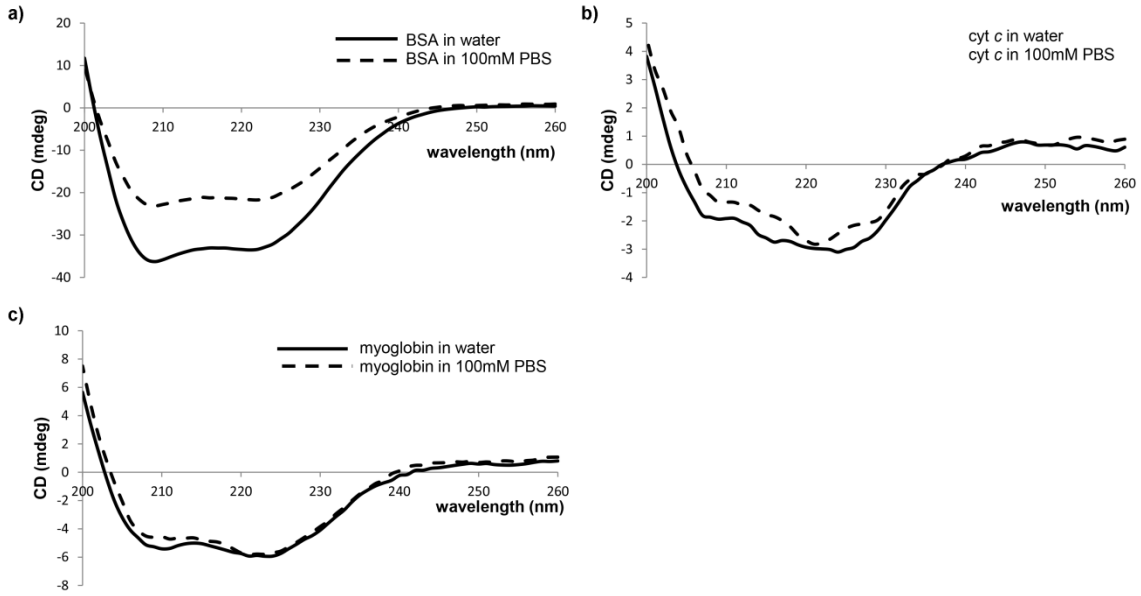

Figure 3.11: CD spectra of 2 μM protein in water (solid line) and 100 mM PBS buffer (dotted line): (a) BSA; (b) cyt *c*; (c) myoglobin.

To test the capability of the system as a bioreactive surface, trypsin was adhered on the surface to perform trypsin digestion test within the system. Trypsin is a well-characterized enzyme known to cleave arginine and lysine residues, and it is positively charged under experimental conditions (the pI of trypsin is 10.5) which helps trypsin to bind at the cavitand **1.14**:SLB surface. TPCK-trypsin, known to limit autolysis, was also tested to minimize the chance of decomposition of the enzyme during trypsin digestion. The immobilization of both trypsin and TPCK-trypsin at the cavitand **1.14**:SLB surface in low and high salt concentrations were observed (Table 3.1 and Figure 3.12). In addition, like other proteins, both enzymes showed no binding affinity for a clean SLB in the absence of cavitand **1.14** (Figure 3.13).

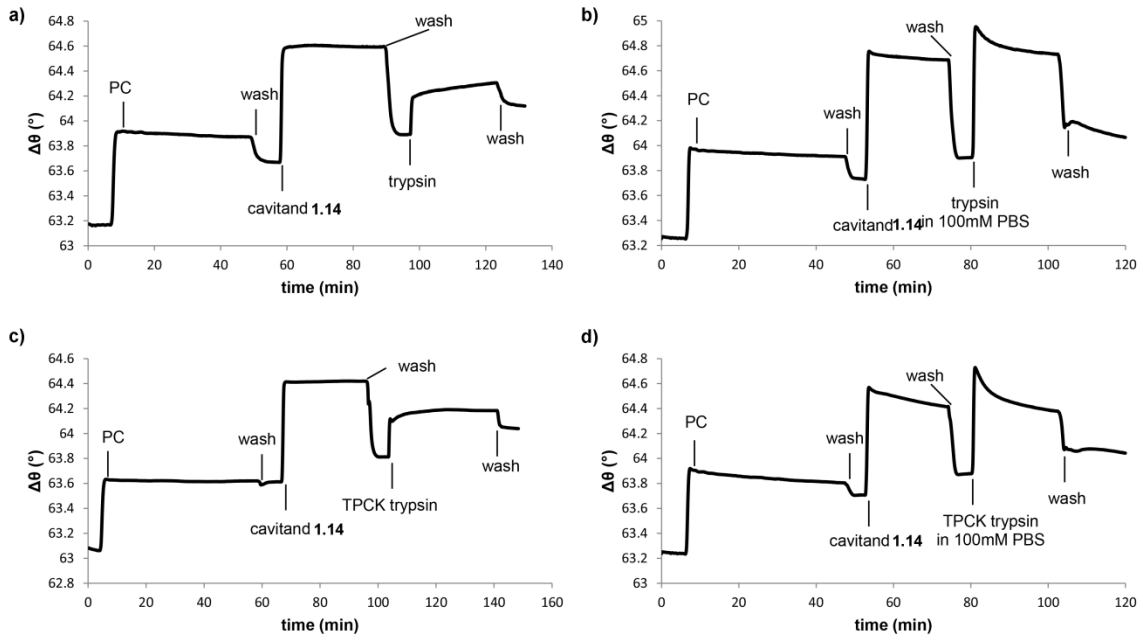

Figure 3.12: SPR sensorgrams of the binding event between cavitand **1.14**:SLB and: (a) trypsin in water; (b) trypsin in 100 mM PBS buffer; (c) TPCK-trypsin in water; (d) TPCK-trypsin in 100 mM PBS buffer.

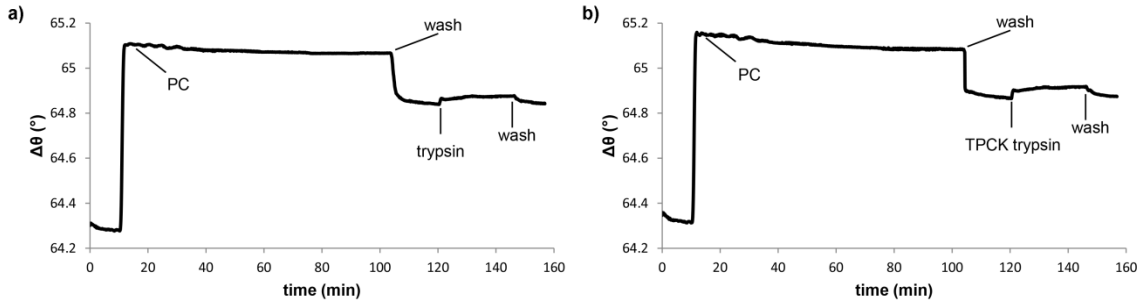

Figure 3.13: SPR sensorgrams of the exposure of enzymes in water at the surface of SLB itself in the absence of cavitand **1.14**: (a) trypsin; (b) TPCK-trypsin.

The potential of the cavitand **1.14**:SLB system as bioreactive surface was tested by injecting a commercially available insulin B into the trypsin adhered surface. Insulin B is a 30-mer oligopeptide possessing an arginine residue at position 22 and a lysine residue at position 29 (sequence shown in Figure 3.14).

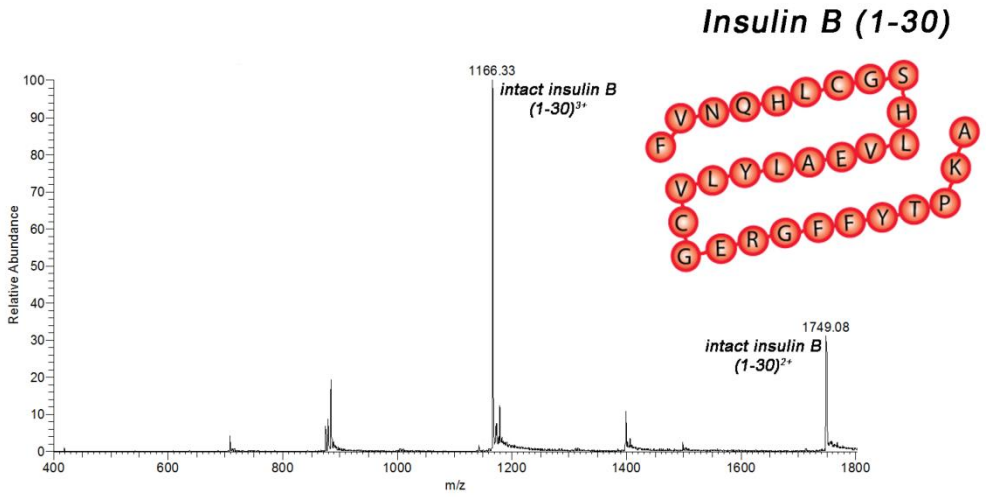

Figure 3.14: A sequence and ESI-MS analysis of oxidized insulin B.

A standard trypsin digestion was also performed in aqueous solution for comparison (Figure 3.15). When 150 µM insulin B was incubated with 7.5 µM trypsin in aqueous solution for 1 h at 298 K, only two fragments were detected by ESI-MS: peptide sequences 1-22 and 23-29 (Figure 3.16). This implies that the C-termini of arginine and lysine residues were successfully cleaved. The alanine (residue 30) formed upon cleavage at lysine group 29, and trypsin itself were not detected in ESI-MS. Similar results were obtained with TPCK-trypsin.

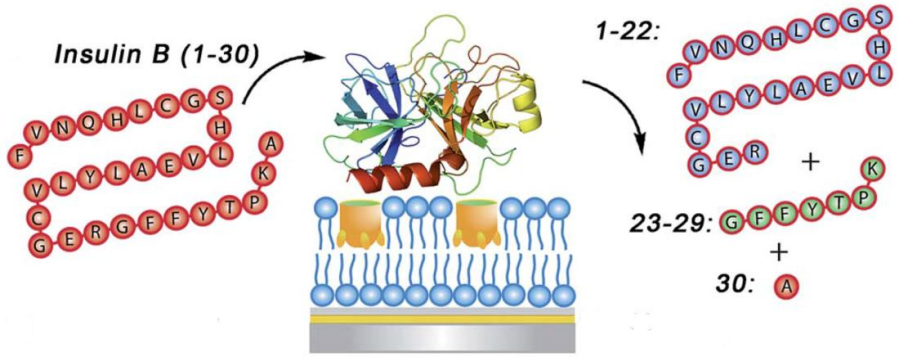

Figure 3.15: A representation trypsin digestion of insulin B in the cavitand **1.14**:SLB system.

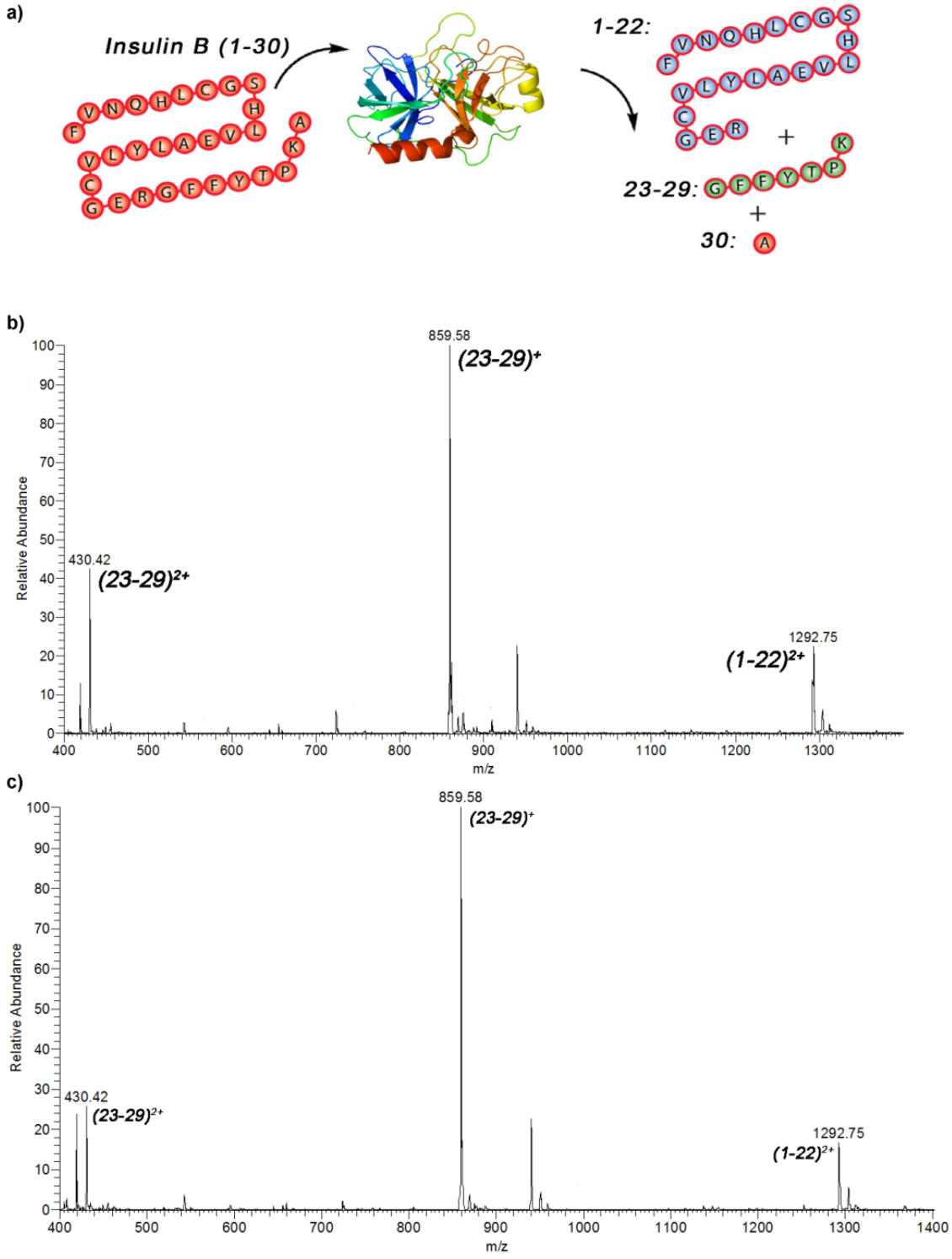

Figure 3.16: (a) A representation of insulin B digestion by immobilized trypsin; ESI-MS analysis of trypsin digestion of insulin B for 1 h at 298 K in aqueous solution: (b) trypsin; (c) TPCK-trypsin.

To perform the trypsin digestion within the cavitand **1.14**:SLB system, 300 μM insulin B was injected into the flowcell and incubated for 1 h (Figure 3.17). The collected product was analyzed by ESI-MS, and interestingly three fragments were detected: peptide sequences 1-22, 23-29, and 23-30. This indicates that the cleavage of lysine residue 29 was incomplete. Unreacted insulin B and peptide 1-29 (complete cleavage of lysine residue but not arginine group) were not observed. This result was expected since the cleavage of an arginine residue is 25 times faster than that of a lysine residue on insulin B by trypsin under similar conditions.[23,24] The peptide fragments in the collected product were separated by HPLC and each fraction was analyzed by ESI-MS. The isolated three components indeed corresponded to peptide sequences 1-22, 23-29, and 23-30 (Figure 3.18). From ESI-MS data of the collected product, trypsin itself was not detected. This implies that trypsin remained adhered at the cavitand **1.14**:SLB surface even after digestion of insulin B. As a control experiment, insulin B was incubated in the cavitand **1.14**:SLB system in the absence of adhered trypsin and no digestion or decomposition of insulin B was observed (Figure 3.19). These results indicate that the cavitand **1.14**: SLB system is a soft, bioreactive surface: the trypsin adhesion at the surface is a mild process, and the immobilized trypsin is fully functional with minimal disruption.

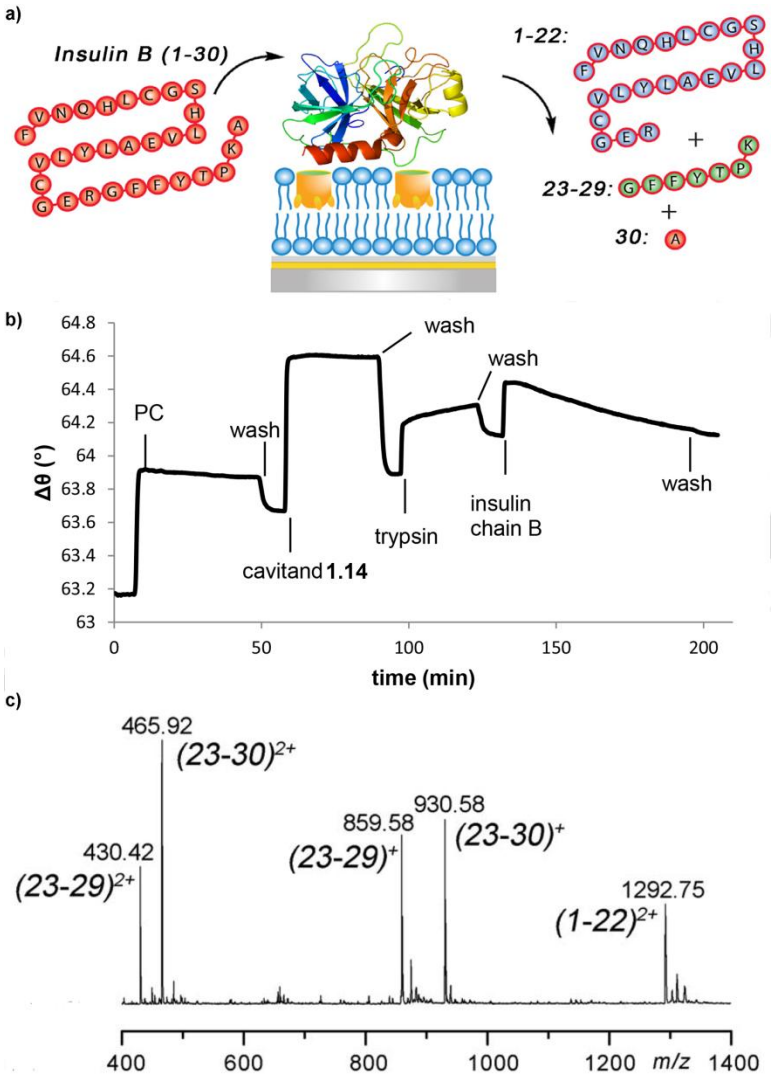

Figure 3.17: (a) A representation of insulin B digestion by immobilized trypsin; (b) SPR sensorgram of trypsin digestion of insulin B for 1 h at 298 K at the surface of cavitand **1.14**:SLB; (c) ESI-MS data for insulin B after injection to cavitand **1.14**:SLB system.

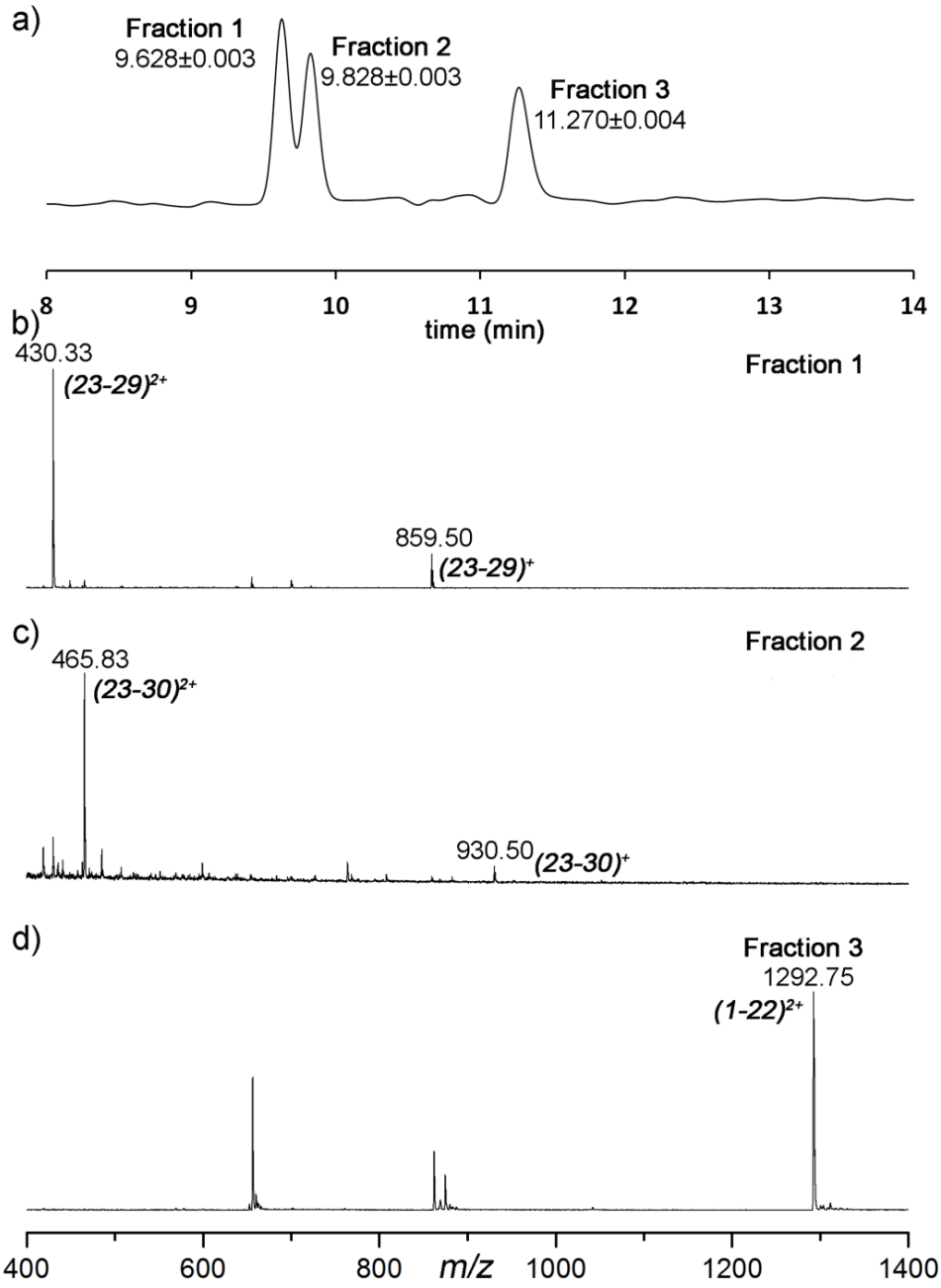

Figure 3.18: HPLC and ESI-MS analysis of trypsin digestion of insulin B for 1 h at 298 K at the surface of cavitand **1.14**:SLB: (a) HPLC data: ESI-MS data of collected fractions from HPLC: (b) fraction 1; (c) fraction 2; (d) fraction 3.

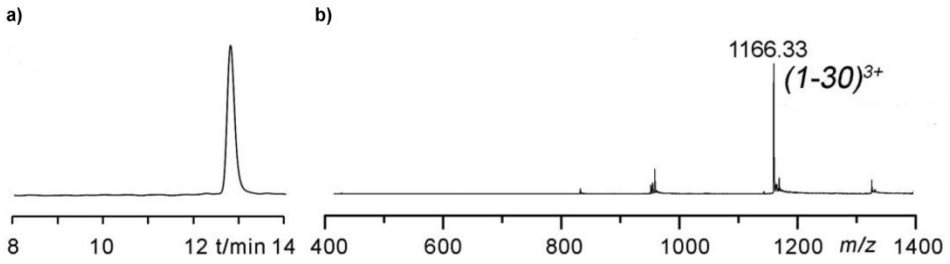

Figure 3.19: HPLC and ESI-MS data for insulin B after injection through the cavitand **1.14**:SLB surface in the absence of immobilized trypsin.

Identical experiments were performed with TPCK-trypsin and similar results were observed (Figure 3.20). If insulin B was incubated with TPCK-trypsin in aqueous solution, only two peptide fragments, 1-22 and 23-29, were detected by ESI-MS. When insulin B was incubated with immobilized TPCK-trypsin at the cavitand **1.14**:SLB surface, another peak corresponded to peptide sequence 23-30, a result of incomplete cleavage of the lysine residue at position 29, was also observed by ESI-MS. In addition, three components were isolated by HPLC whose elution times matched to the ones obtained from insulin B digestion by trypsin in the system.

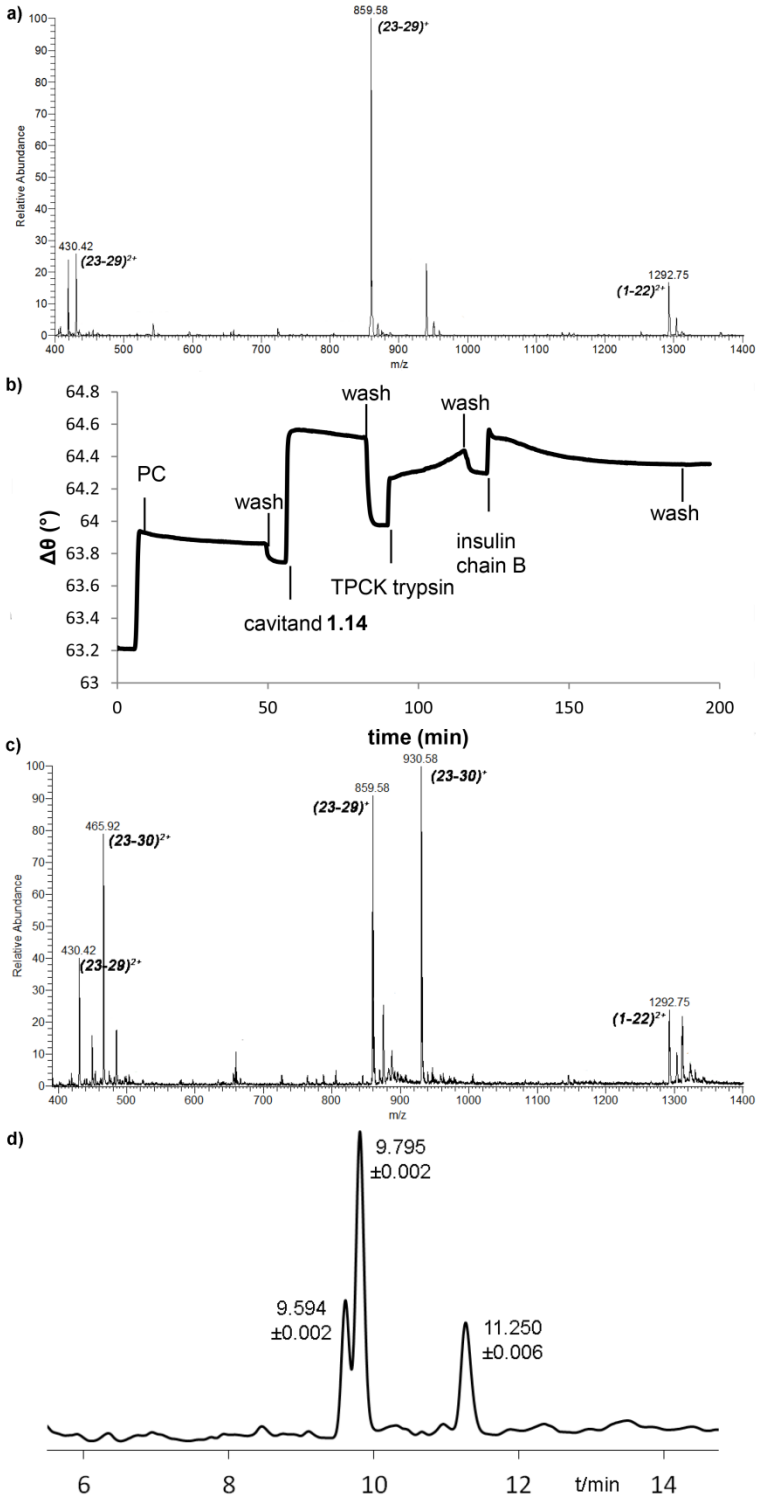

Figure 3.20: (a) ESI-MS analysis of TPCK trypsin (7.5 μM) digestion of insulin B (150 μM) for 1 h at 298 K in aqueous solution; TPCK-trypsin digestion of insulin B in cavitand **1.14**: SLB system for 1 h at 298 K: (b) SPR sensorgram; (c) ESI-MS analysis; (d) HPLC data.

The trypsin digestion within the system was interrupted easily by washing the surface off after a short period of time (10 min) (Figure 3.21). ESI-MS analysis of the collected product showed that unreacted insulin B and two peptide fragments, 1-22 and 23-30, were present. This result was consistent with the fact that the cleavage of an arginine residue is faster than that of a lysine residue in insulin B. In addition, the enzymatic process was chemically inhibited by the addition of benzamidine hydrochloride, a known trypsin inhibitor. If 300 μM insulin B was incubated at the cavitand **1.14**:SLB surface with 100 mM benzamidine hydrochloride for 1 h at 298 K, the unreacted insulin B and minimal resultants of the cleavage of arginine residue was observed (Figure 3.22).

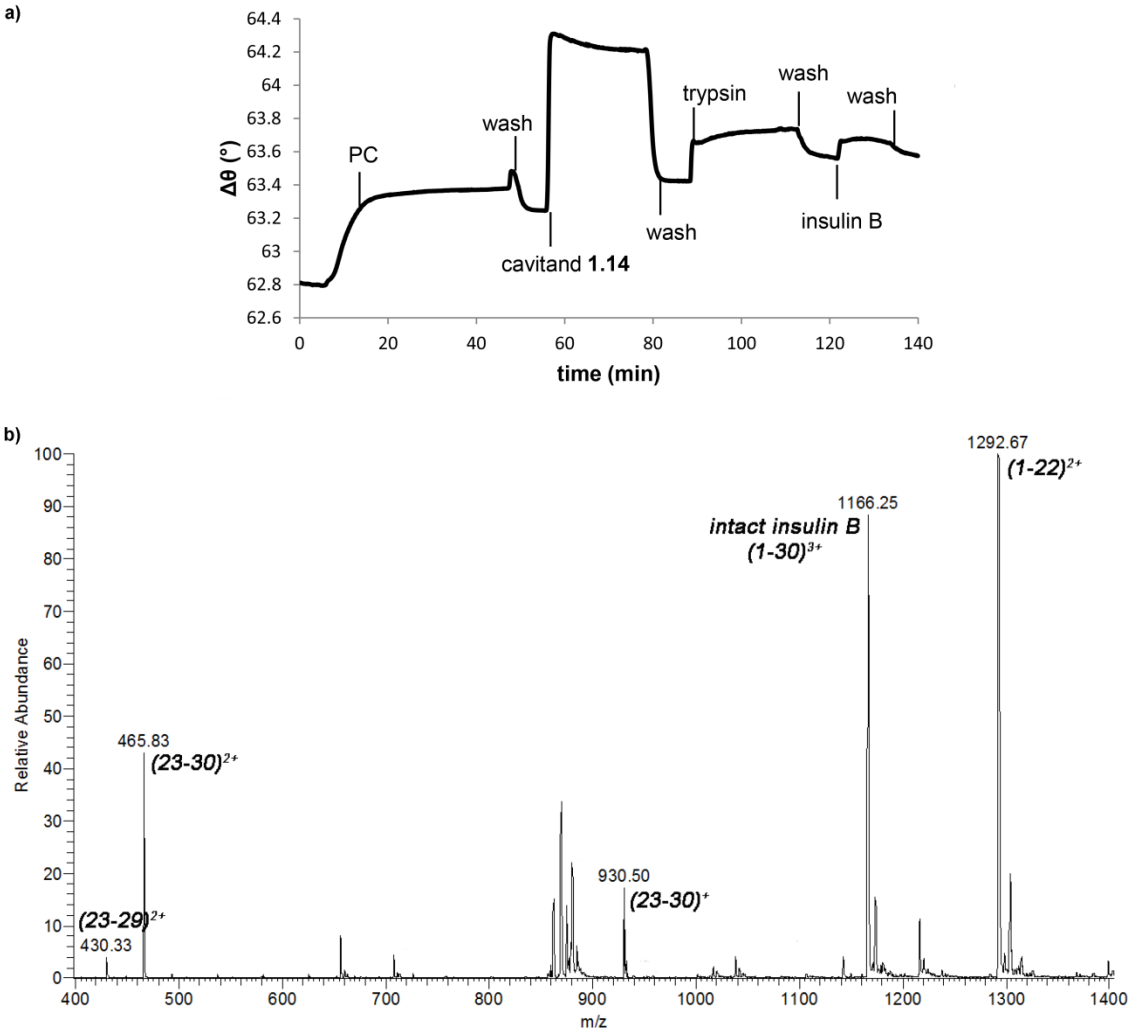

Figure 3.21: Trypsin digestion of insulin B in cavitand **1.14**: SLB system for 10 min at 298 K; (a) SPR sensorgram; (b) ESI-MS data.

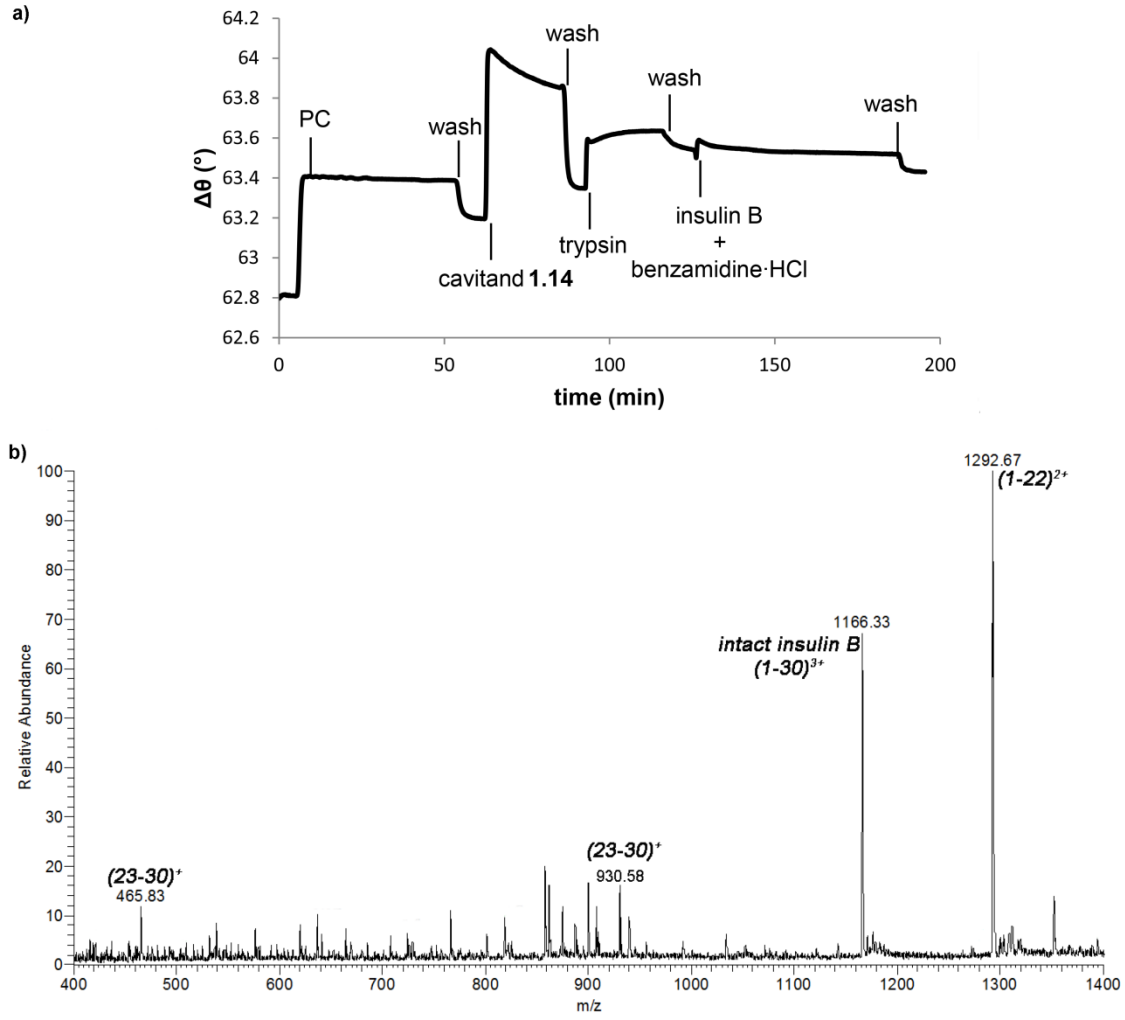

Figure 3.22: Inhibition of trypsin digestion of insulin B with 100 mM benzmidine hydrochloride at the cavitand **1.14**:SLB surface (1 h incubation at 298 K): (a) SPR sensorgram; (b) ESI-MS data.

Furthermore, the enzymatic process at the bioreactive surface was repeatable. Since adhered trypsin was not washed away from the surface, it was allowed to perform multiple trypsin digestions of insulin B at the surface. 300 µM Insulin B was incubated at the trypsin-immobilized cavitand **1.14**:SLB surface for 1 h and the cleaved peptides were washed away. Immediately, another 300 µM insulin B was injected atop the trypsin-immobilized cavitand **1.14**:SLB surface and incubated for 1 h. From both digestion

processes, three peptide fragments, 1-22, 23-29, and 23-30, were detected by ESI-MS, and no intact insulin B or trypsin were observed. This indicates that the enzymatic function of adhered trypsin was not affected by performing multiple digestions and the bioreactive surface was reusable.

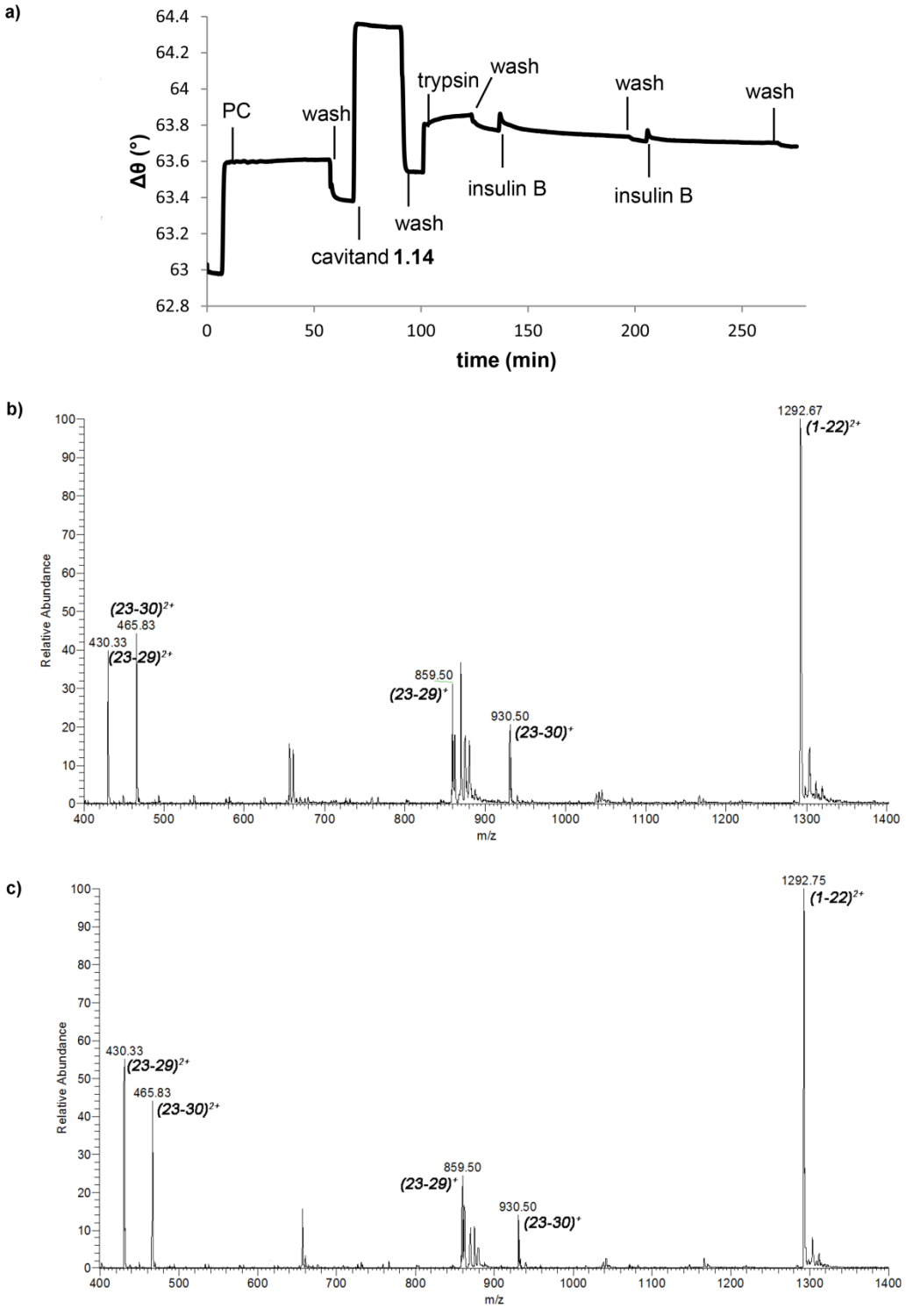

Figure 3.23: Multiple trypsin digestions of insulin B at the trypsin-immobilized cavitand **1.14**:SLB surface (1 h, 298 K): (a) SPR sensorgram; (b) ESI-MS data of product of the first digestion product; (c) ESI-MS data of product of the second digestion.

3.5 Conclusion

Cavitand **1.14** is capable of incorporating into SLBs efficiently and exposes a negatively charged rim at the SLB: water interface. This forms a bioadhesive surface and allows cavitand **1.14** to immobilize proteins atop the surface of the SLB. The binding force is not based on cavity-based interaction but instead is a form of charge-based recognition. The CE experiment showed micromolar range K_d values which mean the recognition event is very strong. Proteins with high pI values show a higher binding strength to cavitand **1.14** under high salt conditions while proteins with low pI values show an affinity for cavitand **1.14** only under low salt concentrations. This means that the selective recognition of proteins is possible by charge differences in this system. The binding event occurs under mild conditions, thus even enzymes like trypsin were immobilized successfully. Moreover, the immobilized trypsin maintained its enzymatic functionality indicating that this system can function as a bioreactive surface.

3.6 References

1. Boonyarattanakalin, S.; Martin, S. E.; Dykstra, S. A.; Peterson, B. R. "Synthetic Mimics of Small Mammalian Cell Surface Receptors." *J. Am. Chem. Soc.*, **2004**, *126*, 16379-16386.

2. Boonyarattanakalin, S.; Martin, S. E.; Sun, Q.; Peterson, B. R. "A Synthetic Mimic of Human Fc Receptors: Defined Chemical Modification of Cell Surface Enables Efficient Endocytic Uptake of Human Immunoglobilin-G." *J. Am. Chem. Soc.*, **2006**, *128*, 11463-11470.

3. Shi, J.; Yang, T.; Kataoka, S.; Zhang, Y.; Diaz, A. J.; Cremer, P. S. "GM1 Clustering Inhibits Cholera Toxin Binding in Supported Phospholipid Membranes." *J. Am. Chem. Soc.*, **2007**, *129*, 5954-5961.

4. Godula, K.; Umbel, M. L.; Rabuka, D.; Botyanszki, Z.; Bertozzi, C. R.; Parthasarathy, R. "Control of the Molecular Orientation of Membrane-Anchored Biomimetic Glycopolymers." *J. Am. Chem. Soc.*, **2009**, *131*, 10263-10268.

5. Rabuka, D.; Forstner, M. B.; Groves, J. T.; Bertozzi, C. R. "Noncovalent Cell Surface Engineering: Incorporation of Bioactive Synthetic Glycopolymers into Cellular Membranes." *J. Am. Chem. Soc.*, **2008**, *130*, 5947-5953.

6. Ludden, M. J. W.; Reinhoudt, D. N.; Huskens, J. "Molecular Printboards: Versatile Platforms for the Creation and Positioning of Supramolecular Assemblies and Materials." *Chem. Soc. Rev.*, **2006**, *35*, 1122-1134.

7. Ludden, M. J. W.; Mulder, A.; Tampé, R.; Huskens, J. "Molecular Printboards as a General Platform for Protein Immobilization: A Supramolecular Solution to Nonspecific Adsorption." *Angew. Chem. Int. Ed.*, **2007**, *46*, 4104-4107.

8. Daze, K. D.; Pinter, T.; Beshara, C. S.; Ibraheem, A.; Minaker, S. A.; Ma, M. C.; Courtemanche, R. J. M.; Campbell, R. E.; Hof, R. "Supramolecular Hosts that Recognize Methyllysines and Disrupt the Interaction between a Modified Histone Tail and its Epigenetic Reader Protein." *Chem. Sci.*, **2012**, *3*, 2695-2699.

9. Daze, K. D.; Hof, F. "The Cation-π Interaction at Protein-Protein Interaction Interfaces: Developing and Learning from Synthetic Mimics of Proteins that Bind Methylated Lysines." *Acc. Chem. Res.*, **2013**, *46*, 937-945.

10. James, L. I.; Beaver, J. E.; Rice, N. W.; Waters, M. L. “A Synthetic Receptor for Asymmetric Dimethyl Arginine.” *J. Am. Chem. Soc.*, **2013**, *135*, 6450-6455.

11. Ingerman, L. A.; Cuellar, M. E.; Waters, M. L. “A Small Molecule Receptor that Selectively Recognizes Trimethyl Lysine in a Histone Peptide with Native Protein-Like Affinity.*” Chem. Commun.*, **2010**, *46*, 1839-1841.

12. McGovern, R. E.; Fernandes, H.; Khan, A. R.; Power, N. P.; Crowley, P. B. “Protein Camouflage in Cytochrome *c*-Calixarene Complexes.” *Nat. Chem.*, **2012**, *4*, 527-533.

13. Chinai, J. M.; Taylor, A. B.; Ryno, L. M.; Hargreaves, N. D.; Morris, C. A.; Hart, P. J., Urbach, A. R. “Molecular Recognition of Insulin by a Synthetic Receptor.” *J. Am. Chem. Soc.*, **2011**, *133*, 8810-8813.

14. Bier, D.; Rose, R.; Brave-Rodriguez, K.; Bartel, M.; Ramirez-Anguita, J. M.; Dutt, S.; Wilch, C.; Klärner, F. –G.; Sanchez-Garcia, E.; Schrader, T.; Ottmann, C. “Molecular Tweezers Modulate 14-3-3 Protein-Protein Interactions.” *Nat. Chem.*, **2013**, *5*, 234-239.

15. Liu, Y.; Liao, P.; Cheng, Q.; Hooley, R. J. “Protein and Small Molecule Recognition Properties of Deep Cavitands in a Supported Lipid Membrane Determined by Calcination-Enhanced SPR Spectroscopy.” *J. Am. Chem. Soc.*, **2010**, *132*, 10383-10390.

16. Ghang, Y. –J.; Lloyd, J. J.; Moehlig, M. P.; Arguelles, J. K.; Mettry, M.; Zhang, X.; Julian, R. R.; Cheng, Q.; Hooley, R. J. “Labeled Protein Recognition at a Membrane Bilayer Interface by Embedded Synthetic Receptors.” *Langmuir*, **2014**, *30*, 10161-10166.

17. Ghang, Y. –J.; Perez, L.; Morgan, M. A.; Si, F.; Hamdy, O. M.; Beecher, C. N.; Larive, C. K.; Julian, R. R., Zhong, W.; Cheng, Q.; Hooley, R. J. “Anionic Deep Cavitands Enable the Adhesion of Unmodified Proteins at a Membrane Bilayer.” *Soft Matter*, **2014**, *10*, 9651-9656.

18. Biros, S. M.; Ullrich, E. C.; Hof, F.; Trembleau, L.; Rebek, J., Jr. “Kinetically Stable Complexes in Water: The Role of Hydration and Hydrophobicity.” *J. Am. Chem. Soc.*, **2004**, *126*, 2870-2876.

19. Rafai Far, A.; Shivanyuk, A.; Rebek, J., Jr. “Water-Stabilized Cavitands.” *J. Am. Chem. Soc.*, **2002**, *124*, 2854-2855.

20. Hooley, R. J.; Rebek, J. Jr. “Chemictry and Catalysis in Functional Cavitands.” *Chem. Biol.*, **2009**, *16*, 255-264.

21. Tseng, W. –L; Chang, H. –T.; Hsu, S. –M.; Chen, R. –J.; Lin, S. “Immunoaffinity Capillary Electrophoresis: Determination of Binding Constant and Stoichiometry for Antibody-Antigen Interaction.” *Electrophoresis*, **2002**, *23*, 836-846.

22. Lindén, M. V.; Meinander, K.; Helle, A.; Yohannes, G.; Riekkola, M. –L.; Butcher, S. J.; Viitala, T.; Weidmer, S. K. “Characterization of Phosphatidylcholine/Polyethylene Glycol-Lipid Aggregates and Their Use as Coatings and Carriers in Capillary Electrophoresis.” *Electropheresis*, **2008**, *29*, 852-862.

23. Wang, S. –S.; Carpenter, F. H. “Kinetics of the Tryptic Hydrolysis of the Oxidized B Chain of Bovine Insulin.” *Biochemistry*, **1967**, *6*, 215-224.

24. Huber, R.; Bode, W. “Structural Basis of the Activation and Action of Trypsin.” *Acc. Chem. Res.*, **1978**, *11*, 114-122.

Chapter Four: Binding Properties of Synthetic Receptors at a Lipid Raft Containing Membrane Bilayer Interface

4.1 Introduction

As shown in Chapter 2 and Chapter 3, our previous work was focused on the molecular recognition by cavitands embedded within POPC lipid bilayers. Membranes in mammalian cells, however, are not consisted with phospholipids alone, but contain many other lipids and sterols. Cholesterol is one of the major sterols found in mammalian cells and is involved in cell proliferation.[1] In addition, sphingomyelin is an enriched lipids found within membranes of mammalian cells. Cholesterol associates with sphingomyelin within plasma membranes due to its tendency to interact with saturated phospholipids rather than unsaturated lipids.[1] Since there is a repulsive interaction between POPC bilayers and cholesterol,[2] this interaction makes cholesterol and sphingomyelin form segregated lipid domains (lipid rafts).[3] Lipid rafts are involved in many important biological events, such as cell signaling.[4] Thus, there have been a lot of efforts to characterize the physical properties of lipid rafts depending on the different compositions and at varying temperatures.[5-9] Since plasma membranes in mammalian cells contain cholesterol and sphingomyelin in high levels, it is important to investigate molecular recognition by cavitand **1.14** in membrane bilayers containing cholesterol /sphingomyelin -rich domains.

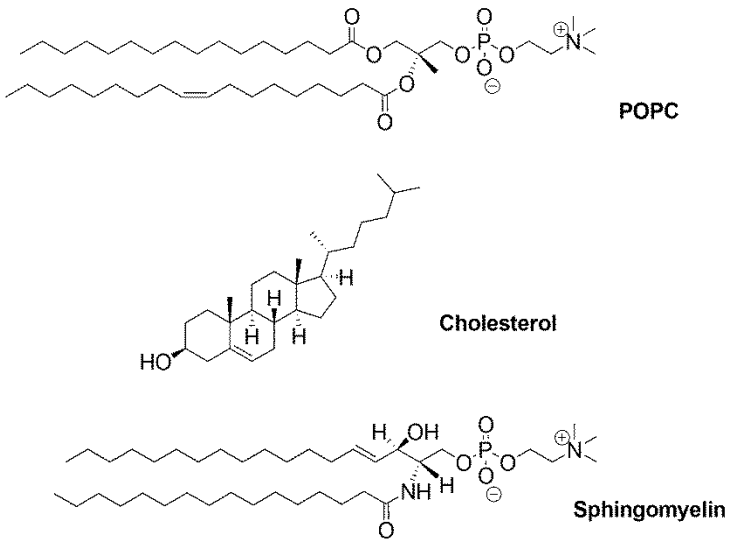

Figure 4.1: Structure of POPC, cholesterol, and sphingomyelin.

4.2 Formation of Lipid Raft Containing Lipid Bilayers

It has been reported that the formation of POPC lipid bilayers with cholesterol does not occur if the concentration of cholesterol exceeds 34 mol %.[10] Thus, as a start of the investigation of the molecular recognition behavior of cavitand **1.14** in lipid bilayers containing lipid rafts, the concentrations of cholesterol or sphingomyelin in POPC vesicles that can form lipid bilayers properly were determined by SPR analysis.

First, various concentrations of cholesterol mixed in POPC vesicles were tested. Vesicles made with binary mixtures of various molar ratios of POPC and cholesterol - 95/5, 90/10, 80/20, and 60/40 - were prepared. Cholesterol dissolved in chloroform was added at the first step of POPC vesicle preparation, and the binary mixed vesicles were prepared via a literature method.[11] These vesicles were injected on a nanoglassified calcinated gold chip, and the resonance angle changes upon the formation of lipid bilayers were monitored by SPR (Figure 4.2). It was observed that lipid bilayers were

formed when as much as 20 mol % cholesterol was mixed in POPC vesicles. If 40 mol % cholesterol or higher was present in POPC vesicles, lipid bilayers were not formed properly based on the observed resonance angle change of <0.05°. This observation corresponds to the literature result that lipid bilayers cannot form with over 34 mol % cholesterol.[10] Interestingly, the formation of lipid bilayers containing 20 mol % cholesterol changed the resonance angle by 0.7° which is larger than the resonance angle change normally observed for the formation of SLB with only POPC (~ 0.4°). This may be due to the thickness of the bilayers. Lipid bilayers containing lipid rafts are thicker than that of regular lipid bilayers,[7] thus the large resonance angle change for the formation of lipid bilayers with lipid rafts was observed.

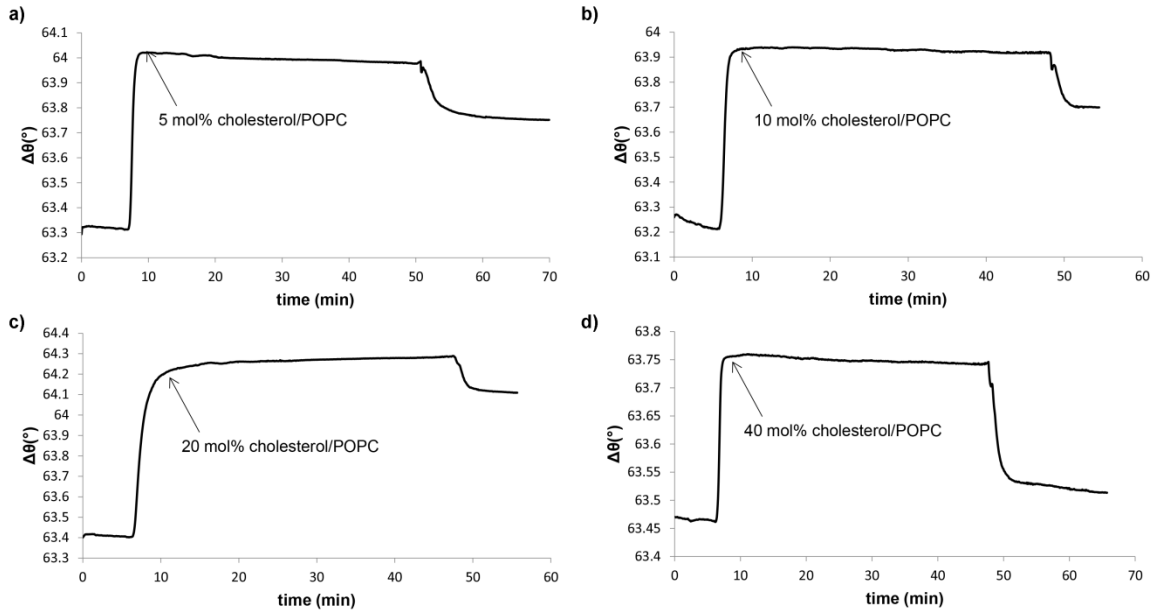

Figure 4.2: SPR sensorgrams of the formation of lipid bilayers by the injection of vesicles prepared from binary mixtures of POPC/cholesterol (mol %): (a) 95/5; (b) 90/10; (c) 80/20; (d) 60/40.

Vesicles made from binary mixtures of POPC and sphingomyelin were also tested for the ability to form lipid bilayers. Vesicles containing POPC and sphingomyelin with two different molar ratios - 90/10 and 80/20 - were prepared. As the preparation of vesicles containing binary mixtures of POPC and cholesterol, sphingomyelin was dissolved in chloroform first and desired amounts of it was mixed with POPC in chloroform. The rest of the steps were identical to those of regular POPC vesicle preparation steps.[11] According to SPR analysis, like vesicles prepared from binary mixtures of POPC and cholesterol, the POPC vesicles containing up to 20 mol % sphingomyelin successfully formed lipid bilayers (Figure 4.3). A larger resonance angle change was also observed from the formation of lipid bilayers containing 80/20 molar ratios of POPC/sphingomyelin than that of POPC lipid bilayers. This may be due to the tighter packing of acyl chains in sphingomyelin, and this caused the thickness of the lipid bilayers to increase.[12]

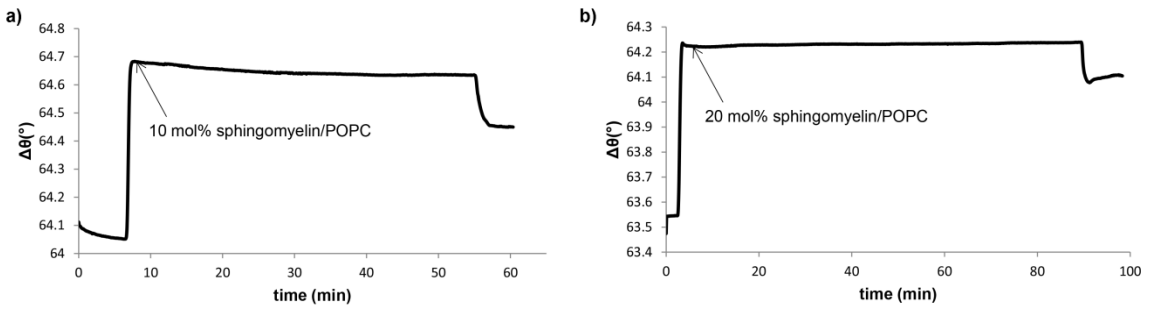

Figure 4.3: SPR sensorgrams of the formation of lipid bilayers by the injection of vesicles prepared from binary mixtures of POPC/sphingomyelin (mol %): (a) 90/10; (b) 80/20.

Vesicles containing ternary mixtures of POPC, cholesterol, and sphingomyelin with two different molar ratios – 80/10/10 and 60/20/20 – were also prepared, and the

formation of lipid bilayers by those were investigated by SPR (Figure 4.4). The successful formation of lipid bilayers from both vesicles was observed. It was surprising that lipid bilayers still formed when cholesterol and sphingomyelin were mixed in concentrations as high as 40 mol % in POPC.

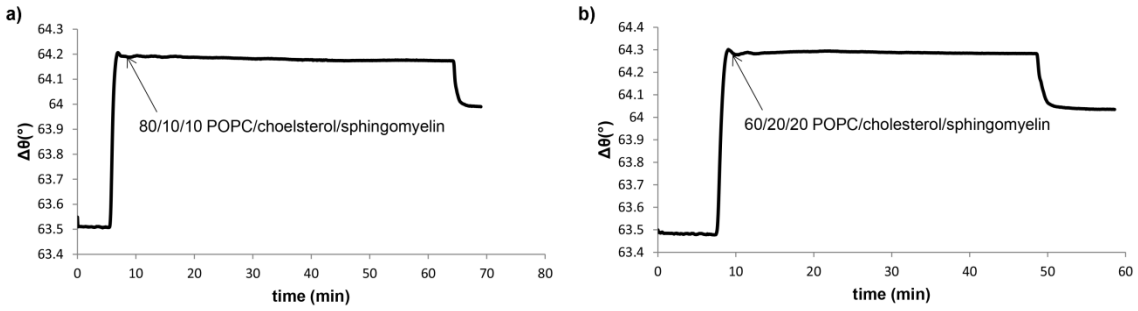

Figure 4.4: SPR sensorgrams of the formation of lipid bilayers by the injection of vesicles prepared from ternary mixtures of POPC/cholesterol/sphingomyelin (mol %): (a) 80/10/10; (b) 60/20/20.

4.3 Physical Properties (Mobility) of Lipid Bilayers Prepared from Ternary Mixtures of POPC/Cholesterol/Sphingomyelin

In order to confirm the existence of lipid rafts within the lipid bilayers formed by ternary mixtures of POPC/cholesterol/sphingomyelin, 2 mol % 1-palmitoyl-2-{12-[(7-nitro-2-1,3-benzoxadiazol-4-yl)amino]hexanoyl}-*sn*-glycero-3-phosphocholine (NBD-PC) was mixed when the vesicles were prepared, and confocal fluorescence microscopy was employed to visualize the lipid bilayers. NBD-PC would be incorporated within POPC, so areas of POPC lipid bilayers would be fluorescent in green while lipid rafts containing only cholesterol and sphingomyelin would be dark without any fluorescence. Unfortunately, none of dark phase was observed when the lipid bilayers were visualized.

There are two possibilities for why lipid rafts were not observed: either there was no formation of lipid rafts, or the formed lipid rafts were too small to visualize by confocal fluorescence microscopy. It has been reported that if the size of the rafts formed by POPC/cholesterol/sphingomyelin system is smaller than 75-100 nm, it is not possible to distinguish these domains by fluorescence microscopy.[13,14] Instead, a special type of microscopy called Brester angle microscopy was employed to visualize lipid rafts successfully.[12] Cho and coworkers were able to visualize lipid rafts within supported lipid bilayers by confocal fluorescence microscopy.[9] The lipid bilayers were, however, made by ~ 60 mol % cholesterol in 1,2-dioleoyl-sn-glycero-3-phosphocholine (DOPC) via a solvent-assisted lipid bilayer formation technique. This high concentration of cholesterol may have induced the formation of larger lipid rafts, thus the visualization of these large lipid rafts was possible.

Since it was not possible to visualize lipid rafts via confocal fluorescence microscopy, the formation of lipid rafts in lipid bilayers was confirmed by alternative methods. In order to confirm the existence of lipid rafts in the lipid bilayers indirectly, fluorescence recovery after photobleaching (FRAP) experiments were performed. FRAP is a technique used to analyze the mobility of lipids in lipid bilayers.[15] A high intensity laser light bleaches a region of fluorescent lipid bilayer sample, and a low intensity laser light measures the recovery of fluorescence of the region. This recovery of fluorescence occurs by the outward diffusion of the bleached fluorescent lipids and the inward diffusion of neighboring non-bleached fluorescent lipids into the bleached region. Here, the assumption was made that the mobility of lipids would be slower for the bilayers

containing rafts than those containing only POPC because lipid rafts would act as obstacles for the diffusion of POPC lipids.

This time, the lipid bilayers were not formed in the SPR flowcell, but it were prepared on a glass slide directly. Circular wells were fabricated on a microscopy cover glass by attaching polydimethylsiloxane (PDMS) punched with holes,[16] and 100 μM vesicles prepared from ternary mixtures of POPC/cholesterol/sphingomyelin with 2 mol % NBD-PC were added into the wells. The vesicles were incubated for 30 min to form lipid bilayers and extensive washing followed to remove any excess lipids. As shown in Figure 4.5, no dark phases but fluorescent lipid bilayers were observed from lipid bilayers containing ternary mixtures of POPC/cholesterol/sphingomyelin in molar ratios of 78/10/10 and 58/20/20 with 2 mol % NBD-PC.

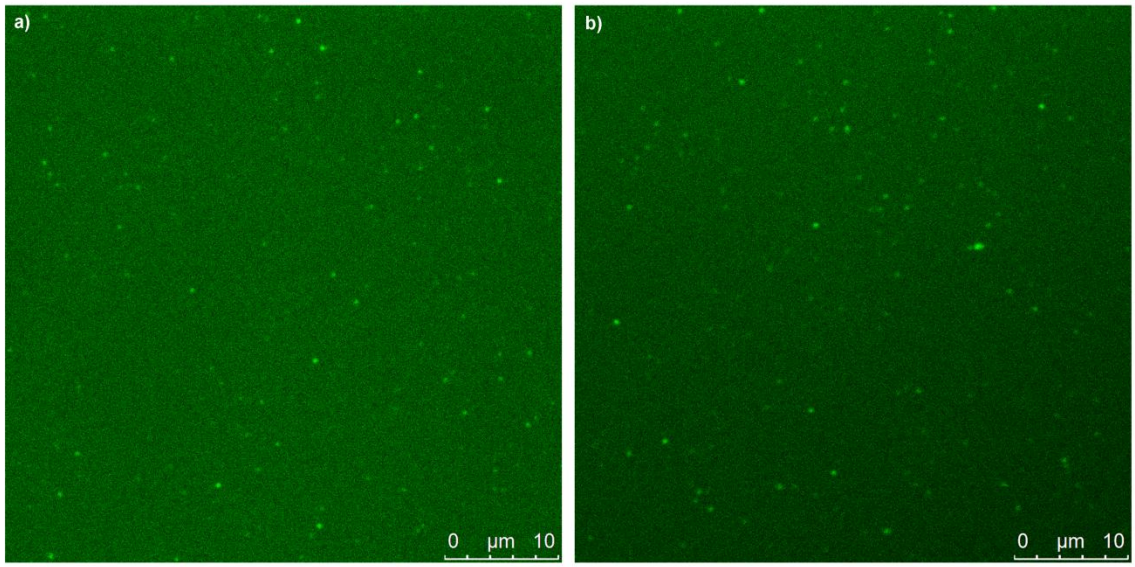

Figure 4.5: Confocal fluorescence microscopy images of lipid bilayers containing 2 mol % NBD-PC and ternary mixtures of POPC/cholesterol/sphingomyelin (mol %): (a) 78/10/10; (b) 58/20/20.

Next, FRAP experiments were performed with these lipid bilayers. As shown in Figure 4.6, the recovery of fluorescence of each bleached spot was observed from both lipid bilayers. The diffusion coefficients were determined by the methods of Axelrod and Soumpasis.[17,18]

$$F_{FRAP} = (F_n - F_0)/(1 - F_0) \qquad \text{(eq 2)}$$

Here, F_n is a normalized value of the intensity of fluorescence of the bleached spot over a fluorescent background region of the same size, and F_0 is a normalized intensity of the bleached spot immediately after bleaching. F_{FRAP} was plotted against time, and the graph was fitted to a first order exponential function.

$$D = (\omega^2/4t_{1/2})\gamma \qquad \text{(eq 3)}$$

The diffusion equation (eq 3) was applied to calculate the diffusion coefficient. Here, D is the diffusion coefficient, ω is the full width at half maximum of the Gaussian profile of the focused laser, $t_{1/2}$ is the half-time recovery obtained from the graph fit, and γ is a correction factor that accounts for the laser beam geometry.

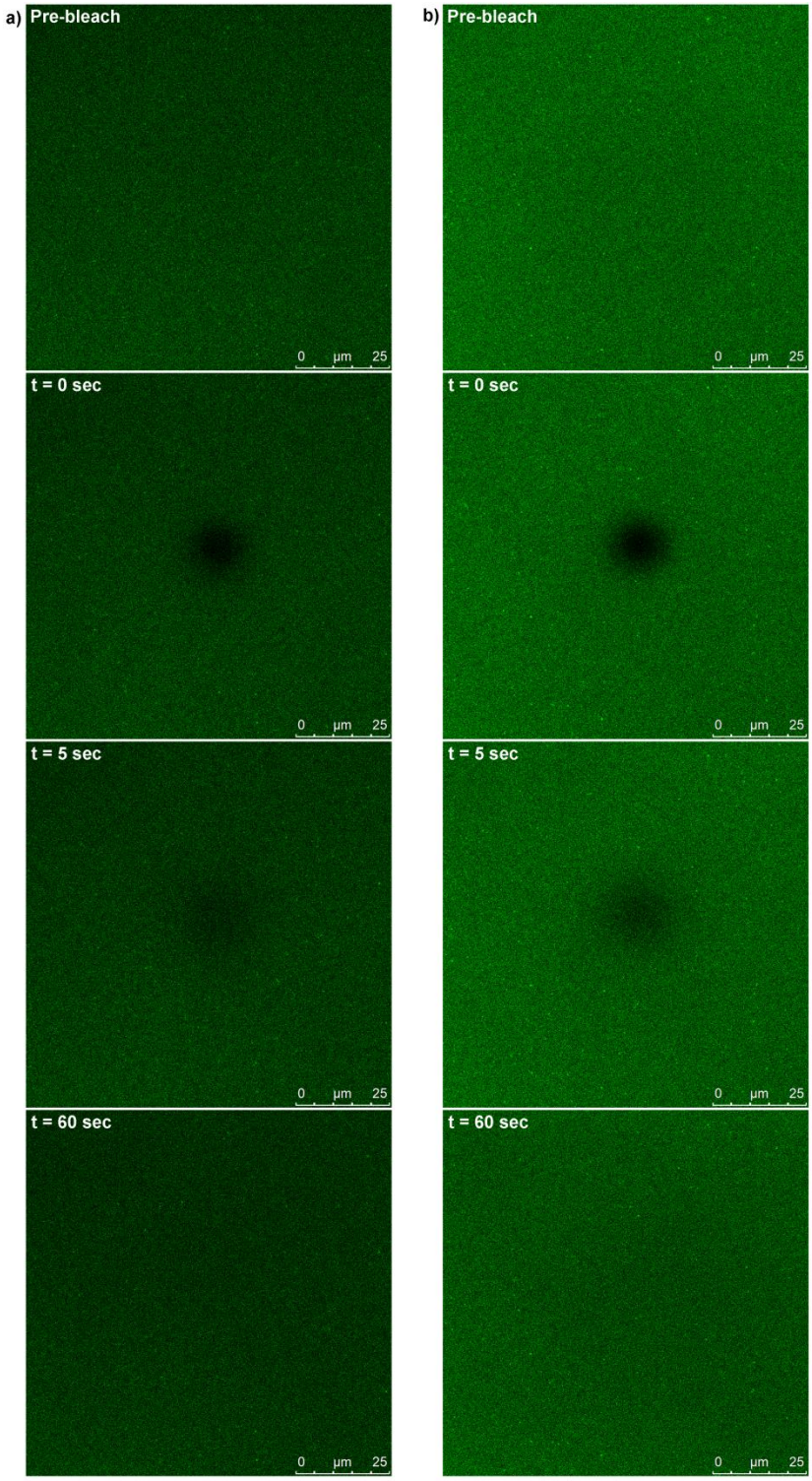

Figure 4.6: Confocal fluorescence microscopy images of the FRAP experiments for lipid bilayers containing 2 mol % NBD-PC and ternary mixtures of POPC/cholesterol/sphingomyelin (mol %): (a) 78/10/10; (b) 58/20/20.

FRAP recovery fitting curves for lipid bilayers containing 2 mol % NBD-PC with ternary mixtures of POPC/cholesterol/sphingomyelin in molar ratios of 78/10/10 and 58/20/20 are shown in Figure 4.7, and the calculated diffusion coefficients were 3.2 $\mu m^2 s^{-1}$ and 3.5 $\mu m^2 s^{-1}$, respectively. These values are smaller than the literature values of pure POPC lipid bilayers (~ 4.0 $\mu m^2 s^{-1}$).[19] These low diffusion coefficients support the assumption that the lipid rafts, formed by the mixture of cholesterol and sphingomyelin in POPC lipid bilayers, obstruct the diffusion of POPC lipids, and provide evidence for the existence of lipid rafts in the system.

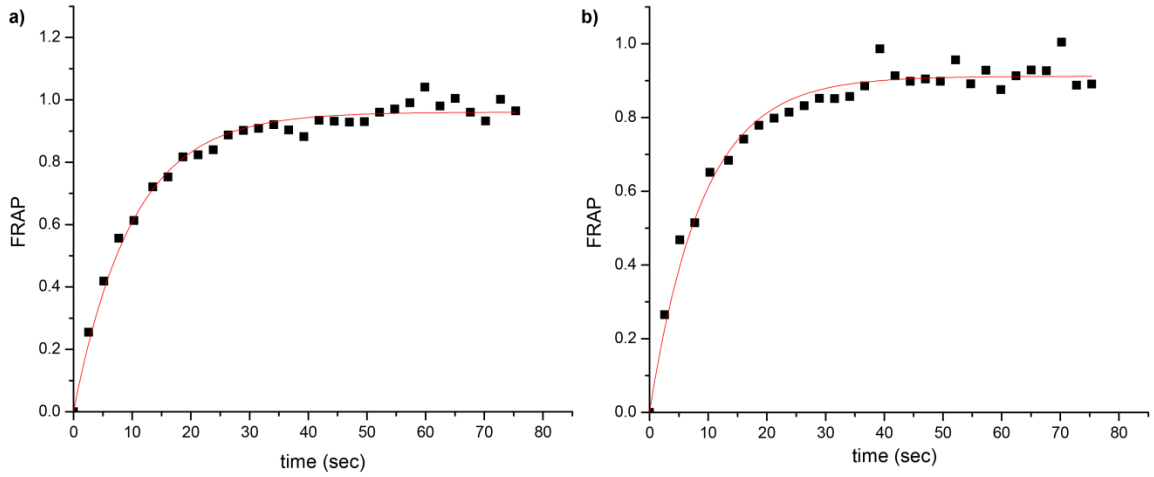

Figure 4.7: FRAP recovery fitting curve obtained with lipid bilayers containing 2 mol % NBD-PC and ternary mixtures of POPC/cholesterol/sphingomyelin (mol %): (a) 78/10/10; (b) 58/20/20.

4.4 Binding Properties of Synthetic Receptors in Lipid Rafts Containing Lipid Bilayers

Since POPC lipid bilayer formation containing cholesterol and sphingomyelin was successful, the binding properties of cavitand **1.14** in sterol-rich membranes were investigated. Lipid bilayers containing POPC/cholesterol in a molar ratio of 80/20 were

formed followed by the injection of cavitand **1.14** and BSA (Figure 4.8). It has already been shown that cavitand **1.14** incorporated within SLB is capable of immobilizing BSA in low salt concentrations.[20] The SLB was replaced with cholesterol-rich bilayers and, the change in resonance angle for the injected cavitand **1.14** was observed via SPR. This indicates that cavitand **1.14** is still capable of self-incorporating within lipid bilayers containing lipid rafts. When BSA in low salt concentrations was injected into the cavitand **1.14**:POPC/cholesterol system, the immobilization of BSA was successfully observed. Similar results were obtained by employing POPC/sphingomyelin lipid bilayers and POPC/cholesterol/sphingomyelin lipid bilayers: cavitand **1.14** was capable of incorporating within the lipid bilayers containing lipid rafts and BSA was successfully immobilized on the systems (Table 4.1).

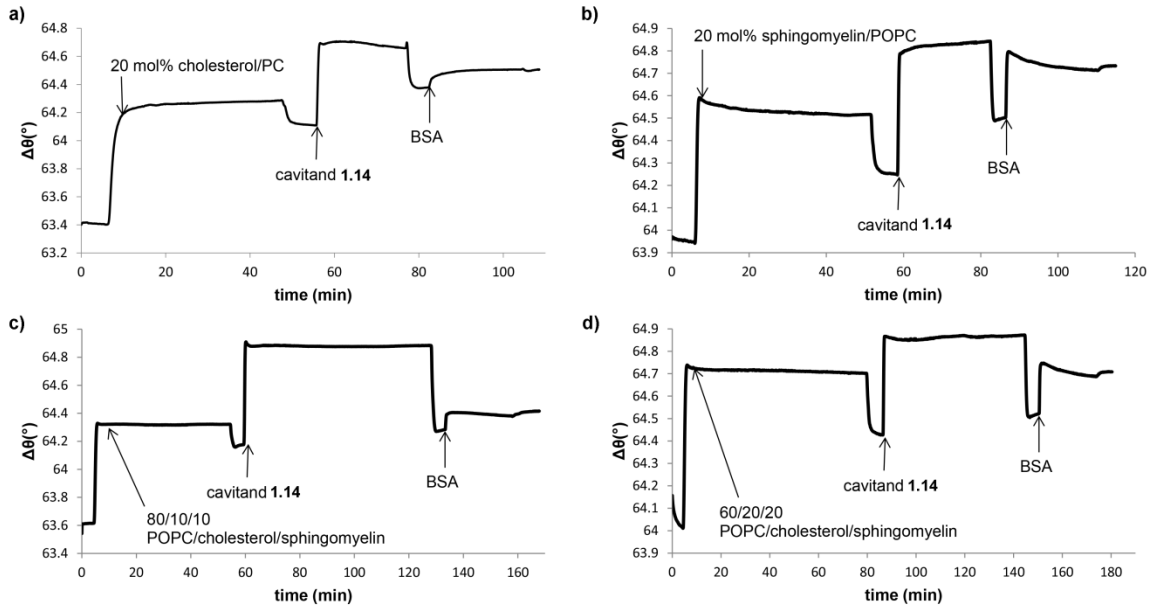

Figure 4.8: SPR sensorgrams of the immobilization of BSA by: (a) the cavitand **1.14**:POPC/cholesterol (80/20) system; (b) the cavitand **1.14**:POPC/sphingomyelin (80/20) system; (c) the cavitand **1.14**:POPC/cholesterol/-sphingomyelin (80/10/10) system; (d) the cavitand **1.14**:POPC/cholesterol/sphingomyelin (60/20/20) system.

Table 4.1: Resonance angle change upon binding of BSA at POPC lipid bilayers containing lipid rafts.

Composition of lipid bilayers	Ratios (mol%)	$\Delta\theta_{cav\ \mathbf{1.14}}$ (°)[a]	$\Delta\theta_{cntl}$ (°)[b]
POPC/cholesterol	80/20	0.12	0.04
POPC/sphingomyelin	80/20	0.23	<0.01
POPC/cholesterol/sphingomyelin	80/10/10	0.11	<0.01
POPC/cholesterol/sphingomyelin	60/20/20	0.18	<0.01

[a]$\Delta\theta_{cav\ \mathbf{1.14}}$ (°) = resonance angle change upon BSA binding in the presence of cavitand 1. [b]$\Delta\theta_{cntl}$(°) = resonance angle change upon target addition to a clean POPC lipid bilayers containing lipid rafts. Injected [cavitand **1.14**] = 1.6 mM; [protein] = 15 μM.

In order to confirm that this immobilization is not due to a non-specific binding of BSA with the POPC lipid bilayers containing cholesterol and sphingomyelin, BSA was exposed to clean lipid bilayers containing lipid rafts in the absence of cavitand **1.14** (Figure 4.9). As shown in Chapter 3, native BSA does not show an affinity for a clean SLB.[20] No non-specific binding between BSA and POPC lipid bilayers containing sphingomyelin only or both cholesterol and sphingomyelin was observed (Table 4.1). On the other hand, a small change in resonance angle was detected ($\Delta\theta_{ctrl}$ = 0.04°) when SLB was replaced with POPC/cholesterol lipid bilayers. This may be due to unknown interactions between BSA and cholesterol. It has been previously reported that there are both hydrophilic and hydrophobic interactions between BSA and cationic lipids in aqueous solutions.[21] The observed binding affinities of cationic lipids in aqueous solution are ~ 10^3 M^{-1}, and the numbers of bound lipids for BSA:lipid complexes are n_{chol} = 1.1 and n_{DOPE} = 1.02. Since BSA was exposed to the interface of packed POPC lipid bilayers containing cholesterol and sphingomyelin, the hydrophobic interactions should be

reduced. As a result, there is no binding observed between BSA and POPC, POPC/sphingomyelin, or POPC/cholesterol/sphingomyelin lipid bilayers. In the case of cholesterol, however, there may be still minimal hydrophilic interactions left between BSA and packed cholesterol itself upon forming homogeneous lipid rafts in the POPC lipid bilayers. Consequently, this may cause a minimal resonance angle change.

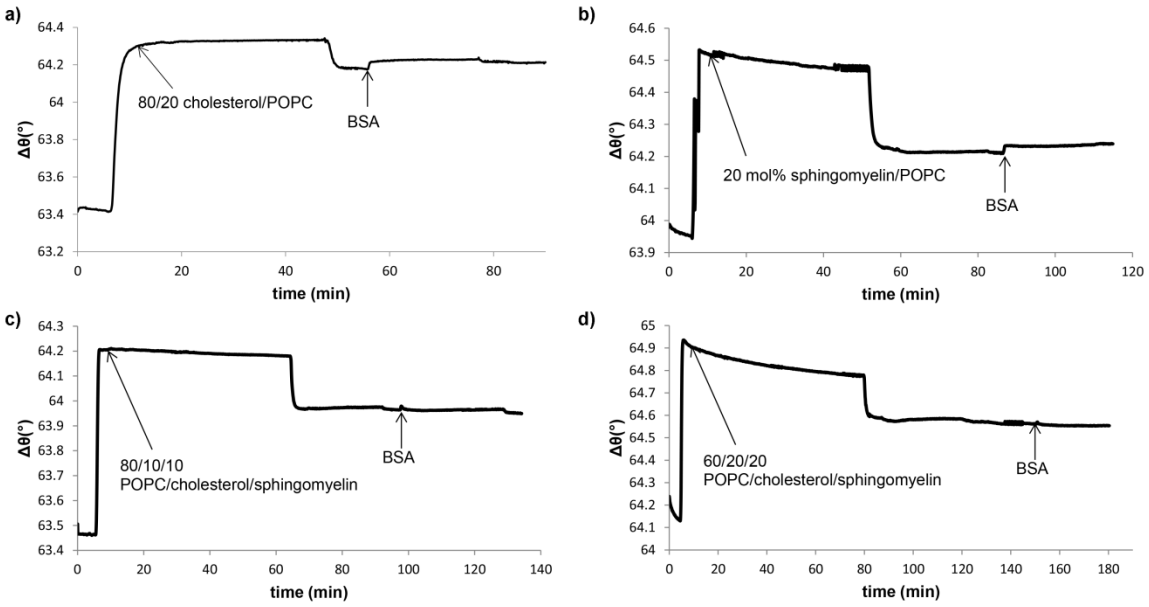

Figure 4.9: SPR sensorgrams of the injection of BSA to: (a) the POPC/cholesterol (80/20) lipid bilayers; (b) the POPC/sphingomyelin (80/20) lipid bilayers; (c) the POPC/cholesterol/sphingomyelin (80/10/10) lipid bilayers; (d) the POPC/cholesterol/sphingomyelin (60/20/20) bilayers.

4.5 Conclusion

POPC lipid bilayers containing lipid rafts of cholesterol or sphingomyelin were successfully formed. The change in resonance angle was observed by SPR upon formation of lipid bilayers. In addition, the smaller diffusion coefficients obtained by FRAP experiments confirmed the existence of lipid rafts within the POPC lipid bilayers

indirectly. When cavitand **1.14** was injected into the lipid bilayer system containing lipid rafts, it was capable of self-incorporating within the bilayers. However, the location of cavitand **1.14** in sterol-rich lipid bilayers is still not clear. Furthermore, embedded cavitand **1.14** maintained its charge-based interactions between carboxylate groups at the rim of cavitand **1.14** and BSA.

4.6 References

1. Ohvo-Rekilä, H.; Ramstedt, B.; Leppimäki, P.; Slotte, J. P. "Cholesterol Interactions withPhospohlipids in Membranes." *Prog.Lipid Res.*, **2002**, *41*, 66-97.

2. Wang, C.; Krause, M. R.; Regen, S. L. "Push and Pull Forces in Lipid Raft Formation: The Push can be as Important as the Pull." *J. Am. Chem. Soc.*, **2015**, *137*, 664-666.

3. McMullen, T. P. W.; Lewis, R. N. A. H.; McElhaney, R. N. "Cholesterol-Phospholipid Interactions, the Liquid-Ordered Phase and Lipid Rafts in Model and Biological Membranes." *Curr. Opin. Colloid Interface Sci.*, **2004**, *8*, 459-468.

4. Simons, K.; Gerl, M. J. "Revitalizing Membranes Rafts: New Tools and Insights." *Nat. Rev. Mol. Cell Biol.*, **2010**, *11*, 688-699.

5. Veatch, S. L.; Keller, S. L. "Separation of Liquid Phase in Giant Vesicles of Ternary Mixtures of Phospholipids and Cholesterol." *Biophys. J.*, **2003**, *85*, 3074-3083.

6. Zheng, L.; McQuaw, C. M.; Ewing, A. G.; Winograd, N. "Sphingomyelin/Phosphatidyl-choline and Cholesterol Interactions Studies by Imaging Mass Spectrometry." *J. Am. Chem. Soc.*, **2007**, *129*, 15730-15731.

7. Bartels, T.; Lankalapalli, R. S.; Bittman, R.; Beyer, K.; Brown, M. F. "Raftlike Mixtures of Sphingomyelin and Cholesterol Investigated by Solid-State ^{2}H NMR Spectroscopy." *J. Am. Chem. Soc.*, **2008**, *130*, 14521-14532.

8. Pathak, P.; London, E. "Measurement of Lipid Nanodomain (Raft) Formation and Size in Sphingomyelin/POPC/Cholesterol Vesicles Shows TX-100 and Transmembrane Helices Increase Domain Size by Coalescing Preexisting Nanodomains but do not Induce Domain Formation." *Biophys. J.*, **2011**, *101*, 2417-2425.

9. Tabaei, S. R.; Jackman, J. A.; Liedberg, B.; Parikh, A. N.; Cho, N. –J. "Observation of Stripe Superstructure in the β-Two Phase Coexistence Region of Cholesterol-Phospholipid Mixtures in Supported Membranes." *J. Am. Chem. Soc.*, **2014**, *136*, 16962-16965.

10. Huang, J.; Buboltz, J. T.; Feigenson, G. W. “Maximun Solubility of Cholesterol in Phosphatidylcholine and Phosphatidylethanolamine Bilayers.” *Biochim. Biophys. Acta*, **1999**, *1417*, 89-100.

11. Liu, Y.; Liao, P.; Cheng, Q.; Hooley, R. J. “Protein and Small Molecule Recognition Properties of Deep Cavitands in a Supported Lipid Membrane Determined by Calcination-Enhanced SPR Spectroscopy.” *J. Am. Chem. Soc.*, **2010**, *132*, 10383-10390.

12. Prenner, E.; Honsek, G.; Hönig, D.; Möbius, D.; Lohner, K. “Imaging of the Domain Organization in Sphingomyelin and Phosphatidylcholine Monolayers.” *Chem. Phys. Lipids*, **2007**, *145*, 106-118.

13. de Almeida, R. F. M.; Loura, L. M. S.; Fedorov, A.; Prieto, M. “Lipid Rafts have Different Sizes Depending on Membrane Composition: A Time-resolved Fluorescence Resonance Energy Transfer Study.” *J. Mol. Biol.*, **2005**, *346*, 1109-1120.

14. Bunge, A.; Müller, P.; Stückl, M.; Herrmann, A.; Huster, D. “Characterization of Ternary Mixture of Sphingomyelin, POPC, and Cholesterol: Support for an Inhomogeneous Lipid Distribution at High Temperatures.” *Biophys. J.*, **2008**, *94*, 2680-2690.

15. Rayan, G.; Guet, J. –E.; Taulier, N.; Pincet, F.; Urbach, W. “Recent Applications of Fluorescence Recovery after Photobleaching (FRAP) to Membrane Bio-Macromolesulces.” *Sensors*, **2010**, *10*, 5927-5948.

16. Costello, D. A.; Millet, J. K.; Hsia, C. –Y.; Whittaker, G. R.; Daniel, S. “Single Particle Assay of Coronavirus Membrane Fusion with Proteinaceous Receptor-Embedded Supported Bilayers.” *Biomaterials*, **2013**, *34*, 7895-7904.

17. Axelrod, D.; Koppel, D. E.; Schlessinger, J.; Elson, E.; Webb, W. W. “Mobility Measurement by Analysis of Fluorescence Photobleaching Recovery Kinetics.” *Biophys. J.*, **1976,** *16*, 1055-1069.

18. Soumpasis, D. M. “Theoretical-Analysis of Fluorescence Photobleaching Recovery Experiments.” *Biophys. J.*, **1983,** *41*, 95-97.

19. Liu, Y.; Young, M. C.; Moshe, O.; Cheng, Q.; Hooley, R. J. “A Membrane-Bound Synthetic Receptor that Promotes Growth of a Polymeric Coating at the Bilayer-Water Interface.” *Angew. Chem. In. Ed.*, **2012**, *51*, 7748-7751.

20. Ghang, Y. –J.; Perez, L.; Morgan, M. A.; Si, F.; Hamdy, O. M., Beecher, C. N.; Larive, C. K.; Julian, R. R., Zhong, W.; Cheng, Q.; Hooley, R. J. "Anionic Deep Cavitands Enable the Adhesion of Unmodified Proteins at a Membrane Bilayer." *Soft Matter*, **2014**, *10*, 9651-9656.

21. Charbonneau, D. M.; Tajmir-Riahi, H. –A. "Study on the Interaction of Cationic Lipids with Bovine Serum Albumin." *J. Phys. Chem. B.*, **2010**, *114*, 1148-1155.

Chapter Five: Cavitand-Mediated Endocytosis of Small Molecules into Live Cells

5.1 Introduction

Developing new methods to transport small molecules into cells selectively is of great interest for effective drug therapies. Small charged molecules can be transported across cellular membrane through membrane-embedded ionophores. Larger molecules are, however, transported into cell via different pathways.[1] There are three different mechanisms for transport of large molecules across living cell membranes in biological systems: phagocytosis, pinocytosis, and receptor-mediated endocytosis.[2] Among these mechanisms, receptor-mediated endocytosis is the most common method used to transport small compounds like proteins or drug candidates into cells.[3] Synthetic receptors transporting small molecules across cellular membranes by mimicking this receptor-mediated endocytosis mechanism have been developed.[4] Current research has been focused on molecular umbrellas[5-9] for effective transport of target molecules, or a synthetic receptor motif that was covalently attached to a lipid or cholesterol anchor for displaying the receptor above the cellular membrane surface, thus promoting receptor-mediated endocytosis of small molecules.[10-13] In this case, the specific interactions between known biological partners such as peptide-protein[10] or drug-bioreceptor[12] were exploited, and target molecules were transported into cells mediated by their own synthetic receptors.

Cavitand **1.14** was applied within the cellular system in order to test its potential as a synthetic receptor that is capable of recognizing target molecules and promoting their

transport into cells via endocytosis (Figure 5.1).[14] Our previous research has shown that a synthetic receptor, cavitand **1.14**, is capable of self-incorporation into SLBs while maintaining its selective recognition of small guests and biomacromolecules.[15,16] This cavitand can be embedded within the biomimetic membrane, and its recognition abilities are controlled by size and shape-based interactions with the guest.

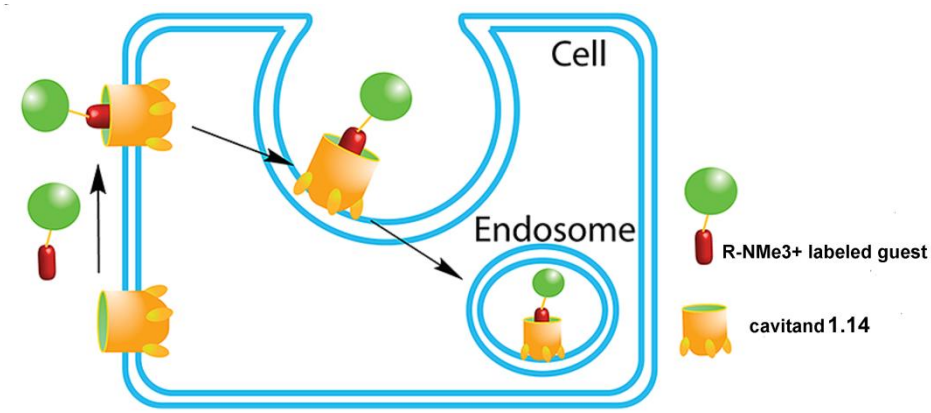

Figure 5.1: A cartoon representation of the transport process mediated by cavitand **1.14**.

5.2 Transport of Small Molecules into Live Cells by Water-Soluble Deep Cavitands

Since this is the first attempt to test cavitand **1.14** in living cells, its location within the membrane should be determined first. In order to track where cavitand **1.14** is located in living cells, visualization using fluorescence microscopy can be used. Direct visualization of the cavitand **1.14** is, however, not possible because cavitand **1.14** itself is not fluorescent and the synthesis of a fluorophore-labeled cavitand would be very challenging. Thus, fluorescently labeled choline derivative **5.1** was employed as an

indirect method of visualization. Guest **5.1** showed a binding affinity for cavitand **1.14** when incorporated into SLB in aqueous solution, and the guest **5.1**:cavitand **1.14** complex within the SLB was visualized by confocal fluorescence microscopy.[15] The fluorescent guest **5.1** can be synthesized in one step by coupling commercially available fluorescein isothiocyanate and (2-aminoetheyl)trimethylammonium chloride hydrochloride (Figure 5.2).

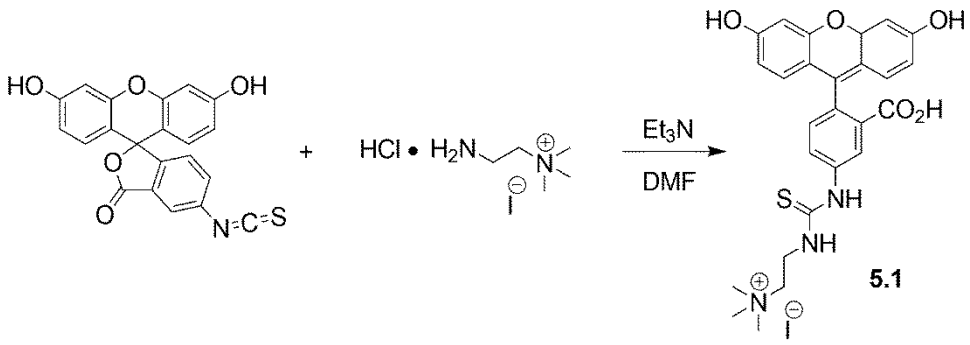

Figure 5.2: Synthesis of fluorescently labeled choline derivative **5.1**.

To investigate the functionality of cavitand **1.14** in living cells, cavitand **1.14** and fluorescent guest **5.1** were tested on human cervical cancer cell lines (HeLa). Cavitand **1.14** and fluorescent guest **5.1** were added into HeLa cell cultures and the cells were incubated for various time periods. After incubating the cells, unincorporated cavitand **1.14** and fluorescent guest **5.1** were removed by washing with PBS buffer. To visualize the cells and incorporated cavitand **1.14**:guest **5.1** complex under confocal fluorescence microscopy, the cells were fixed and the cell nuclei were stained with 4,6-diamidino-2-phenylindole dihydrochloride (DAPI).

First, HeLa cells were incubated with 50 μM fluorescently labeled choline derivative **5.1** under four different conditions: in the presence or absence of 50 μM cavitand **1.14** for 1 h or 24 h. Confocal fluorescence microscopy and differential interference contrast (DIC) microscopy were used to visualize the cells. DIC, cell nuclei (λ_{ex} = 405 nm), and fluorescently labeled choline derivatives (λ_{ex} = 488 nm) images were combined to examine the location of cavitand **1.14**:guest **5.1** complexes within the cells. When comparing the results after a 1 h incubation time, the incorporation rate of fluorescently labeled choline derivative **5.1** increased vastly in the presence of cavitand **1.14** (Figure 5.3). A significant amount of fluorescent guest **5.1** was transported into the cell interior with the aid of cavitand **1.14** only after 1 h. None of the guest molecules were localized in the nuclei of the cells or the cellular membrane, but the guests were transported across the cellular membrane and located in the cytosol. Fluorescently labeled choline derivative **5.1** does not have a high affinity for the cellular membrane. Thus, no fluorescence was observed in the cellular membrane, and minimal incorporation of guest molecules was seen in the absence of cavitand **1.14**. This observation is comparable with previous results obtained from SPR experiments, which showed that fluorescent guest **5.1** is highly water-soluble and shows minimal incorporation into SLBs.[15] The transport of fluorescently labeled choline derivative **5.1** into HeLa cells was observed in small amount when the cells were incubated with guest **5.1** in the absence of cavitand **1.14** for 24 h. Its transport process was slower than in the presence of cavitand **1.14** since smaller amounts of incorporated guest were observed in the absence of cavitand **1.14**.

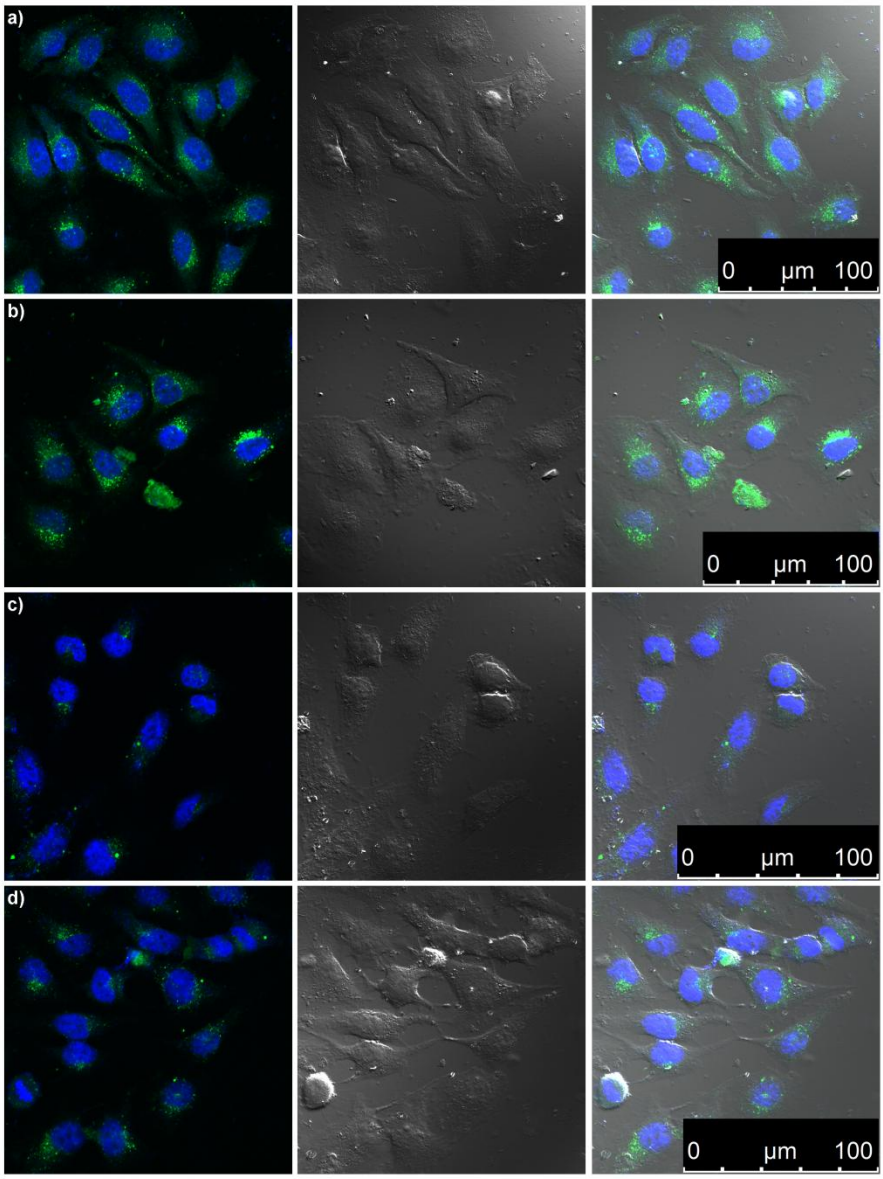

Figure 5.3: Confocal fluorescence microscopy, DIC, and combined images of the addition of fluorescently labeled choline derivative **5.1** to HeLa cells (nuclei stained with DAPI): (a) 50 µM fluorescently labeled choline derivative **5.1**, 50 µM cavitand **1.14**, 1 h incubation; (b) 50 µM fluorescently labeled choline derivative **5.1**, 50 µM cavitand **1.14**, 24 h incubation; (c) 50 µM fluorescently labeled choline derivative **5.1** only, 1 h incubation; (d) 50 µM fluorescently labeled choline derivative **5.1** only, 24 h incubation.

Other cell lines were also tested with cavitand **1.14** and fluorescently labeled choline derivative **5.1**, and it was found that the guest transport process by cavitand **1.14**

is not limited to cancer cell lines, but tolerant to other cell lines. Human skin fibroblast cell lines (GM00637), human foreskin fibroblast cell lines (HFF), and human astrocyte cell lines were all incubated with cavitand **1.14** and fluorescently labeled choline derivative **5.1** for 1 h and 24 h, and the transport of the guest **5.1** was visualized (Figure 5.4). In the case of GM00637, a small amount of transported guest **5.1** was observed in the absence of cavitand **1.14**, but the transport of fluorescently labeled choline derivative **5.1** was still accelerated significantly in the presence of cavitand **1.14** after 1 h incubation. HFF showed results similar to GM00637 when the cells were treated with fluorescently labeled choline derivative **5.1** in the presence of cavitand **1.14**. The rate of guest incorporation into the cells was accelerated after 1 h incubation. The transport efficiency for astrocytes was, however, not as effective as the cases of GM00637 and HFF. Although astrocytes were incubated with fluorescently labeled choline derivative **5.1** and cavitand **1.14** for 1 h, notable incorporation of the guest was not observed unlike HeLa, GM00637 and HFF cell lines. When fluorescent guest **5.1** treated astrocytes were incubated for 24 h, a small amount of fluorescently labeled choline derivative **5.1** transport into the cells was observed. This may be due to the relative growth rate of different cell lines. Since astrocytes are known as slow-growing cells, it is possible that this slow growth gives effects on the rate of the guest transport into cells.

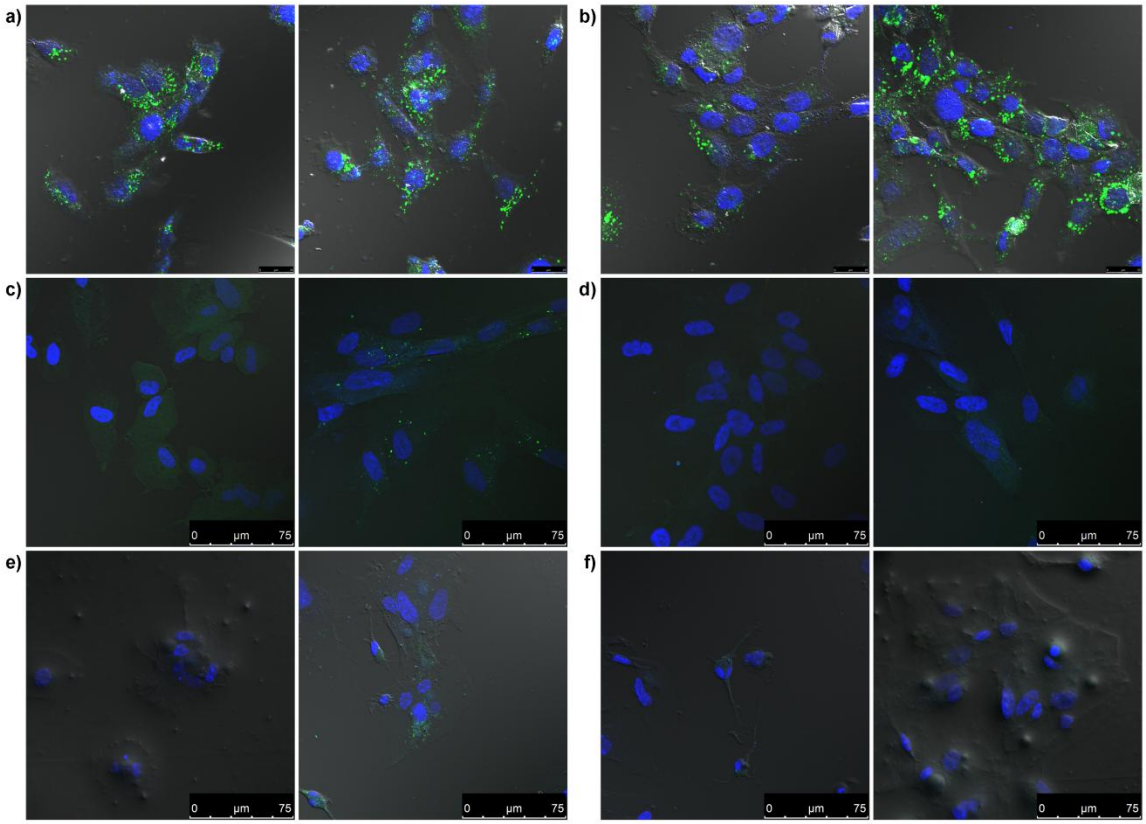

Figure 5.4: DIC/confocal fluorescence microscopy images of the addition of fluorescently labeled choline derivative **5.1** in the presence and absence of cavitand **1.14** to different cell lines (nuclei stained with DAPI): (a) GM00637, 50 µM guest **5.1**, 50 µM cavitand **1.14**, 1 h (left) and 24 h (right) incubation; (b) GM00637, 50 µM guest **5.1**, 1 h (left) and 24 h (right) incubation; (c) HFF, 50 µM guest **5.1**, 50 µM cavitand **1.14**, 1 h (left) and 24 h (right) incubation; (d) HFF, 50 µM guest **5.1**, 1 h (left) and 24 h (right) incubation; (e) astrocyte, 50 µM guest **5.1**, 50 µM cavitand **1.14**, 1 h (left) and 24 h (right) incubation; (f) astrocyte, 50 µM guest **5.1**, 1 h (left) and 24 h (right) incubation.

5.3 Analysis of Efficiency of Small Guest Transport by Cavitands and Cytotoxicity of Cavitands

Various concentrations of cavitand **1.14** and fluorescently labeled choline derivative **5.1** were introduced into HeLa cells as a 1:1 complex: 30 µM, 40 µM, and 50 µM. As shown in Figure 5.5, significant amounts of guest **5.1** were transported when the HeLa cells were incubated with 30 µM or higher concentrations of cavitand **1.14** and fluorescent guest **5.1** for 24 h. The transport efficiency was, however, dependent on the

concentration of cavitand **1.14** and fluorescently labeled choline derivative **5.1** when cells were incubated for only 1 h. The acceleration of guest **5.1** transport into cells in the presence of cavitand **1.14** was less effective at 40 μM or lower concentrations of cavitand **1.14**.

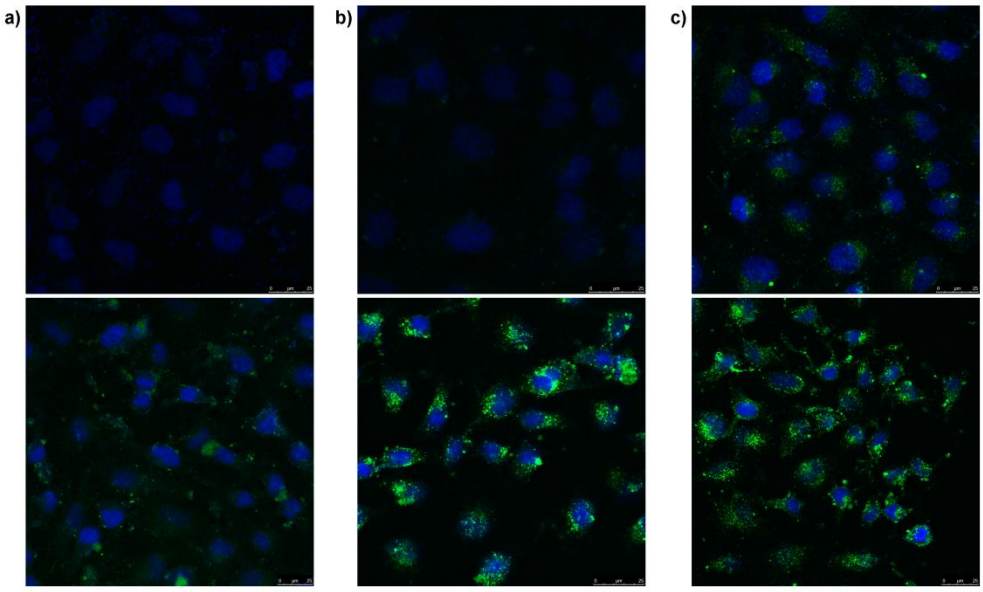

Figure 5.5: Confocal fluorescence microscopy images of the addition of various concentrations of fluorescently labeled choline derivative **5.1** and varying concentrations of cavitand **1.14** to HeLa cells (nuclei stained with DAPI): (a) 30 μM fluorescently labeled choline derivative **5.1**, 30 μM cavitand **1.14**, 1 h (top) and 24 h (bottom) incubation; (b) 40 μM fluorescently labeled choline derivative **5.1**, 40 μM cavitand **1.14**, 1 h (top) and 24 h (bottom) incubation; (c) 50 μM fluorescently labeled choline derivative **5.1**, 50 μM cavitand **1.14**, 1 h (top) and 24 h (bottom) incubation.

For the accurate quantitation of the fluorescent guest **5.1** transported into the cells, flow cytometry experiments were performed. HeLa cells (1 X 10^6 cells) were incubated with fluorescently labeled choline derivative **5.1** for 1 h and 24 h in the presence and absence of cavitand **1.14**, and the fluorescence intensity was measured (Figure 5.5). After 1 h incubation, cells incubated with cavitand **1.14** and fluorescent guest **5.1** showed

stronger fluorescence intensity than the ones incubated with only guest **5.1**. This indicates that HeLa cells transported guest **5.1** at faster rate in the presence of cavitand **1.14**. Following 24 h incubation, the fluorescence intensity of the cells incubated with cavitand **1.14** showed a 10-fold greater intensity than the ones treated with guest **5.1** only. These results imply that cavitand **1.14** indeed accelerates the guest transport into the cells.

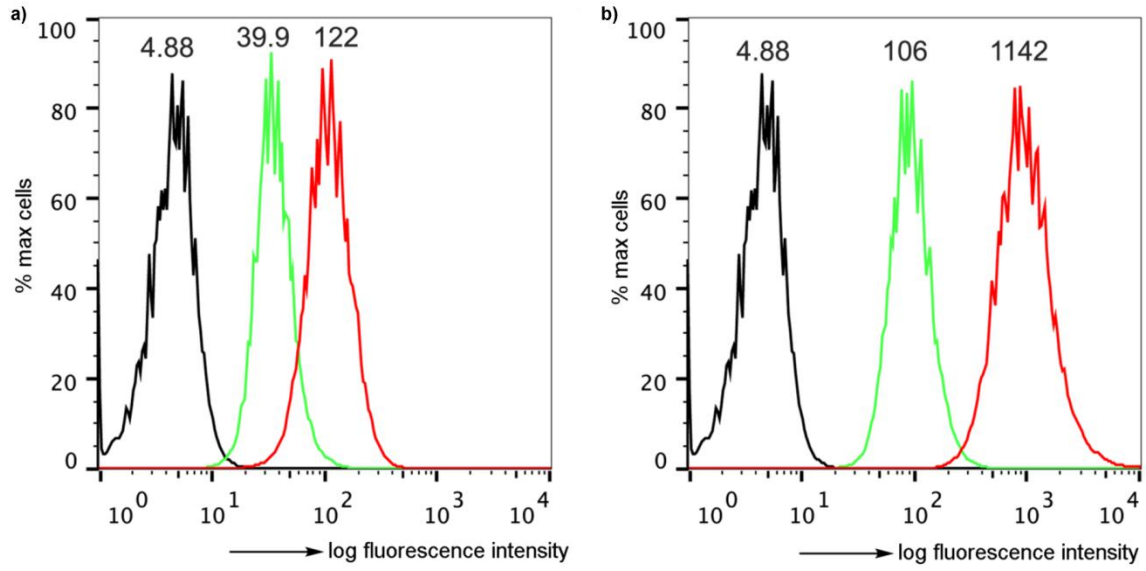

Figure 5.6: Flow cytometry plots of HeLa cells incubated with fluorescently labeled choline derivative **5.1** only (green), fluorescent guest **5.1** and cavitand **1.14** (red) for; (a) 1 h; (b) 24 h. Untreated HeLa cells were plotted in black as a control.

The cytotoxicity of cavitand **1.14** was also tested by performing several assays assisted by Dr. Roger A. Acey at California State University, Long Beach. Human neuroblastoma cells were incubated with varying concentrations of cavitand **1.14** for 24 h under stringent conditions (minimal essential medium with only 0.5 % fetal bovine serum) and cell proliferation assays were performed. The result revealed that cavitand **1.14** does not show any cytotoxicity effect to cells when its concentration is 1 μM or lower (Figure

5.7). When the cavitand concentration was increased to 10 µM or higher, however, it showed 75 % or lower cell proliferation. In addition, if the concentration of cavitand **1.14** was as high as 1 µM, caspase activity (induction of apoptosis) or membrane permeability were not observed (Figure 5.8). These imply that cavitand **1.14** shows little cytotoxicity to cells at 10 µM or higher concentrations. But, this result does not indicate that cavitand **1.14** is entirely cytotoxic to cells because this assay was performed under stringent conditions as previously mentioned.

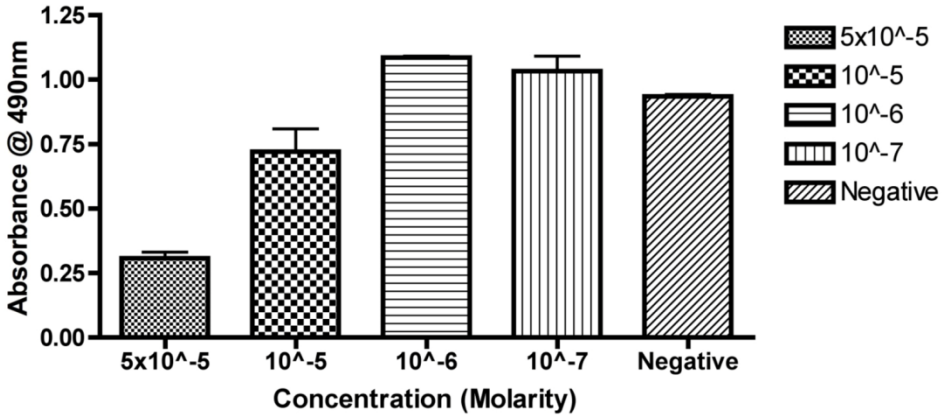

Figure 5.7: Cell proliferation assay. Human neuroblastoma cells were incubated with cavitand **1.14** with 0.5 % fetal bovine serum for 24 h. Results are the average of triplicate assays.

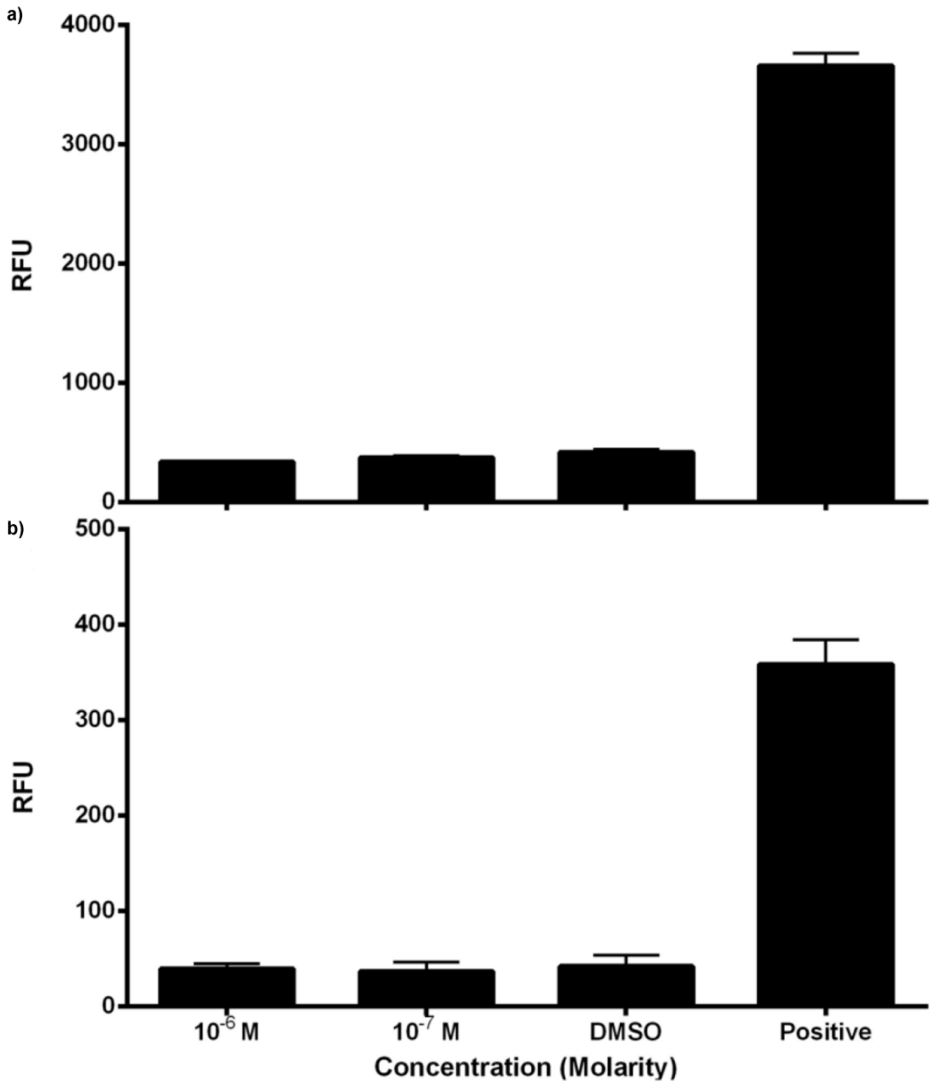

Figure 5.8: Induction of apoptosis and membrane permeability assays: (a) caspase activity; (b) membrane permeability. Human neuroblastoma cells were incubated with cavitand **1.14** with 0.5 % fetal bovine serum for 24 h. Results are the average of triplicate assays.

5.4 Analysis of Selective Recognition by Cavitands for Guest Transport into Live Cells

Cavitand **1.14** is known to show selectivity to molecules labeled with a suitably sized and shaped binding handle, such as R-NMe_3^+. If molecules do not possess a proper binding handle, then the recognition process does not occur. To confirm that the process

of small molecule transport into cells is due to the selective binding of guests containing a binding handle designed for cavitand **1.14**, identical experiments were performed with fluorescein **5.2** in the presence of cavitand **1.14** (Figure 5.9). Fluorescein **5.2** is a fluorophore without the R-NMe_3^+ binding handle and is water-soluble at the concentrations (50 μM) used in the experiments. It also possesses almost identical fluorescence properties to fluorescently labeled choline derivative **5.1**. After 1 h and 24 h incubation times, none of the fluorescein **5.2** was incorporated into cells in the presence of cavitand **1.14**. The transport of fluorescein across the cellular membrane is significantly lower than that of fluorescently labeled choline derivative **5.1**. Furthermore, it was verified that cavitand **1.14** still recognizes molecules selectively within the cellular system and transports them into cells. Without a suitable binding handle present on the molecular targets, the addition of cavitand **1.14** does not have any effect on the transport of molecules into the cell interior. This indicates that the R-NMe_3^+ binding handle is essential for the recognition and transport processes by cavitand **1.14**, and molecules that do not have binding affinity for cavitand **1.14** are not transported into cellular interior.

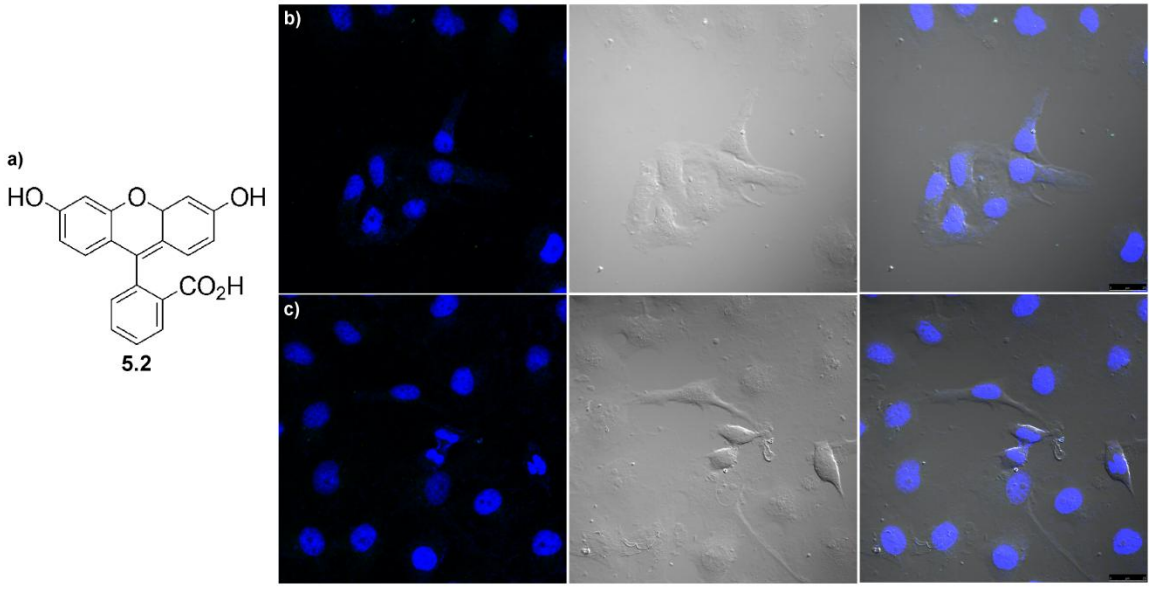

Figure 5.9: (a) A structure of fluorescein **5.2**; Confocal fluorescence microscopy, DIC, and combined images of the addition of fluorescein **5.2** to HeLa cells (nuclei stained with DAPI): (b) 50 µM fluorescein **5.2**, 50 µM cavitand **1.14**, 1 h incubation; (c) 50 µM fluorescein **5.2**, 50 µM cavitand **1.14**, 24 h incubation.

To further verify that the small molecule recognition and transport processes by cavitand **1.14** are due to the interaction between the R-NMe_3^+ binding handle on the guest and a cavity of cavitand **1.14**, neutral cavitand **2.5** was employed. This cavitand does not possess carboxylate groups at the rim, but has a cavity size and shape that is almost identical to that of cavitand **1.14**. HeLa cells were incubated with fluorescently labeled choline derivative **5.1** and cavitand **2.5** for 1 h and 24 h and the incorporation of guest **5.1** was visualized (Figure 5.10). Indeed, the incorporation of guests into cells was observed even after 1 h incubation. Moreover, the greater amount of fluorescently labeled choline derivative **5.1** was transported after extensive incubation (24 h). This confirms that the binding between a R-NMe_3^+ binding handle of the guest and a cavity are crucial for guest transport into cells.

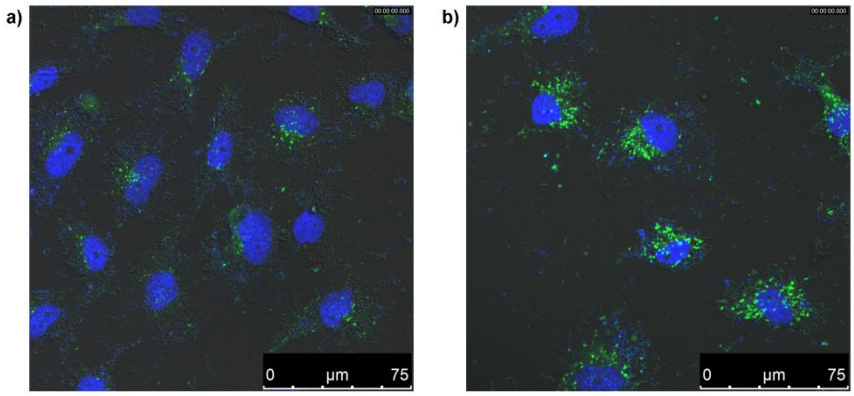

Figure 5.10: DIC/confocal fluorescence microscopy images of the addition of fluorescently labeled choline derivative **5.1** to HeLa cells (nuclei stained with DAPI): (a) 50 µM fluorescently labeled choline derivative **5.1**, 50 µM cavitand **2.5**, 1 h incubation; (b) 50 µM fluorescently labeled choline derivative **5.1**, 50 µM cavitand **2.5**, 24 h incubation.

The selectivity for R-NMe_3^+ binding handle is the key to recognition and transport processes by these cavitands. In some cellular environments, however, this selectivity could be disadvantageous. In the central nervous system, choline and acetylcholine, both containing R-NMe_3^+ binding handles, are abundant because they are essential neurotransmitters. To mimic the choline derivative-rich environment, excess choline (100 µM) were added as a competitive guest during HeLa cell tests with fluorescently labeled choline derivative **5.1** and cavitand **1.14**. Treated cells were incubated for 1 h and 24 h, and the effect of occupation of the cavities of the cavitands in the guest transport process was investigated (Figure 5.11). The addition of competitive guest slowed the incorporation rate of fluorescent guest **5.1** into cells, but it did not prevent the transport process completely. Only a small of fluorescently labeled choline derivative **5.1** was observed after 1 h incubation, but significant amount of guest **5.1** was observed after 24 h incubation. This indicates that the guest binding to cavitand is a reversible process, thus the presence of competitive guest does not stop the transport of desired guest by cavitand

into cells. The binding affinity of choline for cavitand **1.14** is similar to that of fluorescently labeled choline derivative **5.1**. Although the binding constant of choline for cavitand **1.14** when incorporated into SLB could not be determined by SPR analysis, the binding affinity of choline for cavitand **1.14** is 600 M^{-1} in PBS buffer.[16] The fluorescently labeled choline derivative **5.1** showed binding constant for cavitand **1.14** embedded in SLB as 542 M^{-1} by SPR analysis.[15] Previous work showed that the calculated binding constant of guests for cavitand **1.14** incorporated into SLB by SPR analysis provided an approximate their binding affinity in PBS.

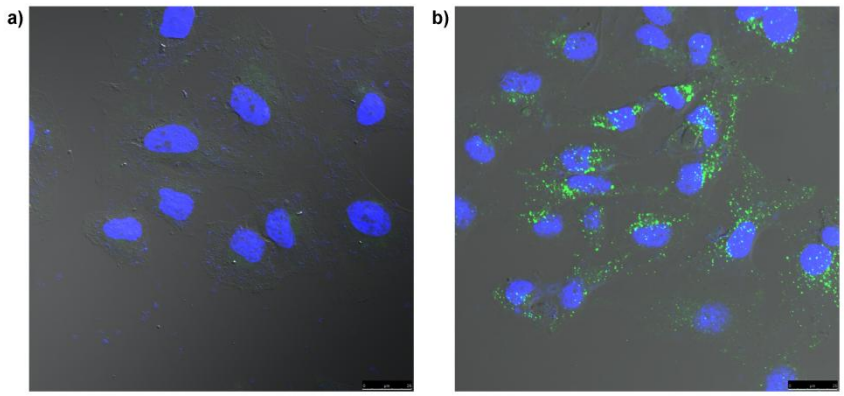

Figure 5.11: DIC/confocal fluorescence microscopy images of the addition of 100 µM choline to HeLa cells with 50 µM fluorescently labeled choline derivative **5.1** and 50 µM cavitand **1.14** (nuclei stained with DAPI): (a) 1 h incubation; (b) 24 h incubation.

5.5 Mechanism of Guest Transport into Cells by Cavitands

The incubation of HeLa cells with cavitand **1.14** and fluorescently labeled choline derivative **5.1**, and subsequent visualization by confocal fluorescence microscopy showed that cavitand **1.14** is capable of selective transport of a suitable guest labeled with the R-NMe_3^+ binding handle. This method, however, does not provide an accurate explanation

of the mechanism of this transport process. Among three major biological mechanisms for transport across cell membranes, pinocytosis and phagocytosis are improbable since the transported guest, fluorescently labeled choline derivative **5.1**, is small. As previous work showed, cavitand **1.14** is known to self-incorporate into SLB.[15] Therefore, there are two possible mechanistic pathways that are realistic (Figure 5.12): cavitand-mediated endocytosis or "flip-flop" membrane translocation similar to phospholipids[18]. When simply analyzing the visualized cell images, it appears that the transport process occurs via endocytosis mechanism. The fluorescently labeled choline derivative **5.1** is punctate in the images. This implies that the guest stays within produced endosomes rather than being released into cytosol and evenly distributed.[19] This is commonly observed with receptor-mediated endocytosis of drug candidates: transported small molecules, mediated by cholesterol-linked receptors, are contained within endosomes without the presence of endosome-disrupting peptides.[19]

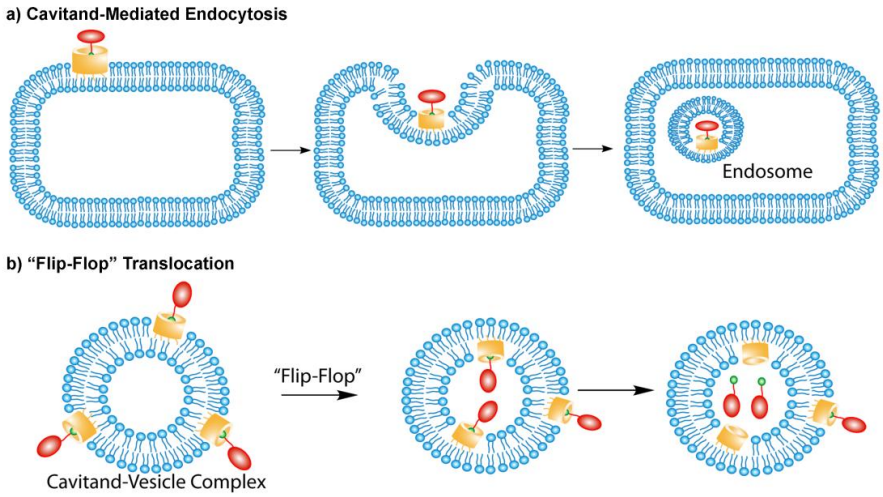

Figure 5.12: Representations of: a) cavitand-mediated endocytosis; b) "flip-flop" translocation mechanism.

To verify that small molecule transport process by cavitand **1.14** occurs via the endocytosis mechanism, depletion of ATP production was forced during the experiment to slow cellular endocytosis.[20] 50 mM 2-deoxy-D-glucose and 10 mM NaN_3 were added to HeLa cells with fluorescently labeled choline derivative **5.1** and cavitand **1.14**, and incubated for 1 h. As shown in Figure 5.13, under ATP-depleted conditions, minimal transport of the guest was observed although cavitand **1.14** was present in cell cultures. This result supports that the transport process occurs via endocytosis mechanism.

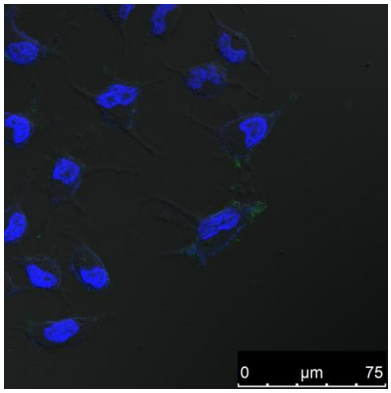

Figure 5.13: DIC/confocal fluorescence microscopy image of HeLa cells incubated with 50 µM fluorescently labeled choline derivative **5.1**, 50 µM cavitand **1.14**, 50 mM 2-deoxy-D-glucose, and 10 mM NaN_3 for 1 h (nuclei stained with DAPI).

The observations from incubating the HeLa cells under ATP-depletion conditions suggest that the transport process is via endocytosis. As mentioned previously, however, the transported fluorescently labeled choline derivative **5.1** is punctate indicating that the guests are contained in endosomes. Therefore, varying concentrations of sucrose (125 – 500 mM) were added into HeLa cell culture for endosome disruption[21] when treated with cavitand **1.14** and fluorescent guest **5.1**, and the cells were incubated for 1 h and 24 h

(Figure 5.14). Unfortunately, the transported fluorescent guest **5.1** still looked punctate even though the concentration of sucrose was increased to 500 mM and the incubation time was extended to 24 h. The addition of high concentration of sucrose may not be the best method to disrupt endosomes containing fluorescently labeled choline derivative **5.1**. The location of transported fluorescent guest **5.1** in endosomes is still remains unclear due to the failure of endosome disruption.

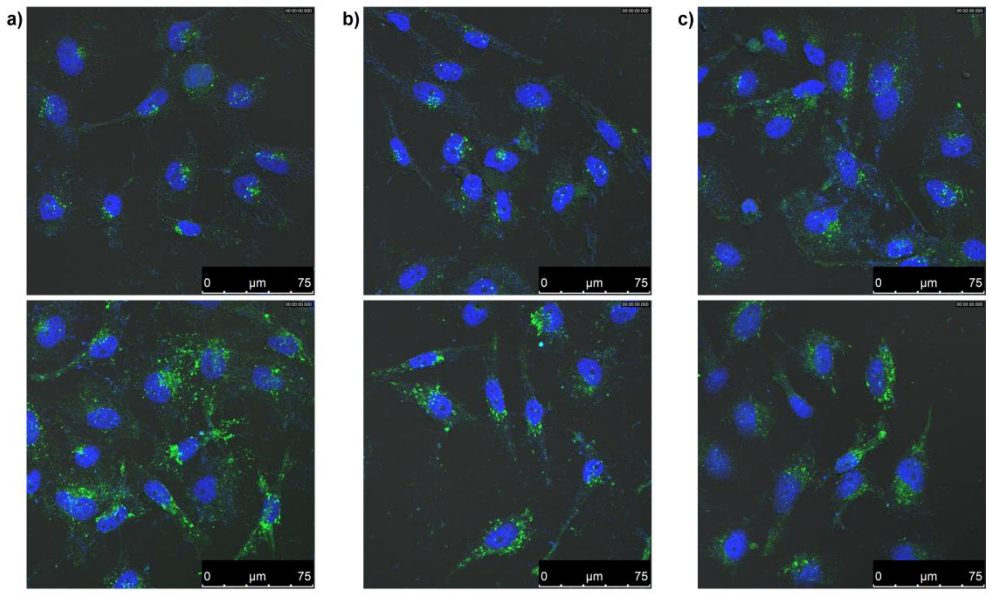

Figure 5.14: DIC/confocal fluorescence microscopy images of HeLa cells incubated with 50 µM cavitand **1.14**, 50 µM fluorescently labeled choline derivative **5.1**, and various concentrations of sucrose (nuclei stained with DAPI): (a) 125 mM sucrose, 1 h (top) and 24 h (bottom) incubation; (b) 250 mM sucrose, 1 h (top) and 24 h (bottom) incubation; (c) 500 mM sucrose, 1 h (top) and 24 h (bottom) incubation.

Visualizing the fluorescently labeled choline derivative **5.1** is not observing the cavitand **1.14** directly. It is not obvious whether the cellular endocytosis is triggered by the molecular recognition process or the cavitand **1.14** is endocytosed and exocytosed constantly by the cells while incubating and the guest is endocytosed into the cells upon

cavitand **1.14**:guest complex formation. Thus, HeLa cells were treated with cavitand **1.14** for 1 h prior to the addition of fluorescently labeled choline derivative **5.1** (Figure 5.15). Even though HeLa cells were pre-incubated with cavitand **1.14**, the incorporation of guest **5.1** was still observed even after 1 h incubation. This does not strongly prove but suggests that the cells allow endocytosis of guest upon its complex formation with cavitand **1.14**.

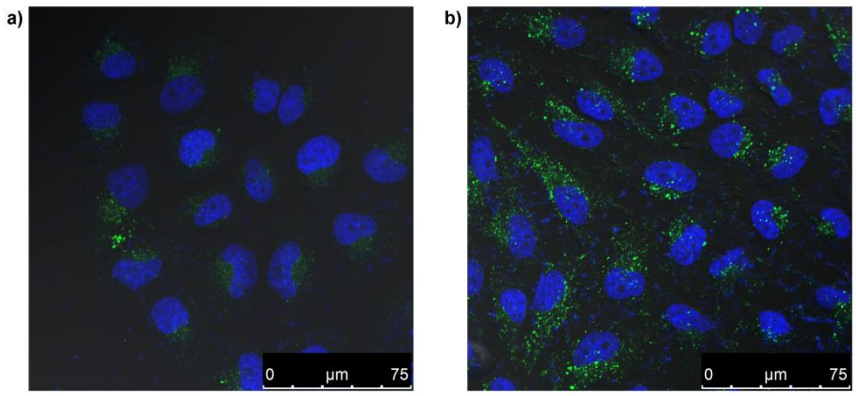

Figure 5.15: DIC/confocal fluorescence microscopy images of HeLa cells incubated with 50 µM fluorescently labeled choline derivative **5.1** after treated with 50 µM cavitand **1.14** for 1 h (nuclei stained with DAPI): (a) 1 h incubation; (b) 24 h incubation.

To further investigate that this transport process occurs via an endocytosis mechanism mediated by the cavitand, guest transport by cavitand **1.14** was tested on the mimic of membrane-containing vesicles, which lack the clathrin-based endocytosis machinery in cells, by Dr. Michael P. Schramm at California State University, Long Beach. Giant unilamellar vesicles (GUVs) are good mimics of cellular membranes, possessing a bilayer membrane with internal cavity whose diameter is ~ 100 nm. They are known to translocate molecules that undergo the "flip-flop" mechanism rapidly at

room temperature, but are not capable of performing endocytosis.[18] GUVs were prepared by POPC lipids via literature methods[22], and the prepared GUVs were doped with 5 % rhodamine-labeled 1,2-dioleoyl-*sn*-glycero-3-phosphoethanolamine lipids (DOPE) for visualization.[23] GUVs were incubated with 20 μM fluorescently labeled choline derivative **5.1** in the presence and absence of 20 μM cavitand **1.14** for 1 h and 24 h, and the location of the guest **5.1** was imaged by confocal fluorescence microscopy (Figure 5.16, 5.17). The results showed that none of the guest **5.1** was transported into the vesicle interior even after 24 h incubation in the presence of cavitand **1.14**. However, it is still possible that cavitand **1.14** can be flip-flopped into the vesicles once it is bound to a bilayer membrane. The transport of cavitand itself via "flip-flop" mechanism is, however, not effective for the incorporation of bound guest **5.1**. Thus, this result provides evidence that this guest transport mechanism in cellular system occurs via cavitand-mediated endocytosis.

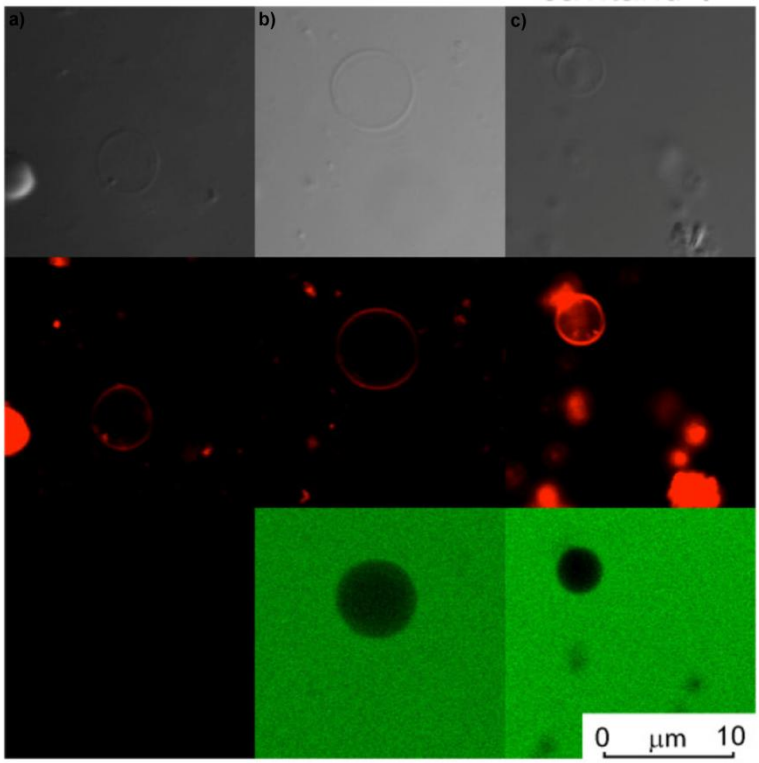

Figure 5.16: DIC, rhodamine, and fluoresein images of the effect of cavitand **1.14**:fluorescently labeled choline derivative **5.1** system on GUVs (POPC+5 % DOPE-Rhod, 10 mM HEPES, 10 mM $MgCl_2$, pH 7.4, 1 h incubation): (a) no additives; (b) 5 mol % fluorescently labeled choline derivative **5.1**; (c) 5 mol % fluorescently labeled choline derivative **5.1** and 2.5 mol % cavitand **1.14**.

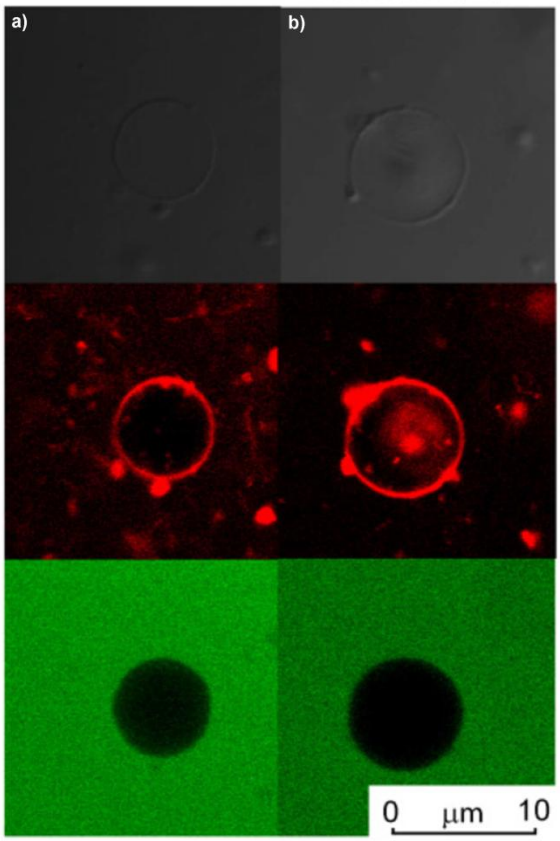

Figure 5.17: DIC, rhodamine, and fluoresein images of the effect of cavitand **1.14**:fluorescently labeled choline derivative **5.1** system on GUVs (POPC+5 % DOPE-Rhod, 10 mM HEPES, 10 mM $MgCl_2$, pH 7.4, 24 h incubation): (a) 5 mol % fluorescently labeled choline derivative **5.1**; (b) 5 mol % fluorescently labeled choline derivative **5.1** and 2.5 mol % cavitand **1.14**.

5.6 Conclusion

Water-soluble cavitand **1.14** has been applied as a synthetic receptor capable of selective and controlled endocytosis of small molecules into different types of human cells with little cytotoxicity observed. In molecular recognition and transport processes, the presence of the R-NMe_3^+ binding handle on target guests plays an important role. In the absence of a suitable binding handle, no transport of guest was observed. This cavitand-mediated endocytosis introduces a novel method of transporting small

molecules into cells by selective shape and size-based molecular recognition. This new method has the potential to be developed into a new drug delivery system.

5.7 References

1. Conner, S. D.; Schmid, S. L. "Regulated Portals of Entry into the Cell." *Nature*, **2003**, *422*, 37-44.

2. Hymel, D.; Peterson, B. R. "Synthetic Cell Surface Receptors for Delivery of Therapeutics and Probes." *Adv. Drug Delivery Rev.*, **2012**, *64*, 797-810.

3. McMahon, H. T.; Boucrot, E. "Molecular Mechanism and Physiological Functions of Clathrin-Mediated Endocytosis." *Nat. Rev. Mol. Cell Biol.*, **2011**, *12*, 517-533.

4. Peterson, B. R. "Synthetic Mimics of Mammalian Cell Surface Receptors: Prosthetic Molecules that Augment Living Cells." *Org. Biomol. Chem.*, **2005**, *3*, 3607-3612.

5. Janout, V.; Lanier, M.; Regen, S. L. "Molecular Umbrellas." *J. Am. Chem. Soc.*, **1996**, 118, 1573-1574.

6. Janout, V.; Lanier, M.; Regan, S. L. "Design and Synthesis of Molecular Umbrellas." *J. Am. Chem. Soc.*, **1997**, *119*, 640-647.

7. Janout, V.; Giorgio, C. D.; Regan, S. L. "Molecular Umbrella-Assisted Transport of Hydrophilic Peptide across a Phospholipid Membrane." *J. Am. Chem. Soc.*, **2000**, *122*, 2671-2672.

8. Kondo, M.; Mehiri, M.; Regen, S. L. "Viewing Membrane-Bound Molecular Umbrellas by Parallax Analyses." *J. Am. Chem. Soc.*, **2008**, *130*, 13771-13777.

9. Mehiri, M.; Chen, W. –H.; Janout, V.; Regen, S. L. "Molecular Umbrella Transport: Exceptions to the Classic Size/Lipophilicity Rule." *J. Am. Chem. Soc.*, **2009**, *131*, 1338-1339.

10. Hussey, S. L.; He, E.; Peterson, B. R. "A Synthetic Membrane-Anchored Antigen Efficiently Promotes Uptake of Antifluorescein Antibodies and Associated Protein A by Mammalian Cells." *J. Am. Chem. Soc.*, **2001**, *123*, 12712-12713.

11. Boonyarattanakalin, S.; Martin, S. E.; Dykstra, S. A.; Peterson, B. R. "Synthetic Mimics of Small Mammalian Cell Surface Receptors." *J. Am. Chem. Soc.*, **2004**, *126*, 16379-16386.

12. Boonyarattanakalin, S.; Hu, J.; Dykstra-Rummel, S. A.; August, A.; Peterson, B. R. "Endocytic Delivary of Vancomycin Mediated by a Synthetic Cell Surface Receptor: Rescue of Bacterially Infected Mammalian Cells and Tissue Targeting In Vivo." *J. Am. Chem. Soc.*, **2007**, *129*, 268-269.

13. Boonyarattanakalin, S.; Martin, S. E.; Sun, Q.; Peterson, B. R. "A Synthetic Mimic of Human Fc Receptors: Defined Chemical Modification of Cell Surface Enables Efficient Endocytic Uptake of Human Immunoglobulin-G." *J. Am. Chem. Soc.*, **2006**, *128*, 11463-11470.

14. Ghang, Y. –J.; Schramm, M. P.; Zhang, F.; Acey, R. A.; David, C. N.; Wilson, E. H.; Wang, Y.; Cheng, Q.; Hooley, R. J. "Selective Cavitand-Mediated Endocytosis of Targeted Imaging Agents into Live Cells." *J. Am. Chem. Soc.*, **2013**, *135*, 7090-7093.

15. Liu, Y.; Liao, P.; Cheng, Q.; Hooley, R. J. "Protein and Small Molecule Recognition Properties of Deep Cavitands in a Supported Lipid Membrane Determined by Calcination-Enhanced SPR Spectroscopy." *J. Am. Chem. Soc.*, **2010**, *132*, 10383-10390.

16. Ghang, Y. –J.; Lloyd, J. J.; Moehlig, M. P.; Arguelles, J. K.; Mettry, M.; Zhang, X.; Julian, R. R.; Cheng, Q.; Hooley, R. J. "Labeled Protein Recognition at a Membrane Bilayer Interface by Embedded Synthetic Receptors." *Langmuir*, **2014**, *30*, 10161-10166.

17. Biros, S. M.; Ullrich, E. C.; Hof, F.; Trembleau, L.; Rebek, J., Jr. "Kinetically Stable Complexes in Water: The Role of Hydration and Hydrophobicity." *J. Am. Chem. Soc.*, **2004**, *126*, 2870-2876.

18. Liu, J.; Conboy, J. C. "Direct Measurement of the Transbilayer Movement of Phospholipids by Sum-Frequency Vibrational Spectroscopy." *J. Am. Chem. Soc.*, **2004**, *126*, 8376-8377.

19. Sun, Q.; Cai, S.; Peterson, B. R. "Selective Disruption of Early/Recycling Endosomes: Release of Disulfide-Linked Charge Mediated by a *N*-Alkyl-3*β*-Cholesterylamine-Capped Peptide." *J. Am. Chem. Soc.*, **2008**, *130*, 10064-10065.

20. Potocky, T. B.; Menon, A. K.; Gellman, S. H. "Membrane Transport, Structure, Function, and Biogenesis." *J. Biol. Chem.*, **2003**, *278*, 50188-50194.

21. Caron, N. J.; Quenneville, S. P.; Tremblay, J. P. “Endosome Disruption Enhances the Functional Nuclear Delivery of Tat-Fusion Proteins.” *Biochem. Biophys. Res. Commun.*, **2004**, *319*, 12-20.

22. Moscho, A.; Orwar, O.; Chiu, D. T.; Modi, B. P.; Zare, R. N. “Rapid Preparation of Giant Unilamellar Vesicles.” *Proc. Natl. Acad. Sci. U.S.A.*, **1996**, *93*, 11443-11447.

23. Dominak, L. M.; Keating, C. D. “Polymer Encapsulation within Giant Lipid Vesicles.” *Langmuir*, **2007**, *23*, 7148-7154.

Chapter Six: Cavitands as New Transfection Agents for Living Cells

6.1 Introduction

Selective recognition and effective transport of target molecules across cellular membrane is crucial for drug or cellular therapeutic. Transport of charged polar species such as drug candidates or proteins across cell membranes is usually challenging. The most common method to transport large polar molecules that are not membrane permeable is the covalent attachment of cell-penetrating peptides (CPPs).[1] Small molecule therapeutics,[2] proteins[3] and nucleic acids[4] were successfully delivered into various cell lines by CPPs with minimal cytotoxicity.[5] Although their ability to transport species that are hard to be delivered into cells is impressive, there are still limitations. It introduces synthetic challenges when linking CPPs covalently to targets. Moreover, CPPs are often contained in endosomes, so efficient intracellular localization is limited.

Cavitand **1.14** can be an alternative candidate for a transfection agent. Our previous research has showed that a synthetic receptor, cavitand **1.14**, is capable of selective recognition and transport of small molecules across cellular membrane and the transported molecules can be visualized by confocal fluorescence microscopy.[6] To extend the scope of application of cavitand **1.14** as a transfection agent, different molecules relevant to biomedical targets were examined.

6.2 Transport of Anticacer Drug Candidates

Cavitand **1.14** showed little cytotoxicity when human neuroblastoma cells were treated with cavitand **1.14** under stringent conditions (minimal essential medium with

only 0.5 % fetal bovine serum).[6] To determine the concentration of cavitand **1.14** that does not show cytotoxicity to cells, HeLa cells were treated with cavitand **1.14** and cell proliferation was examined by sulforhodamine B (SRB) colorimetric assay.[7,8] SRB assay is a large-scale drug-screening method to measure cell preliferation for the purpose of determining cytotoxicity induced by drugs. After treatment of cells with drug candidates for desired time, dead cells are removed by aspirating off media. Live cells are fixed by trichloroacetic acid, and SRB dye is added to fixed cells. SRB dye is capable of binding on protein basic amino acid residues under mild acidic conditions. After extensive washing to remove any unbound dye, the bound dyes are extracted from cells and solubilized by 10 mM Tris base. The optical density (OD) is measure at wavelength of 490 nm for quantitation of live cells. HeLa cells (4×10^3 cells/well in 96-well plate) were incubated with varying concentrations of cavitand **1.14** (5 – 50 μM) for 24 h, and SRB assay was performed (Figure 6.1). The result showed that cavitand **1.14** does not show any significant cytotoxicity effects to cells at concentration of 20 μM or lower. When the concentration of cavitand **1.14** was increased to 30 μM or higher, however, it showed about 70 % or lower cell proliferation. Thus, it was determined that 20 μM cavitand **1.14** should be used for drug candidate transport experiments.

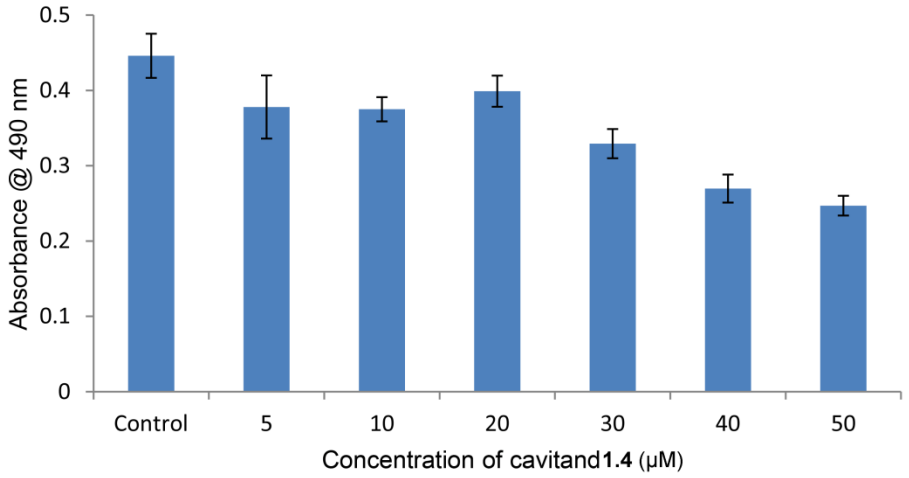

Figure 6.1: SRB assay. HeLa cells treated with various concentrations of cavitand **1.14** for 24 h. Results are the average of triplicate assays.

There have been many efforts to develop effective anticancer drugs. Cisplatin is one well-known anticancer chemotherapeutic agent used to treat various types of cancer effectively, but it has some side effects and tumors often develop resistance to it.[9] As an alternative metal-based drug, it was discovered that gold(III) compounds showed effectiveness on cisplatin resistant tumor cell lines[10] and showed potential as an antitumor drug.[11-13] Gold(III) complexes with polypyridyl ligands also showed anticancer activity against many different types of tumor cell lines.[14] Thus, for an initial test of our system as an enhanced transfection agent, gold(III)-bipyridine complex **6.2** was tested on live cells with cavitand **1.14**. Jessica K. Arguelles at University of California, Riverside synthesized the R-NMe_3^+ binding handle labeled bipyridine ligand **6.1** in two steps. [2,2'-bipyridine]-6-carboxylic acid was coupled with *N*,*N*-dimethylethylenediamine, and subsequent methylation by iodomethane gave bipyridine ligand **6.1**. This bipyridine

ligand **6.1** was mixed with sodium tetrachloroaurate(III) and gold(III)-bipyridine complex **6.2** was formed.

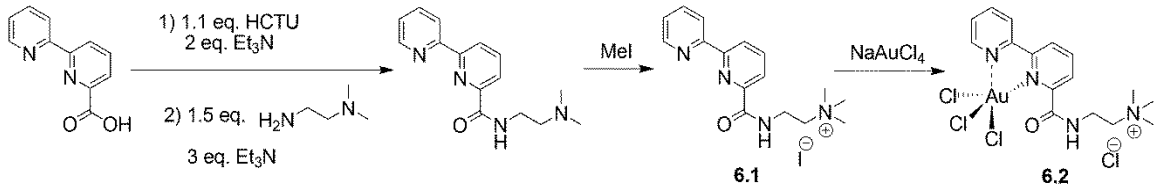

Figure 6.2: Synthesis of R-NMe_3^+ binding handle labeled bipyridine **6.1** and its gold(III) complex **6.2** formation.

HeLa cells were treated with various concentrations of gold(III) complex **6.2** in the presence and absence of 20 μM cavitand **1.14** for 48 h. To test the cytotoxicity of ligand itself, bipyridine ligand **6.1** was also tested with HeLa cells. SRB assay results showed that the cell densities were similar under all conditions. This indicates that neither the gold(III) complex **6.2** nor bipyridine ligand **6.1** were effective at suppressing cell growth in the presence or absence of cavitand **1.14** (Figure 6.3).

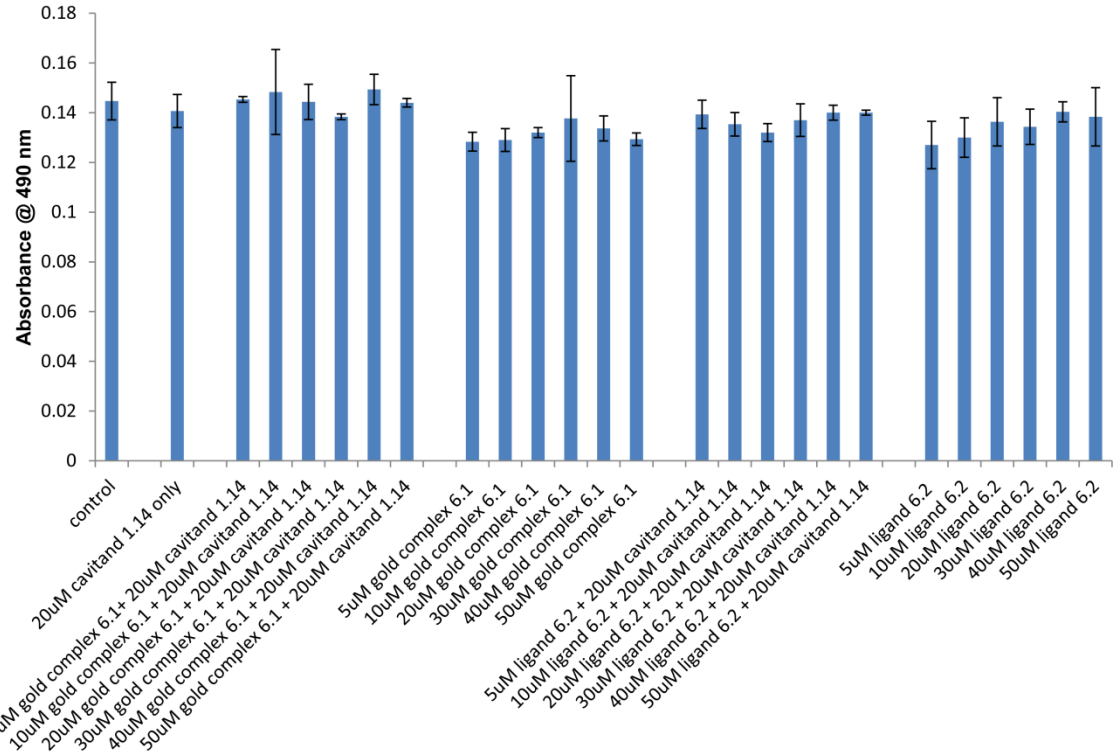

Figure 6.3: SRB assay. HeLa cells treated with various concentrations of gold(III) complex **6.2** or bipyridine ligand **6.1** in the presence and absence of cavitand **1.14** for 48 h. Results are the average of triplicate assays.

As gold(III) complex **6.2** did not show relative cytotoxicity to HeLa cells, another metal was used to form a complex with the bipyridine ligand **6.1**. Since it is well-known that cisplatin is effective on antitumor activity,[10] platinum was employed to synthesize cisplatin-based derivative **6.3**. This was synthesized in one step by the addition of cis-bis(benzonitrile)dicholoroplatinum(II) to bipyridine ligand **6.1** (Figure 6.4).

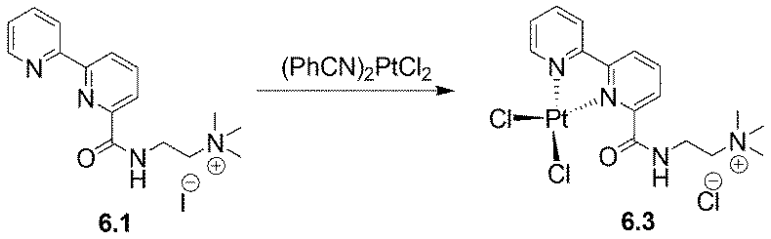

Figure 6.4: Synthesis of cisplatin-based derivative **6.3**.

To test the enhanced transport and cytotoxicity of cisplatin-based derivative **6.3**, HeLa cells were treated with varying concentrations of drug derivative **6.3** (2 – 500 μM) in the presence and absence of 20 μM cavitand **1.14** for 48 h. Since it is already shown that bipyridine ligand **6.1** is not cytotoxic to HeLa cells in the presence and absence of cavitand **1.14**, only cisplatin-based derivative **6.3** was tested. SRB assay results showed that similar OD was observed from all conditions even under high concentrations of cisplatin-based derivative **6.3**. This implies that the cisplatin-based derivative **6.3** is not cytotoxic to HeLa cells (Figure 6.5).

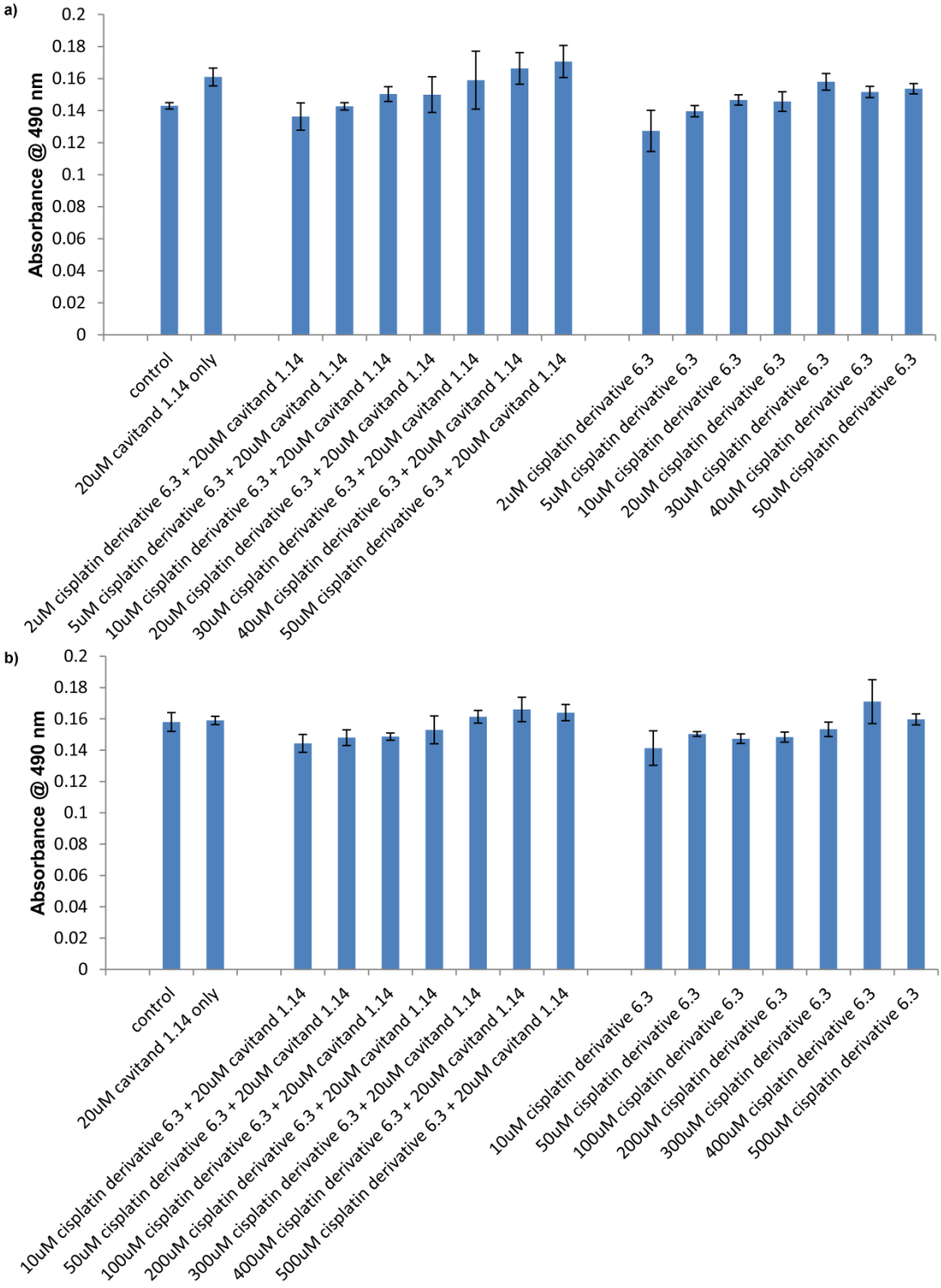

Figure 6.5: SRB assay. HeLa cells treated with various concentrations of cisplatin derivative **6.3** in the presence and absence of cavitand **1.14** for 48 h. Results are the average of triplicate assays: (a) 2-50 µM cisplatin derivative **6.3**; (b) 10-500 µM cisplatin derivative **6.3**.

No cytotoxicity was observed with both gold(III) complex **6.2** and cisplatin-based derivative **6.3** in the presence or absence of cavitand **1.14**. It is still not clear why treatment of HeLa cells with gold complex **6.2** or cisplatin-based derivative **6.3** was not effective. It is possible that the transported drug targets are localized within endosomes, therefore the cells do not get any effects from the drug derivatives. Or, it may be because those drug derivatives are not cytotoxic to HeLa cells. Thus, in order to investigate whether cavitand **1.14** enhances transport of cytotoxic drugs into cells, a commercially available anticancer drug was chosen. The nitrogen mustard chlorambucil is known as an anticancer chemotherapy drug for treatment of chronic lymphocytic leukemia, and it is used to treat many different types of malignancies.[15] Prior to testing derivatized chlorambucil, the cytotoxicity of chlorambucil was examined first. To confirm that chlorambucil itself is cytotoxic to HeLa cells, various concentrations of chlorambucil (10-50 μM) was added into HeLa cell cultures and the cells were incubated for 48 h. In this case, chlorambucil may be transported into HeLa cells via mechanism other than cavitand-mediated endocytosis, but its cytotoxicity on HeLa cells can be still investigated. The % viability of cells after treatment with chlorambucil was determined by counting live and dead cells from the culture (Figure 6.6). % viability was calculated by following.

live cells / (# live cells + # dead cells) (eq 4)

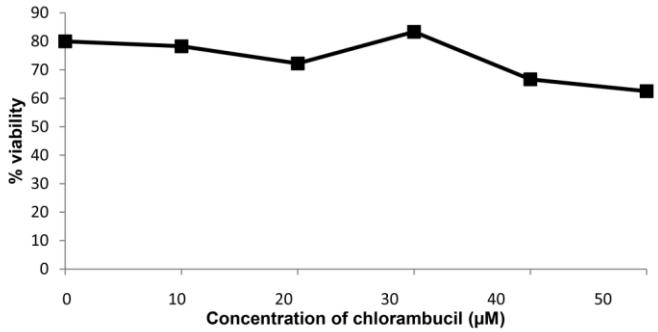

Figure 6.6: The % viability assay. HeLa cells were treated with various concentrations of chlorambucil (10-50 μM) for 48 h.

Interestingly, the % viability was decreased as chlorambucil concentrations were increased, but it was not as effective as expected. Even though 50 μM chlorambucil was added to HeLa cells, only ~ 20 % decrease in viability was observed. This result showed that chlorambucil is cytotoxic, but it is not that effective.

To clarify that chlorambucil is an effective cytotoxic drug, HeLa cells treated with varying concentrations of chlorambucil were incubated for 5 days. SRB assay results showed that even 10 μM chlorambucil is cytotoxic to HeLa cells and reduces more than 40 % cell growth (Figure 6.7). This implies that chlorambucil is obviously cytotoxic to HeLa cells.

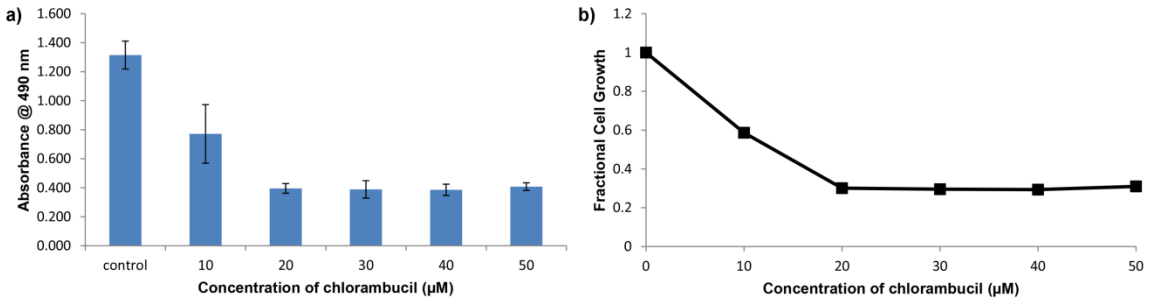

Figure 6.7: SRB assay. HeLa cells were treated with various concentrations of chlorambucil (10-50 μM) for 5 days: (a) absorbance at 490 nm; (b) fractional cell growth. Results are the average of triplicate assays.

Since the cytotoxicity of chlorambucil against HeLa cells was confirmed, it was labeled with a suitable binding handle for transport mediated by cavitand **1.14**. The R-NMe_3^+ binding handle was placed on chlorambucil in two steps (Figure 6.8). The carboxylic acid group on chlorambucil was coupled with *N*,*N*-dimethylethylenediamine and following methylation by iodomethane provides the R-NMe_3^+ labeled chlorambucil derivative **6.4**.

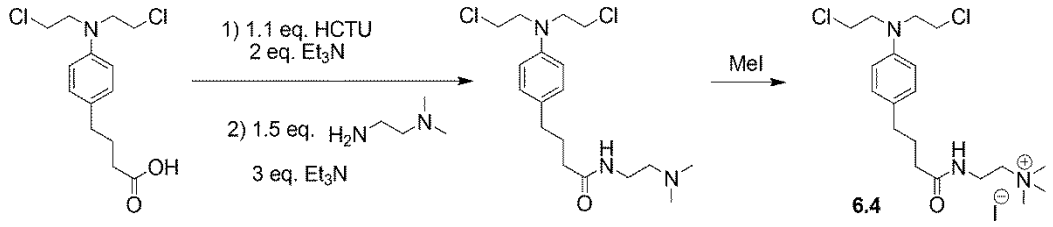

Figure 6.8: Synthesis of R-NMe_3^+ labeled chlorambucil derivative **6.4**.

HeLa cells were treated with various concentrations of chlorambucil derivative **6.4** (10 – 50 μM) in the presence and absence of 20 μM cavitand **1.14** for 5 days. Indeed, cytotoxicity of chlorambucil derivative **6.4** was observed in the presence of cavitand **1.14** in SRB assays, and cell proliferation decreased as the concentration of chlorambucil derivative **6.4** increased (Figure 6.9). Similar results were observed in the absence of cavitand **1.14**, but the cytotoxicity of chlorambucil derivative **6.4** was less effective than in the presence of cavitand **1.14**. Calculated IC_{50} values for chlorambucil derivative **6.4** were 37 μM and 47 μM in the presence and absence of cavitand **1.14**, respectively. This implies that the presence of cavitand **1.14** enhanced the transport of chlorambucil derivative **6.4**.

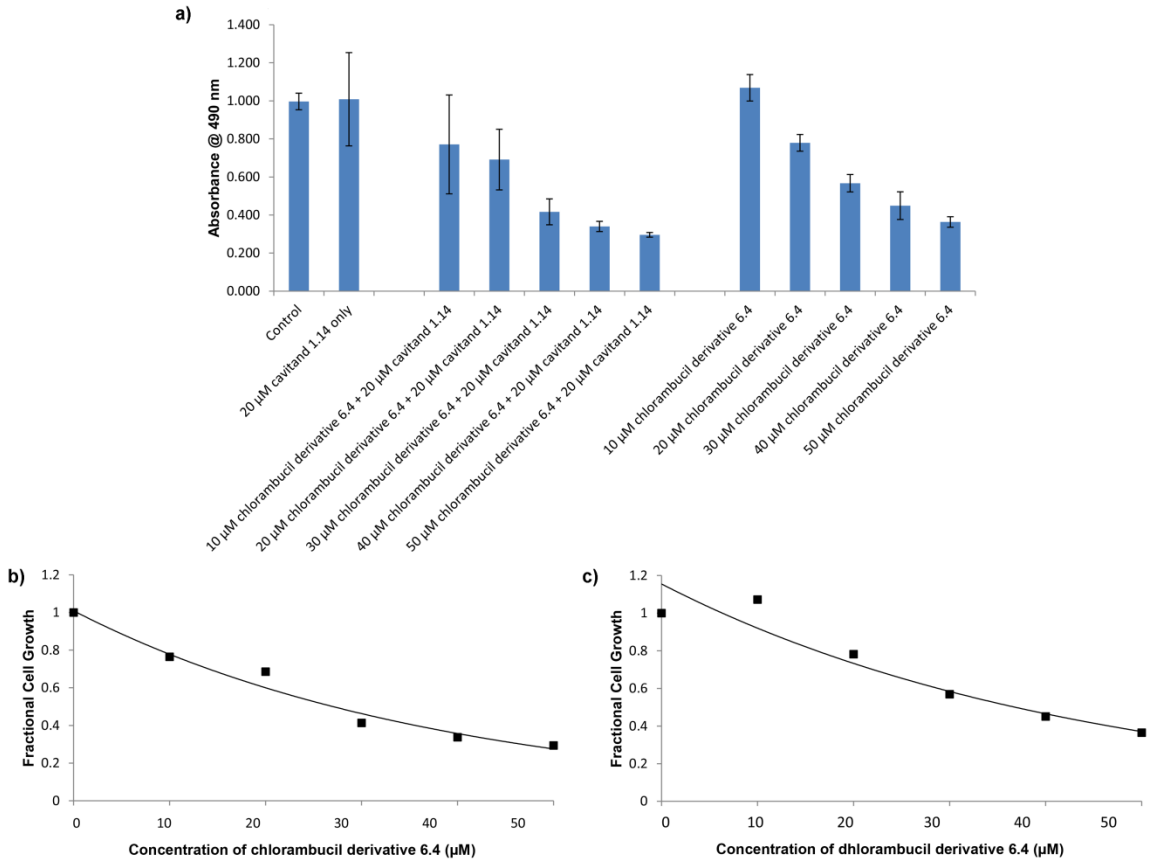

Figure 6.9: SRB assay. HeLa cells were treated with various concentrations of chlorambucil derivative **6.4** (10-50 μM) in the presence and absence of cavitand **1.14** for 5 days: (a) absorbance at 490 nm; (b) fractional cell growth of HeLa cells treated with chlorambucil derivative **6.4** in the presence of cavitand **1.14**; (c) fractional cell growth of HeLa cells treated with chlorambucil derivative **6.4** in the absence of cavitand **1.14**. Results are the average of triplicate assays.

6.3 Transport of Biomacromolecules

The ability of cavitand **1.14** to recognize small molecules with a suitable binding handle and mediating their transport across cell membranes via endocytosis has been shown.[6] Moving on to more challenging targets, the delivery of biomacromolecules like proteins into cells was attempted. Proteins are large and highly charged species that are very soluble in water. It has been reported that hydrophilic molecules show a weaker binding affinity for cavitand **1.14**.[16] Fortunately, previous work showed that a biotin

guest labeled with the R-NMe_3^+ binding handle can be recognized by cavitand **1.14** when incorporated into SLB and NeutrAvidin showed good binding to bound biotin guest in SPR experiments.[17] The binding affinity of NeutrAvidin and biotin is ~ 10^{15} M^{-1} in solution, and the binding constant of biotin guest:NeutrAvidin complex and cavitand **1.14** incorporated into the SLB is 3.64 X 10^5 M^{-1} when measured by SPR analysis. Thus, instead of fluorescently labeled choline derivative **5.1**, a biotin guest **6.5** labeled with the R-NMe_3^+ binding handle was synthesized in two steps (Figure 6.10). Biotin was coupled with *N*-hydroxysuccinimide by *N*, *N'*-dicyclohexylcarbodiimide, and subsequently reacted with (2-aminoethyl)trimethylammonium chloride hydrochloride to introduce the trimethylammonium binding handle to biotin.

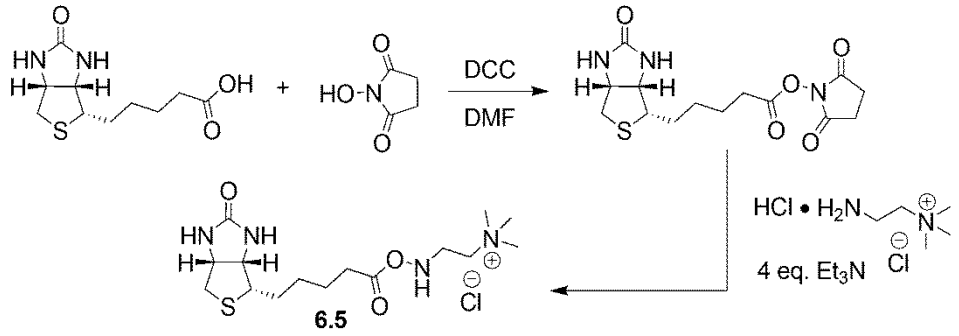

Figure 6.10: Synthesis of biotin labeled with R-NMe_3^+ binding handle **6.5**.

Since neither cavitand **1.14** nor biotin guest **6.5** have a fluorophore, avidin conjugated with fluorescein (MW = 66 kDa) was used for visualization of the location of the protein within the cells. HeLa cells were incubated with the R-NMe_3^+ labeled biotin guest **6.5** and fluorescein conjugated avidin in the presence and absence of cavitand **1.14**

for 1 h and 24 h (Figure 6.11). As another control experiment, HeLa cells were incubated with fluorescein conjugated avidin and cavitand **1.14** in the absence of biotin guest **6.5** for 1 h and 24 h. After 1 h incubation, none of the fluorescein labeled avidin was incorporated into cells under all three conditions. Minimal incorporation of fluorescein labeled avidin was observed after extended incubation time (24 h), but this was shown from HeLa cells incubated under all three different conditions. Therefore, this minimal transport of avidin conjugated with fluorescein may be occurring via a different mechanism that is not cavitand-mediated transport.

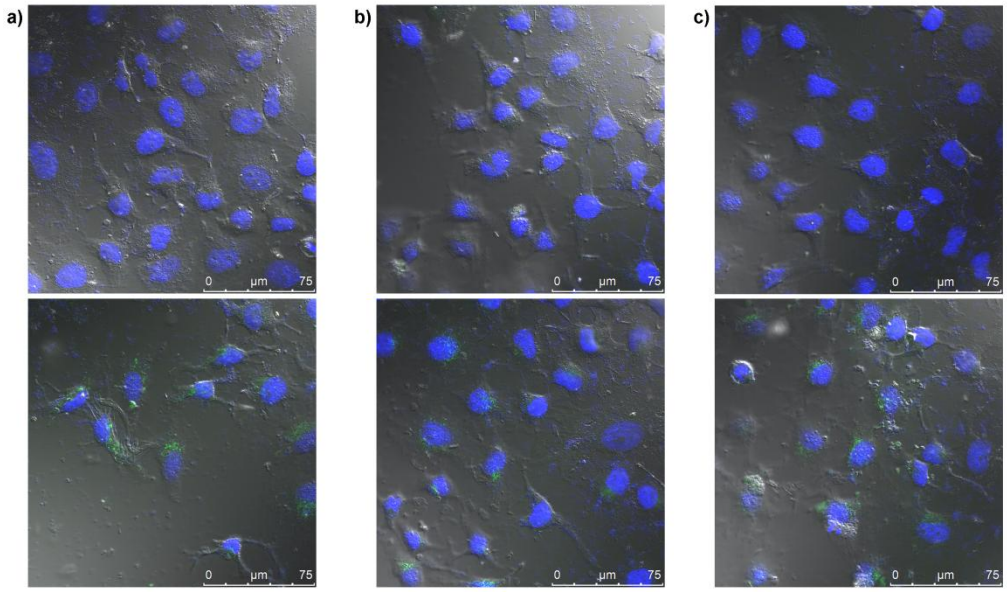

Figure 6.11 DIC/confocal fluorescence microscopy images of the addition of fluorescein conjugated avidin to HeLa cells (nuclei stained with DAPI): (a) 50 µM cavitand **1.14**, 50 µM biotin labeled with a R-NMe_3^+ binding handle **6.5**, 20 µM avidin conjugated with fluorescein, 1 h (top) and 24 h (bottom) incubation; (b) 50 µM biotin labeled with a R-NMe_3^+ binding handle **6.5**, 20 µM avidin conjugated with fluorescein, 1 h (top) and 24 h (bottom) incubation; (c) 50 µM cavitand **1.14**, 20 µM avidin conjugated with fluorescein, 1 h (top) and 24 h (bottom) incubation.

The transport of fluorescein labeled avidin into cells is complicated since the protein has to form a complex with the biotin guest **6.5** and the huge complex has to be recognized by free cavitand **1.14** in cell cultures or cavitand **1.14** incorporated into the cellular membrane. Therefore, proteins directly labeled with the R-NMe_3^+ binding handle was tested. Our preliminary research showed that the R-NMe_3^+ binding handle **2.4** can be labeled on external lysine groups on proteins and cavitand **1.14** was capable of immobilizing the derivatized proteins at biomimetic membrane interfaces.[18] The observed binding constants of cyt *c* and myoglobin, both labeled with the R-NMe_3^+ binding handle, for cavitand **1.14** incorporated into SLB were ~10^5 M^{-1}. The ESI MS analysis of derivative cyt *c* revealed that one and two R-NMe_3^+ binding handles were labeled on cyt *c*. Since proteins are not usually fluorescent, fluorescein was tagged on external lysine groups in proteins by the addition of fluorescein isothiocyanate in the binding handle labeling process. First, HeLa cells were incubated with 10 μM derivatized cyt *c* in the presence and absence of cavitand **1.14** for 1 h and 24 h, and the localization of derivatized cyt *c* was visualized (Figure 6.12). The results showed that none of the derivatized cyt *c* was transported into cells after 1 h incubation, both in the presence and absence of cavitand **1.14**. After 24 h incubation, small amounts of cyt *c* labeled with a suitable binding handle were transported into HeLa cells in both cases; in the presence and absence of cavitand **1.14**. This indicates that the transport of the R-NMe_3^+ labeled cyt *c* was not mediated by cavitand **1.14**, but occurred via a different mechanism. Furthermore, transported cyt *c* tagged with the R-NMe_3^+ binding handle and fluorescein seems to remain within endosomes because the fluorescence is punctate, as shown in

Figure 6.12. Cyt *c* is a membrane-impermeable protein and known to be released into cytoplasm from mitochondria during cellular apoptosis. In order to transport cyt *c* from the external cellular environment to induce apoptosis, electroporation technique[19] or covalent attachment of cyt *c* into nanoparticles method[20] are employed to increase permeability of cyt *c*. Since the transport of cyt *c* without evident cell death was not observed, it supports the assumption that the transported cyt *c* were contained within endosomes and not released to the cytosol.

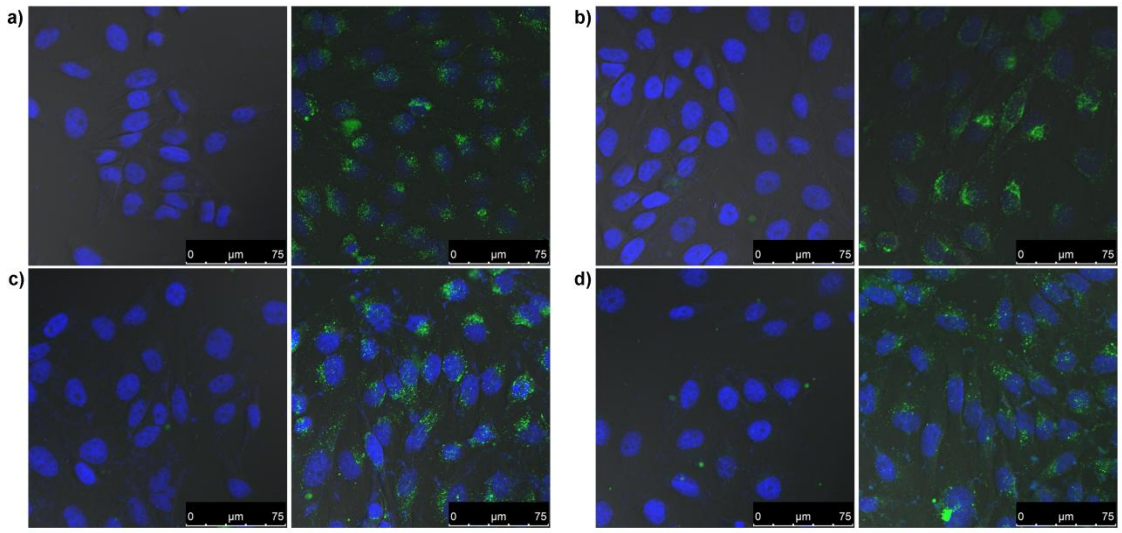

Figure 6.12: DIC/confocal fluorescence microscopy images of the addition of both fluorescein and R-NMe_3^+ binding handle labeled proteins in the presence and absence of cavitand **1.14** to HeLa cells (nuclei stained with DAPI): (a) 10 µM fluorescein and R-NMe_3^+ binding handle labeled cyt *c*, 50 µM cavitand **1.14**, 1 h (left) and 24 h (right) incubation; (b) 10 µM fluorescein and R-NMe_3^+ binding handle labeled cyt *c*, 1 h (left) and 24 h (right) incubation; (c) 10 µM fluorescein and R-NMe_3^+ binding handle labeled myoglobin, 50 µM cavitand **1.14**, 1 h (left) and 24 h (right) incubation; (d) 10 µM fluorescein and R-NMe_3^+ binding handle labeled myoglobin, 1 h (left) and 24 h (right) incubation.

HeLa cells were also incubated with 10 µM derivatized myoglobin in the presence and absence of cavitand **1.14** for 1 h and 24 h (Figure 6.12). Unfortunately,

transport of derivatized myoglobin into cells was not observed after 1 h incubation, both in the presence and absence of cavitand **1.14**. Small amounts of myoglobin tagged with the R-NMe_3^+ binding handle were incorporated into HeLa cells after 24 h incubation in the presence and absence of cavitand **1.14**. This indicates that the transport of myoglobin labeled with the R-NMe_3^+ binding handle was not assisted by cavitand **1.14**, but promoted via different mechanism.

As mentioned previously, the R-NMe_3^+ binding handle labeling efficiency on cyt *c* was not high.[18] Only one or two binding handles were labeled on cyt *c*. Thus, our attempt to label both fluorescein and the R-NMe_3^+ binding handle on proteins might have been too complicated. It is possible that only fluorescein was labeled on proteins and the fluorescein tagged proteins without the binding handle was transported into cells via a different mechanism. To solve this complicated labeling problem, mWasabi, kindly provided by Dr. Huiwang Ai at University of California, Riverside, was employed. mWasabi is a monomeric green fluorescent protein (MW = 27 kDa) that can be easily visualized by confocal fluorescence microscopy since the protein itself is a fluorophore. For the recognition by cavitand **1.14**, mWasabi was labeled with the R-NMe_3^+ binding handle **2.4** via literature method.[15] The total number of R-NMe_3^+ binding handles labeled on mWasabi could not be determined clearly because this protein is too large for ESI MS, but the presence of R-NMe_3^+ on mWasabi after the labeling reaction was confirmed by SPR analysis (Figure 6.13). HeLa cells were incubated with a suitable binding handle labeled mWasabi (2 μM) and cavitand **1.14** (50 μM) for 1 h and 24 h (Figure 6.14). The results showed that none of derivatized mWasabi was transported into the cells after 1 h

incubation, both in the presence and absence of cavitand **1.14**. However, small amounts of mWasabi labeled with a suitable binding handle were transported into HeLa cells in both cases; in the presence and absence of cavitand **1.14** after 24 h incubation. mWasabi is also a membrane-impermeable protein like cyt *c*, thus this indicates that the R-NMe_3^+ labeled mWasabi was transported into cells via a different mechanism, but it was not mediated by cavitand **1.14**.

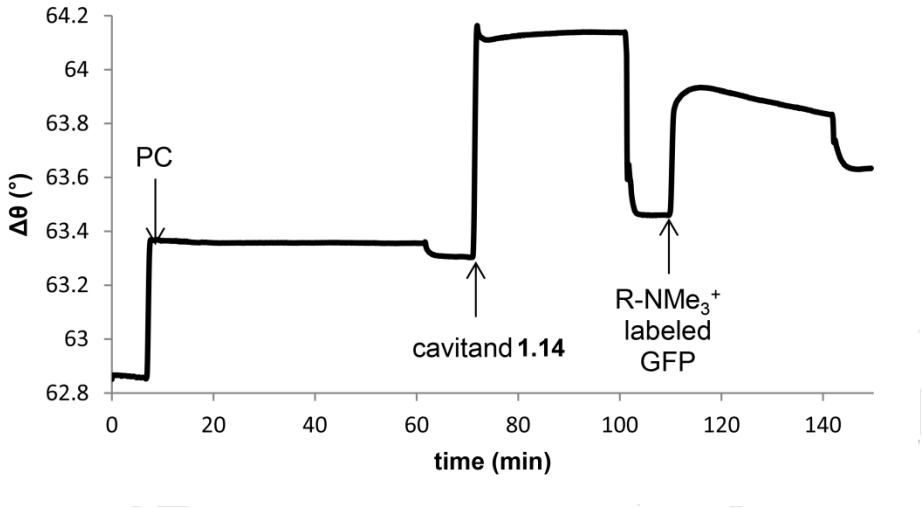

Figure 6.13: SPR sensorgram of R-NMe_3^+ labeled mWasabi recognition by membrane-bound cavitand **1.14**.

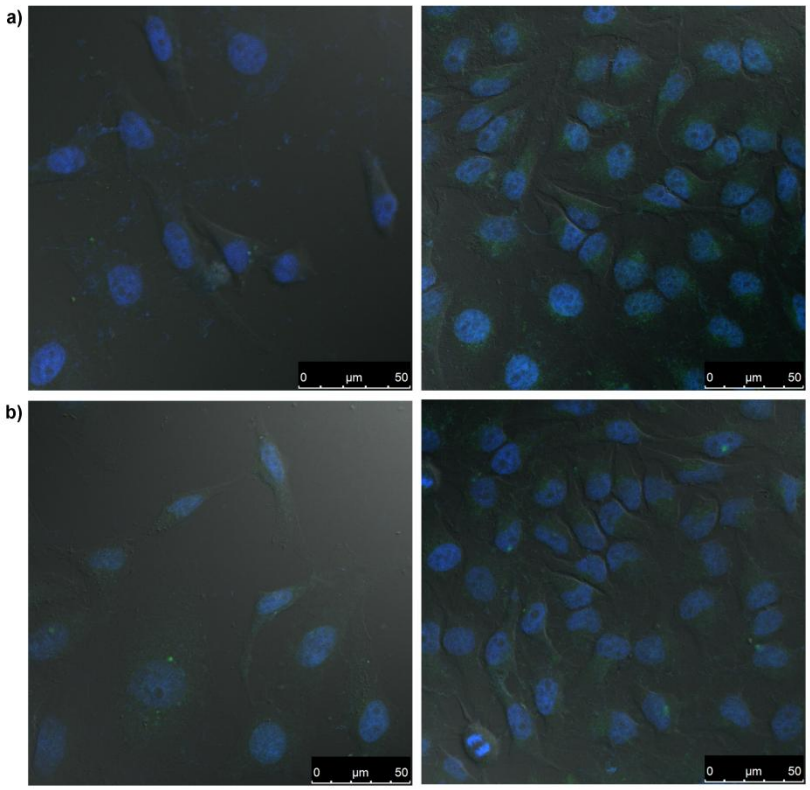

Figure 6.14: DIC/confocal fluorescence microscopy images of mWasabi labeled with R-NMe_3^+ binding handle to HeLa cells (nuclei stained with DAPI): (a) 50 µM cavitand **1.14**, 50 µM R-NMe_3^+ labeled mWasabi, 1 h (left) and 24 h (right) incubation; (b) 50 µM R-NMe_3^+ labeled mWasabi, 1 h (left) and 24 h (right) incubation.

6.4 Conclusion

In order to investigate enhanced transport assisted by cavitand **1.14**, several anticancer drug candidates were labeled with a R-NMe_3^+ binding handle and their cytotoxicity was tested on HeLa cells in the presence and absence of cavitand **1.14**. Chlorambucil labeled with R-NMe_3^+ binding handle showed cytotoxicity under both conditions, in the presence and absence of cavitand **1.14**. But, lower IC_{50} value was obtained when cells were treated with the drug derivative in the presence of cavitand.

This indicates that the presence of cavitand **1.14** enhances the transport of drug candidates labeled with a suitable binding handle.

Since cavitand **1.14** was capable of transporting small molecules into cells, larger proteins were tested on the system to investigate the scope of guest that can be transported into cells by cavitand **1.14**. Fluorescein labeled avidin with R-NMe_3^+ labeled biotin guest **6.5** and R-NMe_3^+ labeled proteins were introduced on HeLa cells in the presence and absence of cavitand **1.14**, but the transport of the proteins obviously mediated by cavitand **1.14** was not observed.

6.5 References

1. Koren, E.; Torchilin, V. P. "Cell-Penetrating Peptides: Breaking Through to the Other Side." *Trends Mol. Med.*, **2012**, *18*, 385-393.

2. Rothbard, J. B.; Garlington, S.: Lin, Q.; Kirschberg, T.; Kreider, E.; McGrane, P. L.; Wender, P. A.; Khavari, P. A. "Conjugation of Arginine Oligomers to Cycloporin A Facilitates Topical Delivery and Inhibition of Inflammation." *Nat. Med.*, **2000**, *6*, 1253-1257.

3. Fawell, S.; Seery, J.; Daikh, Y.; Moore, C.; Chen, L. L.; Pepinsky, B.; Barsoum, J. "Tat-Mediated Delivery of Heterologous Proteins into Cells." *Proc. Natl. Acad. Sci. U. S. A.*, **1994**, *91*, 664-668.

4. Chiu, Y. L.; Ali, A.; Chu, C. Y.; Cao, H.; Rana, T. M. "Visualizing a Correlation between siRNA Localization, Cellular Uptake, and RNAi in Living Cell." *Chem. Biol.*, **2004**, *11*, 1165-1175.

5. Nagahara, H.; Vocero-Akbani, A. M.; Snyder, E. L.; Ho, A.; Latham, D. G.; Lissy, N. A.; Becker-Hapak, M.; Ezhevsky, S. A.; Dowdy, S. F. "Transduction of Full-Length TAT Fusion Proteins into Mammalian Cells: TAT-p27Kip1 Induces Cell Migration." *Nat. Med.*, **1998**, *4*, 1449-1452.

6. Ghang, Y. –J.; Schramm, M. P.; Zhang, F.; Acey, R. A.; David, C. N.; Wilson, E. H.; Wang, Y.; Cheng, Q.; Hooley, R. J. "Selective Cavitand-Mediated Endocytosis of Targeted Imaging Agents into Live Cells." *J. Am. Chem. Soc.*, **2013**, *135*, 7090-7093.

7. Vichai, V.; Kirtikara, K. "Sulforhodamine B Colorimetric Assay for Cytotoxicity Screening." *Nature Protocols*, **2006**, *1*, 1112-1116.

8. Houghton, P.; Fang, R.; Techatanawat, I.; Steventon, G.; Hylands, P.; Lee, C. C. "The Sulphorhodamine (SRB) Assay and Other Approaches to Testing Plant Extracts and Derived Compounds for Activities Related to Reputed Anticancer Activity." *Methods*, **2007**, *42*, 377-387.

9. Florea, A. –M.; Büsselberg, D. “Cisplatin as an Anti-Tumor Drig: Cellular Mechanisms of Activity, Drug Resistance and Induced Side Effects.” *Cancers*, **2011**, *3*, 1351-1371.

10. Fritz-Wolf, K.; Urig, S.; Becker, K. “The Structure of Human Thioredoxin Reductase 1 Provides Insights into C-terminal Rearrangements During Catalysis.” *J. Mol. Biol.*, **2007**, *370*, 116-127.

11. Wein, A. N.; Stockhausen, A. T.; Hardcastle, K. I; Peng, S.; Saadein, M. R.; Peng, S.; Wang, D.; Shin, D. M.; Chen, Z. ; Eichler, J. F. “Tumor Cytotoxicity of 5,6-Dimethyl-1,10-Phenanthroline and its Corresponding Gold(III) Complex.” *J. Inorg. Biochem.*, **2011**, *105*, 663-668.

12. Hudson, Z. D.; Sanghvi, C. D.; Rhine, M. A.; Ng, J. J.; Bunge, S. D.; Hardcastle, K. I.; Saadein, M. R.; MacBeth, C. E.; Eichler, J. F. “Synthesis and Characterization of Gold(III) Complexes Possessing 2,9-Dialkylphenanthroline Ligands: To Bind or Not to Bind?” *Dalton. Trans.*, **2009**, 7473-7480.

13. Sanghvi, C. D.; Olsen, P. M.; Elix, C.; Peng, S.; Wang, D.; Chen, Z.; Shin, D.; Hardcastle, K. I.; Macbeth, C. E.; Eichler, J. F. “Antitumor Properties of Five-Coordinating Gold(III) Complexes Bearing Substituted Polypyridyl Ligands.” *J. Inor. Biochem.*, **2013**, *128*, 68-76.

14. Olsen, P. M.; Ruiz, C.; Lussier, D.; Le B. K.; Angel, N.; Smith, M.; Hwang, C.; Khatib, R.; Jenkins, J.; Adams, K.; Getcher, J.; Tham, F.; Chen, Z.; Wilson, E. H.; Eichler, J. F. “Synthesis, Characterization, and Antitumor Activity of Unusual Pseudo Five Coordinate Gold(III) Complexes: Distinct Cytotoxic Mechanism or Expensive Ligand Delivery Systems?” *J. Inorg. Biochem.*, **2014**, *141*, 121-131.

15. Begleiter, A.; Mowat, M.; Israels, L. G.; Johnston, J. B. “Chlorambucil in Chroni Lymphocytic Leukemia: Mechanism of Action.” *Leuk. Lymphoma*, **1996**, *23*, 187-201.

16. Hooley, R. J.; van Anda, H. J.; Rebek, J. Jr. “Extraction of Hydrophobic Species into a Water-Soluble Synthetic Receptor.” *J. Am. Chem. Soc.*, **2007**, *129*, 13464-13473.

17. Liu, Y.; Liao, P.; Cheng, Q.; Hooley, R. J. “Protein and Small Molecule Recognition Properties of Deep Cavitands in a Supported Lipid Membrane

Determined by Calcination-Enhanced SPR Spectroscopy." *J. Am. Chem. Soc.*, **2010**, *132*, 10383-10390.

18. Ghang, Y. –J.; Lloyd, J. J.; Moehlig, M. P.; Arguelles, J. K.; Mettry, M.; Zhang, X.; Julian, R. R.; Cheng, Q.; Hooley, R. J. "Labeled Protein Recognition at a Membrane Bilayer Interface by Embedded Synthetic Receptors." *Langmuir*, **2014**, *30*, 10161-10166.

19. Garland, J. M.; Rudin, C. "Cytochrome c Induces Caspase-Dependent Apoptosis in Intact Hematopoietic Cells and Overrides Apoptosis Suppression Mediated by bcl-2, Growth Factor Signaling, MAP-Kinase-Kinase, and Malignant Change." *Blood*, **1998**, *92*, 1235-1246.

20. Méndez, J.; Cruz, M. M., Delgado, Y.; Figueroa, C. M.; Orellano, E. A.; Morales, M.; Monteagudo, A.; Griebenow, K. "Delivery of Chemically Glycosylated Cytochrome c Immobilized in Mesoporous Silica Nanoparticles Induces Apoptosis in HeLa Cancer Cells." *Mol. Parmaceutics*, **2014**, *11*, 102-111.

Chapter Seven: Experimental

7.1 General Information

^{1}H and ^{13}C NMR spectra were recorded on a Varian Inova 300 or 400 MHz NMR spectrometer and processed using MestReNova by Mestrelab Research S.L. Proton (^{1}H) chemical shifts are reported in parts per million (δ) with respect to tetramethylsilane (TMS, $\delta = 0$), and referenced internally with respect to the protio solvent impurity. Carbon (^{13}C) chemical shifts were reported in parts per million (δ) with respect to TMS ($\delta = 0$), and referenced internally with respect to the solvent ^{13}C signal (either $CDCl_3$ or DMSO-d_6). Deuterated NMR solvents were obtained from Cambridge Isotope Laboratories, Inc., Andover, MA, and used without further purification. Victor^2 1420 multilable counter (PerkinElmer, Waltham, MA) was used for Bradford assay and SRB assay. A P/ACE PA800 capillary electrophoresis system equipped with a diode array detector (Beckman Coulter, Fullerton, CA) was used for all CE experiments. Mass spectra were recorded by electrospray ionization on an LTQ-XL linear ion trap mass spectrometer (Thermo Scientific, San Jose, CA). HPLC measurements were performed on an Agilent 1100 HPLC (Agilent Technologies, Santa Clara, CA) using a Waters (Milford, MA) 4.6 x 150 mm XTerra MS C18 column with 5 μm pore size. HPLC-grade acetonitrile was purchased from Fisher Scientific (Pittsburgh, PA), and trifluoroacetic acid (TFA) was purchased from Acros (Geel, Belgium). HPLC-grade water was obtained from Burdick and Jackson (Muskegon, MI). 1-Palmitoyl-2-oleoyl-*sn*-glycero-3-phosphocholine, 1-palmitoyl-2-{12-[(7-nitro-2-1,3-benzoxadiazol-4-yl)amino]hexanoyl}-*sn*-glycero-3-phosphocholine, and sphingomyelin were purchased from Avanti Polar

Lipids (Alabaster, AL). Bradford Protein Assay solution was purchased from Bio-Rad (Hercules, CA). CE solutions were prepared in the deionized water purified by the Milli·Q water purification system (Billerica, MA). Fluorescence and DIC images of SLB and cells were taken and FRAP experiments were performed by Confocal Leica SP5 fluorescence microscopy (Buffalo Grove, IL). All other materials were obtained from Aldrich Chemical Company (St. Louis, MO), Fisher Scientific (Fairlawn, NJ), or TCI (Tokyo, Japan) and were used as received. Solvents were dried through a commercial solvent purification system (Pure Process Technologies, Inc.). Dulbecco's Modification of Eagle's Medium (DMEM) and fetal bovine serum (FBS) were purchased from ATCC. The HeLa cell line was purchased from ATCC (Manassas, VA), and the GM00637 cell line was kindly provided by Prof. Gerd P. Pfeifer (City of Hope, CA). HeLa, GM00637, HFF, and astrocyte cells were maintained in DMEM supplemented with 10 % FBS in a humidified incubator with 5 % CO_2 at 37 °C. Molecular modeling (semi-empirical calculations) was performed using the AM1 force field using SPARTAN. Cavitand **1.14** and **2.5** were synthesized according to literature procedures.[1,2]

7.2 Chapter Two Experimental

Synthesis of New Compounds

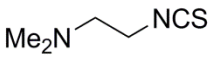

2-isothiocyanato-*N*,*N*-dimethylaminoethane 2.1: In a 50 mL round bottom flask, *N*,*N*-dimethylethylenediamine (0.48 mL, 4.36 mmol) was dissolved in 5 mL EtOH. To this solution was added NEt_3 (0.61 mL, 4.36 mmol) followed by CS_2 (2.64 mL, 43.6 mmol).

The reaction mixture was stirred for 1h at room temperature before cooling to 0 ºC and adding a solution of Boc_2O (0.95 g, 4.33 mmol) in 1 mL EtOH followed by the addition of a solution of a solution of 4-dimethylaminopyridine (11 mg, 0.09 mmol) in 1mL EtOH. The reaction mixture was stirred for 1h at room temp before removing the solvent and all volatiles under reduced pressure to yield an off-white solid (592 mg, 99% yield). ^{1}H NMR ($CDCl_3$, 400 MHz): δ 3.56 (t, *J* = 6.3 Hz, 2H), 2.56 (t, *J* = 6.3 Hz, 2H), 2.25 (s, 6H). ^{13}C NMR ($CDCl_3$, 100 MHz): δ 131.7, 58.5, 45.4, 43.5. MS (ESI) *m/z* $(M+H)^+$ 131.0639, expected *m/z* 131.0637.

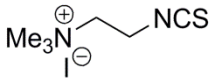

2-isothiocyanatoethane-1-*N,N,N*-trimethylammonium iodide 2.2: 2-isothiocyanato-*N,N*-dimethylaminoethane (100 mg, 0.77 mmol) was dissolved in THF (2 mL). To this solution was added MeI (50 μL, 0.77 mmol). The reaction mixture was stirred for 2h before filtering off the precipitate and washing with diethyl ether. A pale yellow solid was obtained (175 mg, 84 % yield). ^{1}H NMR (DMSO-d_6, 400 MHz): δ 4.33 (t, *J* = 5.3 Hz, 2H), 3.70 (t, *J* = 5.4 Hz, 2H), 3.15 (s, 9H). ^{13}C NMR (DMSO-d_6, 100 MHZ): δ 129.9, 63.3, 52.6, 40.1. MS (ESI) *m/z* $(M-I)^+$ 145.0801, expected *m/z* 145.0794.

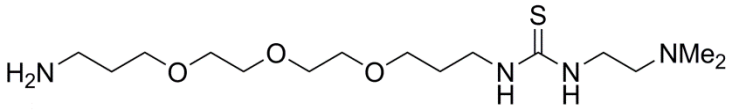

1-[3-[2-[2-(3-aminopropoxy)ethoxy]ethoxy]propyl]-3-(2-dimethylaminoethyl)thio-urea 2.3: 2-isothiocyanato-*N,N*-dimethylaminoethane (100 mg, 0.77 mmol) was dissolved in EtOH (5 mL) before adding 4,7,10-trioxa-1,13-tridecanediamine (168 μL, 0.77 mmol). The reaction mixture was stirred for 18h at room temperature. The solvent

was removed under reduced pressure and the product was purified on a basic alumina gradient column (0% to 10% MeOH in CH_2Cl_2). Yellow oil was obtained (37 mg, 14 % yield). ^{1}H NMR ($CDCl_3$, 400 MHz): δ 3.54-3.28 (m, 16H), 3.27 (broad s, 4H), 2.72 (t, *J* = 6.7 Hz, 2H), 2.38 (t, *J* = 5.7 Hz, 2H), 2.13 (s, 6H), 1.75 (qn, *J* = 6.2 Hz, 2H), 1.65 (qn, *J* = 6.3 Hz, 2H). ^{13}C NMR ($CDCl_3$, 100 MHz): δ 182.1, 70.2, 69.9, 69.4, 69.2, 58.2, 45.0, 41.9, 39.3, 32.0, 29.5, 28.8, 28.6. MS (ESI) *m/z* $(M+Na)^+$ 373.2244, expected *m/z* 373.2244.

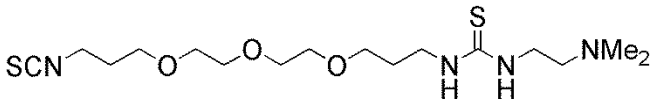

1-(2-dimethylaminoethyl)-3-[3-[2-[2-(3-isothiocyanatopropoxy)ethoxy]ethoxy]-propyl]thiourea: 1-[3-[2-[2-(3-aminopropoxy)ethoxy]ethoxy]propyl]-3-(2-dimethyl-aminoethyl)thiourea (160 mg, 0.46 mmol), CS_2 (0.28 mL, 4.56 mmol), and NEt_3 (63 μL, 0.46 mmol) were combined in EtOH (2 mL). The mixture was stirred for 1h at room temperature before being cooled to 0 ºC and adding a solution of Boc_2O (98 mg, 0.45 mmol) in 0.5 mL EtOH followed by a solution of 4-dimethylaminopyridine (1 mg, 0.008 mmol) in 0.5 mL EtOH. The reaction mixture was stirred at room temperature for 1h before removing solvent under reduced pressure to yield viscous yellow oil (177 mg, 99% yield). ^{1}H NMR ($CDCl_3$, 400 MHz): δ 3.63-3.43 (m, 18H), 2.40 (t, *J* = 5.5 Hz, 2H), 2.16 (s, 6H), 1.84 (qn, *J* = 6.2 Hz, 2H), 1.76 (qn, *J* = 6.2 Hz, 2H). ^{13}C NMR ($CDCl_3$, 100 MHz): δ 182.2, 129.9, 70.4, 70.3, 70.2, 70.1, 67.2, 58.4, 58.1, 45.1, 42.1, 31.2, 30.1, 28.7, 28.1. MS (ESI) *m/z* $(M+H)^+$ 393.1976, expected *m/z* 393.1989.

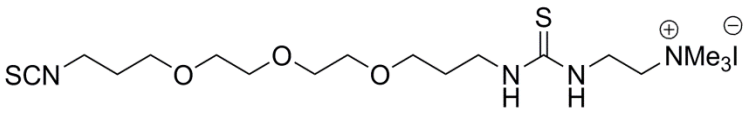

2-[3-[2-[2-(3-isothiocyanatopropoxy)ethoxy]ethoxy]propylcarbamothioylamino]-ethyl-trimethylammonium iodide 2.4: To a solution of 1-(2-dimethylaminoethyl)-3-[3-[2-[2-(3-isothiocyanatopropoxy)ethoxy]ethoxy]propyl]thiourea (41 mg, 0.11 mmol) in THF (2 mL) was added MeI (7 μL, 0.11 mmol). The reaction was stirred for 4h before removing the solvent and sonicating in hexanes. The solvent was decanted off to yield a viscous yellow wax. ^{1}H NMR ($CDCl_3$, 400 MHz): δ 3.74 (t, J = 5.5 Hz, 2H), 3.66-3.52 (m, 18H), 3.42 (s, 9H), 1.92 (qn, *J* = 6.2 Hz, 2H), 1.84 (qn, *J* = 6.2 Hz, 2H). ^{13}C NMR ($CDCl_3$, 100 MHz): δ 183.4, 129.6, 70.5, 70.4, 70.1, 69.8, 69.2, 67.2, 65.1, 54.7, 54.5, 42.2, 30.2, 30.0, 29.9. MS (ESI) *m/z* $(M-I)^+$ 407.2215, expected *m/z* 407.2151.

Labeling Proteins with a Trimethylammonium Binding Handle 2.2 and 2.4

Trimethylammonium tag **2.2** or **2.4** was dissolved in DMSO to a concentration of 1 M. Protein was dissolved in 0.1 M PBS buffer (pH 7.4), and 20 μM fo 1 M tag solubion was added into the protein solution to make the final concentration of tag range 20 mM. The mixture was incubated at 37 °C for 24 h. The labeled protein was separated from unreacted or hydrolyzed tag by Amicon Ultra Centrifugal Filter (EMD Millipore, Billerica, MA), and the purified labeled protein concentration was determined by Bradford Assay. The desired concentration of labeled protein was achieved by the dilution of purified labeled protein with 0.1 M PBS buffer.

Bradford assay

The 20 μM of BSA standard solutions - blank, 0.125 mg/mL, 0.25 mg/mL, 0.5 mg/mL, 1.0 mg/mL, and 2/0 mg/mL - were prepared in PBS buffer, and 1 mL of commassie blue dye were added to each solution. An unknown labeled protein sample solution was prepared by combining 20 μM unknown labeled protein and 1 mL of commassie blue dye. These solutions were mixed well and incubated for 5 min at room temperature. the solutions were transferred to 1 mL disposable cuvettes and spectrophotometer was set to 595 nm. The blank sample was measure in order to zero the instrument. The absorbance of the standards and the unknown labeled protein sample were measures.

Calcinated Chip Preparation

Gold substrates were fabricated with a 2 nm thick chromium adhesion layer, followed by the deposition of a 46 nm thick gold layer via e-beam evaporation on cleaned glass slides. The nanoglassified layers were constructed on the surface based on a previous layer-by-layer protocol.[3] Clean gold substrates were immersed in 10 mM 3-mercaptopropionic acid (MPA) ethanol solution overnight to form a self-assembly monolayer. After extensive rinsing with ethanol and nanopure water and drying with nitrogen gas, modified gold substrates were alternated dipped into poly(allylamine hydrochloride) solution (1 mg/mL, adjusted to pH 8.0) and sodium silicate solution (22 mg/mL, adjusted to pH 9.5) for 1 min to form a layer by layer assembly structure, with sufficient ultrapure water rinsing between layers. This dipping process was repeated six times to build up a multilayer membranes gold chip, followed by calcinated in a furnace by heating to 450 °C at a rate of 17 °C/min and allowing cooling to room temperature 4 hours later.

Vesicle Preparation

1-Palmitoyl-2-oleoyl-*sn*-glycero-3-phosphocholine lipid stock solution in chloroform was transferred to a small vial and the organic solvent was purged from the vial with nitrogen gas to form a dry lipid film on the vial wall, which was then rehydrated with 20 mM PBS (150 mM NaCl, pH 7.4) to a lipid concentration of 1 mg/mL. The resuspended lipids were probe sonicated for 20 min, followed by centrifuged at 8,000 rpm for 15 min to remove any titanium particles released from the probe tip. The supernatant was then extruded with 11 passes through a polycarbonate membrane of pore size 100 nm to ensure formation of small unilamellar vesicles. The solution was then incubated at 4 °C for at least 1 h before use. For the preparation of vesicle preincorporated with cavitand **2.5**, 1-Palmitoyl-2-oleoyl-*sn*-glycero-3-phosphocholine lipid stock solution in chloroform was transferred to a small vial and was added cavitand **2.5** stock solution in chloroform to a final concentration of 2 wt%. The rest of the preparation steps were identical.

Fabrication of Cavitand Receptor Layer and Protein Binding Measurement

The fabrication of cavitand **1.14**-membrane complex and subsequent guest binding was monitored through surface plasmon resonance (SPR) spectrometry.[4] The shift of SPR minimum angle characterized surface thickness and surface refractive index change, demonstrating adsorption or binding on the surface. The calcinated gold substrate was first rinsed with ethanol and nanopure water and after drying under gentle stream of nitrogen gas was then clamped down by a flow cell on a high-refractive index prism for SPR measurement. PC vesicles (1 mg/mL) in 20 mM PBS (150 mM NaCl, pH 7.4) were injected through a flow-injection system and incubated for 1 h to allow vesicle fusion on

the hydrophilic calcinated gold surface, forming a smooth bilayer membrane. After 10 min of rinsing to remove excess vesicle from the surface, 2 mg/mL cavitand **1.14** in 10 % DMSO solution was subsequently injected and incubated for 30 min. The surface was extensively rinsed with nanopure water, followed by incubation with 15 μM R-NMe_3^+ labeled protein in water for 30 min. Excess proteins were rinsed with water. Control experiments were performed under identical conditions in the absence of cavitand **1.14**, or by the injection of PC vesicles pre-incorporated with cavitand **2.5**.

ESI-MS Analysis of Trypsinized Fragments

Solutions containing 10 μM labeled protein in 100% water were directly infused into an LTQ linear ion trap with a standard electrospray ionization source (Thermo Scientific, San Jose, CA).

Binding Analysis

Saturation binding mode (eq 1)[5] was applied to determine the equilibrium dissociation constant (K_d) value for the interaction between cavitand **1** and labeled protein guests. Increasing concentrations of labeled protein guests (3 μM to 15 μM) were injected over the cavitand **1**:membrane complex, and the minimum angle shift was recorded:

$$AB_{eq} = AB_{max}(1/(1+K_d/[A])) \qquad \text{(eq 1)}$$

where AB_{eq} is the average of response signal at equilibrium and AB_{max} is the maximum response that can be obtained for guest binding and [A] is the concentration of labeled protein injection. AB_{max}/AB_{eq} was plotted against 1/[A], and the slope is equal to K_d value. K_a, the equilibrium association constant can be determined by the reciprocal value of K_d.

7.3 Chapter Three Experimental

Fabrication of Cavitand Receptor Layer and Protein Binding Measurement

The fabrication of cavitand **1.14**-membrane complex and subsequent guest binding was monitored through surface plasmon resonance (SPR) spectrometry. The shift of SPR minimum angle characterized surface thickness and surface refractive index change, demonstrating adsorption or binding on the surface. The calcinated gold substrate was first rinsed with ethanol and nanopure water and after drying under gentle stream of nitrogen gas was then clamped down by a flow cell on a high-refractive index prism for SPR measurement. PC vesicles (1 mg/mL) in 20 mM PBS (150 mM NaCl, pH 7.4) were injected through a flow-injection system and incubated for 1 h to allow vesicle fusion on the hydrophilic calcinated gold surface, forming a smooth bilayer membrane. After 10 min of rinsing to remove excess vesicle from the surface, 2 mg/mL cavitand **1.14** in 10 % DMSO solution was subsequently injected and incubated for 30 min. The surface was extensively rinsed with nanopure water, followed by incubation with 15 μM protein in water for 30 min. Excess proteins were rinsed with water. Control experiments were performed under identical conditions in the absence of cavitand **1.14**, or by the injection of PC vesicles pre-incorporated with cavitand **2.5**.

Capillary Electrophoresis

The 50 cm fused-silica capillary (75 μm id, 365μm od; PolymicroTechnologies, Phoenix, AZ) with an effective length of 40 cm was sequentially rinsed at 20 psi with 0.1 M NaOH (2 min), deionized water (1 min), 0.1 M HCl (2 min), deionized water (1 min), and the running buffer (4 min) prior to injection. Different concentrations of cavitand **1.14** (3

μM-30 μM) in the presence/absence of 0.012 mg/ml POPC were included in the running buffer of 17.5 mM phosphate (pH 7.4). DMSO at 0.01% was co-injected with 3 μM cytochrome *c* to serve as the EOF marker. All CE separations were done at 25 kV with UV-absorption detection at 191 nm in room temperature. The sample was injected by pressure at 1 psi for 5 s.

Sample Preparation of Trypsin Digestion of Insulin B in SPR for ESI MS and HPLC

Once 15 μM trypsin was immobilized on cavitand **1.14**-membrane complex, 300 μM oxidized insulin chain B from bovine pancreas in water was injected and incubated for 1 h. The digested insulin chain B was collected while rinsing with nanopure water. The collected sample was lyophilized overnight and reconstituted with water to the desired concentration.

Sample Preparation for Solution Phase Trypsin Digestion

Trypsin and insulin chain B were mixed in water to final concentrations of 8 μM and 150 μM, respectively. The mixture was incubated at room temperature for 1 h, lyophilized overnight and reconstituted with water into desired concentration.

HPLC Analysis of Trypsinized Fragments

The measurements were performed on an Agilent 1100 HPLC with UV detection at 215 nm based on previous methods.[6] Separations were performed on a Waters (Milford, MA) 4.6 x 150 mm XTerra MS C18 column with 5 μm pore size. The digested insulin was eluted using a mobile phase A, consisting of 0.1% TFA in H_2O, and a mobile phase B, consisting of 0.1% TFA in acetonitrile. The retention of the insulin components were

evaluated using a gradient of 10-60 % B over 20 mins at a flow rate of 1.0 mL/min. The column temperature was held at 25 ºC. Solutions were introduced into the system using 20 μL injections, each at a concentration of 50 μM. Fractions were collected from SPR experiments over a series of four injections to confirm their identity by mass spectrometry.

ESI-MS Analysis of Trypsinized Fragments

Solutions containing 10 μM peptides in 100% water were directly infused into an LTQ linear ion trap with a standard electrospray ionization source (Thermo Scientific, San Jose, CA). Collision induced dissociation (CID) was performed on peptides to verify sequence.

7.4 Chapter Four Experimental

Vesicle Preparation

A desired amount of 1-Palmitoyl-2-oleoyl-*sn*-glycero-3-phosphocholine lipid stock solution in chloroform, cholesterol stock solution in chloroform, and sphingomyelin stock solution in chloroformed were transferred to a small vial and the organic solvent was purged from the vial with nitrogen gas to form a dry lipid film on the vial wall, which was then rehydrated with 20 mM PBS (150 mM NaCl, pH 7.4) to a lipid concentration of 1 mg/mL. The resuspended lipids were probe sonicated for 20 min, followed by centrifuged at 8,000 rpm for 15 min to remove any titanium particles released from the probe tip. The supernatant was then extruded with 11 passes through a polycarbonate

membrane of pore size 100 nm to ensure formation of small unilamellar vesicles. The solution was then incubated at 4 °C for at least 1 h before use.

Fabrication of Cavitand Receptor Layer and Protein Binding Measurement

The fabrication of cavitand **1.14**-membrane complex and subsequent guest binding was monitored through surface plasmon resonance (SPR) spectrometry. The shift of SPR minimum angle characterized surface thickness and surface refractive index change, demonstrating adsorption or binding on the surface. The calcinated gold substrate was first rinsed with ethanol and nanopure water and after drying under gentle stream of nitrogen gas was then clamped down by a flow cell on a high-refractive index prism for SPR measurement. PC, PC/cholesterol, or PC/cholesterol/sphingomyelin vesicles in 20 mM PBS (150 mM NaCl, pH 7.4) were injected through a flow-injection system and incubated for 40 min to allow vesicle fusion on the hydrophilic calcinated gold surface, forming a smooth bilayer membrane. After 10 min of rinsing to remove excess vesicle from the surface, 2 mg/mL cavitand **1.14** in 10 % DMSO solution was subsequently injected and incubated for 20 min. The surface was extensively rinsed with nanopure water, followed by incubation with 15 μM BSA in water for 20 min. Excess proteins were rinsed with water. Control experiments were performed under identical conditions in the absence of cavitand **1.14**.

Fabrication of Polydimethylsiloxane (PDMS) Wells

PDMS wells were formed on a microscopy glass coverslip via literature method.[7] A thin layer of PDMS was prepared in a Petri dish using 10:1 elastomer/crosslinker mixture of Sylgard 184 (Robert McKeown Company; Branchburg, NJ). The PDMS was baked at

80 °C for 3 h, and cut into the same size as a coverslip. In order to form the wells, holes were punched through each square. The PDMS squares with holes were attached to a clean glass coverslip.

The Formation of Lipid Bilayers in PDMS Wells

100 μL of POPC vesicles containing cholesterol and sphingomyelin with 2 mol % NBD-PC were transferred to PDMS wells formed on a microscopy coverslip and vesicles were incubated under dark. After 30 min incubation, excess lipids were extensively washed with water.

Fluorescence Recovery After Photobleaching (FRAP)

The diffusion coefficients were determined by the methods of Axelrod and Soumpasis.[8,9]

$$F_{FRAP} = (F_n - F_0)/(1 - F_0) \qquad \text{(eq 2)}$$

Here, F_n is a normalized value of the intensity of fluorescence of the bleached spot over a fluorescent background region of the same size, and F_0 is a normalized intensity of the bleached spot immediately after bleaching. F_{FRAP} was plotted against time, and the graph was fitted to a first order exponential function.

$$D = (\omega^2/4t_{1/2})\gamma \qquad \text{(eq 3)}$$

The diffusion equation (eq 3) was applied to calculate the diffusion coefficient. Here, D is the diffusion coefficient, ω is the full width at half maximum of the Gaussian profile of the focused laser, $t_{1/2}$ is the half-time recovery obtained from the graph fit, and γ is a correction factor that accounts for the laser beam geometry.

7.5 Chapter Five Experimental

Synthesis of New Compounds

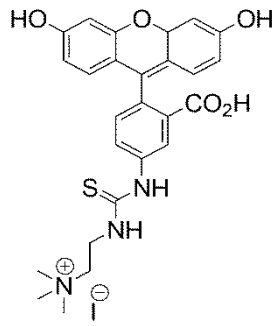

2-(3-(3-carboxy-4-(3,6-dihydroxy-4aH-xanthen-9-yl)phenyl)thioureido)-*N*,*N*,*N*-trimethylethanaminium iodide 5.1: In a 10 mL round bottom flask, (2-aminoethyl)trimethylammonium chloride hydrochloride(44 mg, 0.25 mmol) was dissolved in 1 mL DMF. To this solution Et_3N (70 µL, 0.5 mmol) was added and the solution was stirred for 10 min at room temperature. Fluorescein 5(6)-isothiocyanate was added, and the mixture was stirred at room temperature overnight under dark. The reaction solution was transferred to a centrifugal tube, and the mixture was centrifuged. The supernatant was removed and the pellet was suspended in DCM. This centrifugation step was repeated five times to remove the solvent and Et_3N. The product was dried under high vacuum and dark orange powder was obtained.[4]

Cellular Transport Imaging Assays of the Guest 5.1:Cavitand 1.14 System

1 h Incubation: HeLa, GM00637, HFF, or astrocyte cells (5 x 10^4 cells/well) were seeded on a glass cover slip in 24-well plate for 23 h at 37 °C and was added cavitand **1.14** (final concentration = 50 µM) and varying concentrations of fluorescein guest **5.1**. These cells were incubated at 37 °C for 1 h and washed with PBS buffer (3 x 500 µL) to

remove unincorporated cavitand **1.14** and guest **5.1**. The cells were fixed with 4 % paraformaldehyde and the cover slip was removed from the 24-well plate. The nuclei of the cells were stained with 4,6-diamidino-2-phenylindole dihydrochloride (DAPI) and a glass slide was mounted on the cover slip and fixed. Fluorescence microscopy of the cells was carried out on a Leica SP5 confocal microscope. Confocal fluorescence microscopy and differential interference contrast (DIC) microscopy were used to image the cells and the three images (DIC, 405 nm DAPI, 488 nm guest **5.1**) were combined to form the images shown.

24 h Incubation: To HeLa, GM00637, HFF, or astrocyte cells (5 x 10^4 cells/well) on a glass cover slip in a 24-well plate was added cavitand **1.14** (final concentration = 50 μM) and various concentrations of fluorescein guest **5.1**. These cells were incubated at 37 °C for 24 h and washed with PBS buffer (3 x 500 μL) to remove unincorporated cavitand **1.14** and guest **5.1**. The cells were fixed with 4 % paraformaldehyde and the cover slip was removed from the 24-well plate. The nuclei of the cells were stained with DAPI and a glass slide was mounted on the cover slip and fixed. Fluorescence microscopy of the cells was carried out as above.

Other Assays: All other assays were performed as described above, varying only in the species added (e.g. ± cavitand **1.14**, fluorescein **5.2** or choline chloride).

Flow Cytometry

1x10^6 HeLa cells were placed in FACS tubes (BD Falcon™, MA, USA), centrifuged at 1200 rpm for 5 minutes at 4 °C and resuspended in FACS buffer (1X PBS containing 4 % BSA, 0.01 % EDTA). After a further round of centrifugation the cells were fixed by

adding ice cold 4 % PFA in PBS slowly whilst gently mixing cells. Following a 10 minute incubation on ice, cells were centrifuged and resuspended in 300μL FACS buffer then analyzed using the BD FACSCantoTM II flowcytometer and FlowJo analysis software v.8.7.3.

Cytotoxicity Experiments

Compounds were tested for their effect on cell proliferation/viability, membrane integrity, and induction of apoptosis using human neuroblastoma cells. Cells were cultured at 37 ^{o}C and 5 % CO_2 in a 96 well dish with Minimum Essential Medium containing Earl's Balanced Salts, 0.5% fetal bovine serum, Glutamax, and antibiotic. The negative control was DMSO used to solubilize the compound.

Cell proliferation/viability was determined using the CellTiter 96 Aqueous One Cell Proliferation Assay (Promega). Cells were cultured in the presence of varying concentration of the compound for 24 hrs. Twenty microliters of CellTiter96 Reagent was added to each sample and the plate incubated in the dark for 4 hrs at 37°C. Results are expressed as 490 nm absorbance and reflect cell proliferation.

Membrane integrity was determined with CytoTox-One Homogeneous Membrane Integrity Assay (Promega). Cells were cultured in the presence of varying concentration of the compound for 24 hrs.. The culture dish was then placed at room temperature for 30 min. Subsequently, 100 μl of CytoTox-ONE reagent was added to each sample and the plate incubated at room temperature for 10 minutes. The reaction was terminated by addition of 50 μl of stop solution. Fluorescence was measured at an excitation wavelength of 560 nm and emission wavelength of 590 nm. The positive control was 2%

(v/v) lysis solution. Results are expressed as relative fluorescence units (RFU) and reflect membrane permeability.

Induction of apoptosis was determined with Apo-ONE Homogeneous Caspase-3/7 Assay (Promega). Cells were cultured in the presence of varying concentration of the compound for 24 hrs. Next, 100 µl of Apo-ONE reagent was added to each sample and the plate incubated at room temperature for 18 hours. Fluorescence was measured at an excitation wavelength of 499 nm and emission wavelength of 521 nm. The positive control (cells undergoing apoptosis) was medium containing 1µM Staurosporine. Results are expressed as relative fluorescence units (RFU) and reflect the degree of apoptosis.

ATP Depletion

HeLa cells (5 x 10^4 cells/well) were seeded on a glass cover slip in 24-well plate for 23 h at 37 °C and was added cavitand **1.14** (final concentration = 50 µM), fluorescein guest **5.1** (final concentration = 50 µM), 50 mM 2-deoxy-D-glucose, and 10 mM NaN_3. These cells were incubated at 37 °C for 1 h and washed with PBS buffer (3 x 500 µL). The cells were fixed with 4 % paraformaldehyde and the cover slip was removed from the 24-well plate. The nuclei of the cells were stained with 4,6-diamidino-2-phenylindole dihydrochloride (DAPI) and a glass slide was mounted on the cover slip and fixed. Fluorescence microscopy of the cells was carried out on a Leica SP5 confocal microscope. Confocal fluorescence microscopy and differential interference contrast (DIC) microscopy were used to image the cells and the three images (DIC, 405 nm DAPI, 488 nm guest **5.1**) were combined to form the images shown.

Endosome Disruption

HeLa cells (5 x 10^4 cells/well) were seeded on a glass cover slip in 24-well plate for 23 h at 37 °C and was added cavitand **1.14** (final concentration = 50 μM), fluorescein guest **5.1** (final concentration = 50 μM), and various concentrations of sucrose (125 – 500 mM). These cells were incubated at 37 °C for 1 h and 24 h, and washed with PBS buffer (3 x 500 μL). The cells were fixed with 4 % paraformaldehyde and the cover slip was removed from the 24-well plate. The nuclei of the cells were stained with 4,6-diamidino-2-phenylindole dihydrochloride (DAPI) and a glass slide was mounted on the cover slip and fixed. Fluorescence microscopy of the cells was carried out on a Leica SP5 confocal microscope. Confocal fluorescence microscopy and differential interference contrast (DIC) microscopy were used to image the cells and the three images (DIC, 405 nm DAPI, 488 nm guest **5.1**) were combined to form the images shown.

Vesicle Preparation

POPC, (151 μL, 13.2 mM in chloroform), DOPE-Rhod (ammonium salt) (13 μL, 0.769 mM in chloroform), chloroform (121 μL), and 10 mM HEPES buffer (3 mL, with 10 mM $MgCl_2$, pH 7.4) were added in sequence to a 20 mL scintillation vial. The solvent was slowly removed by rotary evaporation (10 mmHg, 40 °C, 40 rpm) for 4–5 min and after one vigorous distillation event gave ~ 2.5 mL of an opaque pink liquid.[10] The solution of vesicles was then divided into 500 μL aliquots and treated separately with fluorescent guest **5.1** (21 μL, 0.94 mM in water, 5 mol % with respect to POPC), or fluorescent guest **5.1** (21 μL) and cavitand **1.14** (34 μL, 0.29 mM in water, 2.5 mol % with respect to POPC).

Vesicle Imaging: Fluorescence microscopy was carried out on a Zeiss LSM 510 confocal laser scanning microscope with 488 nm argon laser excitation and a CCD camera.

7.6 Chapter Six Experimental

Synthesis

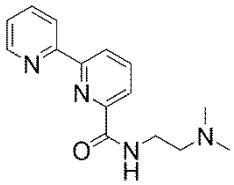

***N*-(2-(dimethylamino)ethyl)-2,2'-bipyridine-6-carboxamide:** In a 500 mL round bottom flask, [2,2'-bipyridine]-6-carboxylic acid (2.5 g, 12.49 mmol), 2-(6-chloro-1H-benzotriazole-1-yl)-1,1,3,3-tetramethylaminium hexafluorophosphate (5.68 g, 13.74 mmol), and triethylamine (3.48 mL, 24.98 mmol) were dissolved in 190 mL of 1:1 acetonitrile:chloroform, and the solution was stirred for 1 h at room temperature. To this solution were added *N*,*N*-dimethylethylenediamine (2.06 mL, 18.74 mmol) and triethylamine (5.2 mL, 37.47 mmol). The reaction mixture was stirred overnight at room temperature. The solvent was removed under reduced pressure and $NaHCO_3$ was added to the crude product and the product was extracted by dichloromethane. The collected organic layer was dried with $MgSO_4$ and filtered. The dichloromethane was removed under reduced pressure. The crude product was purified by running column (1-10 % MeOH in DCM). $NaHCO_3$ was added to the purified product and the product was extracted by dichloromethane. The collected organic layer was dried with $MgSO_4$ and filtered. The dichloromethane was removed under reduced pressure to yield dark brown

oil (670 mg, 20 % yield). ^{1}H NMR ($CDCl_3$, 400 MHz): δ 8.67 (dd, *J* = 8.0, 1.2 Hz, 1H), 8.52 (dd, *J* = 8.0, 1.2 Hz, 1H), 8.38 (dd, *J* = 8.0, 1.2 Hz, 1H), 8.19 (dd, *J* = 8.0, 1.2 Hz, 1H), 7.95 (t, *J* = 8.0 Hz, 1H), 7.81 (dt, *J* = 8.0, 1.2 Hz, 1H), 7.32 (dq, *J* = 8.0, 1.2 Hz, 1H), 3.60 (q, *J* = 8.0 Hz, 2H), 2.60 (t, *J* = 8.0 Hz, 2H), 2.34 (S, 6H).

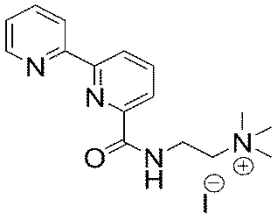

2-(2,2'-bipyridine-6-carboxamido)-*N*,*N*,*N*-trimethylethanaminium iodide 6.1: In a 50 mL sealed tube, *N*-(2-(dimethylamino)ethyl)-2,2'-bipyridine-6-carboxamide (670 mg, 2.48 mmol) was suspended in 10 mL toluene, and was added DMSO until *N*-(2-(dimethylamino)ethyl)-2,2'-bipyridine-6-carboxamide dissolved completely. Iodomethane (0.161 mL, 2.60 mmol) was added and the solution was stirred and heated at 112 °C for 5 h. Light brown precipitate was formed after 1 h stirring. The reaction solution was cool downed to room temperature and ether was added. The formed precipitate was vacuum filtered to yield light brown powder (848 mg, 85 % yield). ^{1}H NMR (D_2O, 400 MHz): δ 8.70 (dd, *J* = 8.0, 1.2 Hz, 1H), 8.35 (dd, *J* = 8.0, 1.2 Hz, 2H), 8.20 (t, *J* = 10.4 Hz, 2H), 8.16 (dd, *J* = 8.0, 1.2 Hz, 1H), 8.09 (dt, *J* = 8.0, 1.2 Hz, 1H), 7.60 (dt, *J* = 8.0, 1.2 Hz, 1H), 4.02 (t, *J* = 8.0 Hz, 2H), 3.70 (t, *J* = 8.0 Hz, 2H), 3.27 (s, 9H).

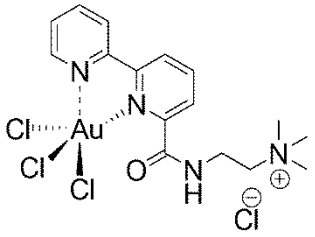

Gold(III)2-(2,2'-bipyridine-6-carboxamido)-*N*,*N*,*N*-trimethylethanaminium chloride 6.2: In a 250 mL round bottom flask, 2-(2,2'-bipyridine-6-carboxamido)-*N*,*N*,*N*-trimethylethanaminium iodide (100 mg, 0.24 mmol) was dissolved in 40 mL acetonitrile, and was added $NaAuCl_4$ (99.4 mg, 0.25 mmol). The reaction solution was refluxed for 2 h. The solvent was removed under reduced pressure to yield brown oil (235 mg). ^{1}H NMR (D_2O, 400 MHz): δ 9.22 (dd, *J* = 4.0, 0.8 Hz, 1H), 8.94 (dd, *J* = 4.0, 0.8 Hz, 1H), 8.73 (d, *J* = 8.0 Hz, 1H), 8.71 (dt, *J* = 8.0, 1.2 Hz, 1H), 8.56 (q, *J* = 8.0 Hz, 1H), 8.35 (d, *J* = 4.0 Hz, 1H), 8.14 (t, *J* = 8.0 Hz, 1H), 4.06 (t, *J* = 8.0 Hz, 2H), 3.72 (t, *J* = 8.0 Hz, 2H), 3.28 (s, 9H).

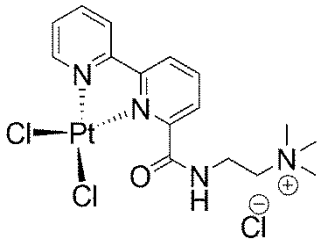

Platinum(II) 2-(2,2'-bipyridine-6-carboxamido)-*N*,*N*,*N*-trimethylethanaminium chloride 6.3: In a 50 mL round bottom flask, 2-(2,2'-bipyridine-6-carboxamido)-*N*,*N*,*N*-trimethylethanaminium iodide (82.5 mg, 0.2 mmol) was dissolved in 10 mL acetonitrile, and was added cis-bis(benzonitrile)dichloroplatinum(II) (94.5 mg, 0.2 mmol). The reaction solution was stirred at room temperature overnight. The precipitate was vacuum filtered and the filtrate solvent was removed under reduced pressure to yield orange

powder (53 mg, 45 % yield). ^{1}H NMR (D_2O, 400 MHz): δ 8.70 (dd, *J* = 4.0, 0.8 Hz, 1H), 8.35 (dd, *J* = 4.0, 0.8 Hz, 1H), 8.19 (d, *J* = 8.0 Hz, 1H), 8.14 (q, *J* = 8.0 Hz, 1H), 7.80 (dd, *J* = 4.0, 0.8 Hz, 1H), 7.64 (dt, *J* = 8.0, 1.2 Hz, 1H), 7.57 (t, *J* = 8.0 Hz, 1H), 4.02 (t, *J* = 8.0 Hz, 2H), 3.70 (t, *J* = 8.0 Hz, 2H), 3.27 (s, 9H).

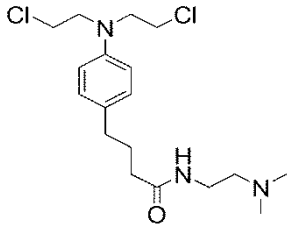

4-(4-(bis(2-chloroethyl)amino)phenyl)-*N*-(2-(dimethylamino)ethyl)butanamide: In a 50 mL round bottom flask, chlorambucil (100 mg, 0.33 mmol), 2-(6-chloro-1H-benzotriazole-1-yl)-1,1,3,3-tetramethylaminium hexafluorophosphate (149 mg, 0.36 mmol), and triethylamine (0.09 mL, 0.66 mmol) were dissolved in 10 mL chloroform, and the solution was stirred for 1 h at room temperature. To this solution were added *N*,*N*-dimethylethylenediamine (0.062 mL, 0.56 mmol) and triethylamine (0.14 mL, 1.00 mmol). The reaction mixture was stirred overnight at room temperature. The solvent was removed under reduced pressure and $NaHCO_3$ was added to the crude product and the product was extracted by dichloromethane. The collected organic layer was dried with $MgSO_4$ and filtered. The dichloromethane was removed under reduced pressure to yield light yellow oil (60 mg, 49 % yield). ^{1}H NMR ($CDCl_3$, 400 MHz): δ 7.04 (d, *J* = 12.0 Hz, 2H), 6.59 (d, *J* = 12.0 Hz, 2H), 3.67 (d, *J* = 8.0 Hz, 4H), 3.61 (d, *J* = 8.0 Hz, 4H), 3.38 (q, *J* = 8.0 Hz, 2H), 2.57 (t, *J* = 8.0 Hz, 2H), 2.52 (t, *J* = 8.0 Hz, 2H), 2.35 (s, 6H), 2.17 (t, *J* = 8.0 Hz, 2H), 1.88 (qn, *J* = 8.0 Hz, 2H).

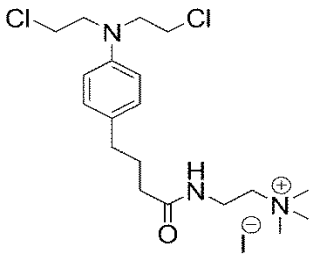

2-(4-(4-(bis(2-chloroethyl)amino)phenyl)butanamido)-*N*,*N*,*N*-trimethylethan-aminium iodide 6.4: In a 25 mL round bottom flask, 4-(4-(bis(2-chloroethyl)amino)phenyl)-*N*-(2-(dimethylamino)ethyl)butanamide (60 mg, 0.16 mmol) was dissolved in 4 mL dry THF, and was added iodomethane (0.01 mg, 0.17 mmol). The reaction solution was stirred at room temperature for 3 h. The solvent was removed under reduced pressure to yield dark brown oil. NMR (D_2O, 400 MHz): δ 7.07 (d, *J* = 12.0 Hz, 2H), 6.61 (d, *J* = 12.0 Hz, 2H), 3.68 (d, *J* = 8.0 Hz, 4H), 3.63 (d, *J* = 8.0 Hz, 4H), 3.48 (q, *J* = 8.0 Hz, 2H), 3.36 (s, 9H), 2.54 (t, *J* = 8.0 Hz, 2H), 2.30 (t, *J* = 8.0 Hz, 2H), 1.90 (qn, *J* = 12.0 Hz, 2H), 1.21 (t, *J* = 12.0 Hz, 2H).

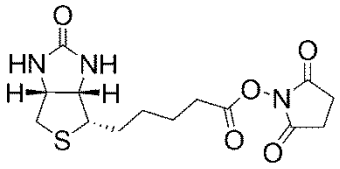

2,5-dioxopyrrolidin-1-yl 5-((3aS,4S,6aR)-2-oxohexahydro-1H-thieno[3,4-d]imidazol-4-yl)pentanoate: In a 25 mL round bottom flask, biotin (196 mg, 0.8 mmol) was dissolved in 6 mL DMF at 60 °C under N_2, and treated with *N,N'*-dicyclohexylcarbodiimide (168 mg, 0.88 mmol) and *N*-hydroxysuccinimide (104 mg, 0.8 mmol). The mixture was stirred at 60 °C for 2 h and kept stirring for 24 h at room temperature. The white precipitate formed during reaction was filtered and the volume of

the solvent was concentrated to 1 mL under reduced pressure, and then excess acetone was added into the mixture until no more precipitate formed. The precipitate was collected and washed with acetone. The product was recrystallized in isopropanol, and white powder was obtained (85 mg, 31 % yield). ^{1}H NMR (DMSO, 400 MHz): δ 6.42 (s, 1H), 6.35 (s, 1H), 4.30 (m, 1H), 4.15 (m, 1H), 3.12 (m, 1H), 2.85 (d, *J* = 4 Hz, 1H), 2.81 (s, 4H), 2.67 (t, *J* = 8.0 Hz, 2H), 2.58 (d, *J* = 16 Hz, 1H), 1.51 (m, 6H).

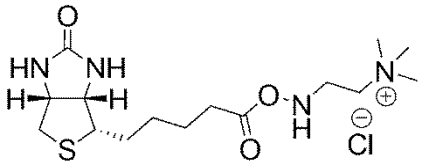

***N*,*N*,*N*-trimethyl-2-(5-((3aS,4S,6aR)-2-oxohexahydro-1H-thieno[3,4-d]imidazol-4-yl)pentanoyloxyamino)ethanaminium chloride 6.5:** In a 10 mL round bottom flask, (2-aminoethyl)trimethylammonium chloride hydrochloride (34 mg, 0.22 mmol) was dissolved in 1 mL DMF, and treated with Et_3N (56 µM, 0.4 mmol). 2,5-dioxopyrrolidin-1-yl 5-((3aS,4S,6aR)-2-oxohexahydro-1H-thieno[3,4-d]imidazol-4-yl)pentanoate (69 mg, 0.2 mmol) was added and the mixture was stirred at room temperature overnight. Another Et_3N (56 µM, 0.4 mmol) was added to the solution and the reaction was stirred at room temperature overnight. Excess diethylether was added to the solution and the product was precipitated out. The product was filtered and washed with excess diethylether, and white powder was obtained (29 mg, 36 % yield). ^{1}H NMR (DMSO, 400 MHz): δ 6.41 (s, 1H), 6.37 (s, 1H), 4.31 (m, 1H), 4.13 (m, 1H), 3.47 (q, *J* = 8 Hz, 2H), 3.11 (m, 1H), 3.09 (s, 9H), 2.85 (d, *J* = 4 Hz, 1H), 2.81 (t, *J* = 8.0 Hz, 2H), 2.58 (d, *J* = 16 Hz, 1H), 2.11 (t, *J* = 8 Hz, 2H), 1.50 (m, 6H).

Cytotoxicity Test

HeLa cells (4 x 10^3 cells/well) were cultured in 96-well plate for 24 h at 37°C and was added cavitand **1.14** (final concentration = 20 μM) and various concentrations of R-NMe_3^+ labeled compounds. These cells were incubated at 37 °C for various incubation times and SRB assay was performed.

SRB Assay

SRB assay was performed via literature method.[11] Cell media were removed from each well. Cells were fixed by the addition of 100 μL cold 10 wt % trichloroacetic acid and incubated at 4 °C for 1 h. The solution was removed and each well was washed with water five times and air dried. The addition of 50 μL SRB solution (0.4 wt % in 1 wt % acetic acid) was added into each well and the fixed cells were incubated for 10 min at room temperature. After discarding the solution, each well was washed with 1 wt % acetic acid for five time and air dried. 100 μL of 10 mM Tris buffer (pH 10) were added into each well to solubilize the bound dye. The 96-well plate was shaken on a plate reader and the absorbance at 490 nm was measured.

Cell Counting

HeLa cells (8 x 10^4 cells/well) were cultured in 6-well plate for 24 h at 37°C and was added various concentrations of chlorambucil (10 – 50 μM). These cells were incubated at 37 °C for 48 h. After incubation, dead HeLa cells were collected from media and adhered live HeLa cells were detached by trypsin. Both dead cells and live cells were combined and collected by centrifugation. Those cells were stained with trypan blue and

counted using hemocytometer. The % viability of cells was determined by the equation below.

$$\#\ \text{live cells} / (\#\ \text{live cells} + \#\ \text{dead cells}) \qquad \text{(eq 4)}$$

7.7 References

1. Biros, S. M.; Ullrich, E. C.; Hof, F.; Trembleau, L.; Rebek, J., Jr. "Kinetically Stable Complexes in Water: The Role of Hydration and Hydrophobicity." *J. Am. Chem. Soc.*, **2004**, *126*, 2870-2876.

2. Rafai Far, A.; Shivanyuk, A.; Rebek, J., Jr. "Water-Stabilized Cavitands." *J. Am. Chem. Soc.*, **2002**, *124*, 2854-2855.

3. Phillips, K. S.; Han, J. –H.; Martinez, M.; Wang, Z.; Carter, D., Cheng, Q. "Nanoscale Glassification of Gold Substrates for Surface Plasmon Resonance Analysis of Protein Toxins with Supported Lipid Membranes." *Anal. Chem.*, **2006**, *78*, 596-603.

4. Liu, Y.; Liao, P.; Cheng, Q.; Hooley, R. J. "Protein and Small Molecule Recognition Properties of Deep Cavitands in a Supported Lipid Membrane Determined by Calcination-Enhanced SPR Spectroscopy." *J. Am. Chem. Soc.*, **2010**, *132*, 10383-10390.

5. Bieri, C.; Ernst, O. P.; Heyse, S.; Hofmann, K. P.; Vogel, H. "Micropatterned Immobilization of a G Protein-Coupled Receptor and Direct Detection of G Protein Activation." *Nat. Biotechnol.*, **1999**, *11*, 1105-1108.

6. Vestling, M. M. "Insulin: HPLC Mapping of Protease Digestion Products: A Biochemistry Laboratory Experiment." *J. Chem. Educ.*, **1991**, *68*, 958-960.

7. Costello, D. A.; Millet, J. K.; Hsia, C. –Y.; Whittaker, G. R.; Daniel, S. "Single Particle Assay of Coronavirus Membrane Fusion with Proteinaceous Receptor-Embedded Supported Bilayers." *Biomaterials*, **2013**, *34*, 7895-7904.

8. Axelrod, D.; Koppel, D. E.; Schlessinger, J.; Elson, E.; Webb, W. W. "Mobility Measurement by Analysis of Fluorescence Photobleaching Recovery Kinetics." *Biophys. J.*, **1976,** *16*, 1055-1069.

9. Soumpasis, D. M. "Theoretical-Analysis of Fluorescence Photobleaching Recovery Experiments." *Biophys. J.*, **1983,** *41*, 95-97.

10. Dominak, L.M.; Keating, C.D. "Polymer Encapsulation within Giant Lipid Vesicles." *Langmuir*, **2007**, *23*, 7148-7154.

11. Houghton, P.; Fang, R.; Techatanawat, I.; Steventon, G.; Hylands, P.; Lee, C. C. "The Sulphorhodamine (SRB) Assay and Other Approaches to Testing Plant

Extracts and Derived Compounds for Activities Related to Reputed Anticancer Activity." *Methods*, **2007**, *42*, 377-387.